

COMPARISON OF TWO-PHASE NUMERICAL MODELLING TECHNIQUES IN APPLICATIONS
WITH ELECTROHYDRODYNAMICS

By

James M. LeMoine B.Eng

A Thesis

Submitted to the School of Graduate Studies

in Partial Fulfilment of the Requirements

for the Degree

MASTER OF APPLIED SCIENCE

MASTER OF APPLIED SCIENCE (2022)
(Mechanical Engineering)

McMaster University
Hamilton, Ontario

TITLE: Comparison of Two-Phase Numerical Modelling Techniques in
Applications with Electrohydrodynamics

AUTHOR: James LeMoine

SUPERVISOR: Dr. James S. Cotton, Professor
Department of Mechanical Engineering

PAGE COUNT: xviii, 125

“Essentially, all models are wrong, but some are useful” – George E.P. Box

Acknowledgments

I'd like to give thanks my supervisor Dr. Jim Cotton for his support over the last 3 years. It was a pleasure working with you and your guidance throughout this thesis was crucial. The pandemic was a difficult time and its arrival midway through this thesis came with so many challenges. Your help and understanding is appreciated throughout these hard times.

I'd like to give thanks to all my lab mates that gave advise on my work and provided a space to work through issues I had. Everyone was so helpful and there was always someone willing to help with any issue that arose.

I'd like to give thanks to my friends that supported me and were there to talk when models were not working, and things got stressful. All of you were there whenever I needed a break away from my work. Whether it was going for food or playing games, it was much needed so I could come back to work with a clear mind.

I'd like to thank my family that has supported me all of these years. I'd like to give a special thank you to my mother that made sure I only had to focus on my studies my whole life. I would not have had the same success without everything you've done for me. I'd also like to thank all of my aunts that are always there to talk whenever I need someone to listen. You all have taught me so much of our culture which you had to teach yourself.

I'd like to give thanks to the Mississauga of the Credit First Nation for the support they gave me and the cultural guidance. The support they gave through my undergraduate degree made it possible to get to where I am now. All of the events that have been hosted like the three fires powwows have been a great learning opportunity.

I'd like to give thanks to McMaster University and NSERC for the support given throughout this thesis. The financial assistance makes this research possible.

I'd like to thank all the staff. The members of the mechanical engineering machine lab do great work to help all the students with everything they need. The secretary staff that make sure that there's no additional stress on us. All the other workers at McMaster that are crucial to keep the university running and clean. Everyone's work is truly appreciated.

I'd like to give thanks to my partner Rhea that has always been there for me. I knew I could talk to you about anything and everything. You probably have heard more about EHD than any Biology student would ever want to hear. Even when I would talk about the same problems, you were there to listen and help. This thesis would not be what it is without your time editing my poor spelling and run on sentences.

Chi-miigwech to everyone that supported me financially, emotionally, and spiritually. Without all of the people that surrounded me I don't think I could be as successful as I have been.

Abstract

Three two-phase numerical modelling techniques were employed to study the effect of electrohydrodynamics (EHD) on the redistribution of fluid and flow patterns created. One model uses an interface tracking technique to differentiate the fluids in different domains. The other modelling techniques have a volume of fluids approach that uses a variable to represent the volume of each phase that is present in a control volume and is subjected to advection from the velocity field and diffusion to stabilize the interface. These models were testing in two cases, the deformation of a bubble from EHD forces and liquid redistribution in a stratified pipe cross-section causing liquid extraction, to investigate the limitations of each of the modelling techniques and compare the results to find the right model to use in different situations.

It was found, in the bubble deformation model, that the EHD polarization forces are centralized on the interface between the fluids. Both the dielectrophoretic and electrostrictive forces were found to be significant in this scenario where previous models thought the electrostrictive component to be negligible [1]–[4]. These forces act to spread the phase parameter in the volume of fluids methods due to the force being variable across the interface control volumes which leads to a destabilization of the model. This unstable interface expansion degrades the forces dependent on the gradient of the phase parameter, in particular EHD and surface tension forces. The surface tension degradation led to bubble detachment or phase infiltration across the interface which made the model results nonphysical. The interface tracking method maintained stability as the force applied was a surface pressure on the moving interface and could not expand as the interface was infinitesimal. The steady state results of this method matched experimental data from previous investigations within 5% of interface position [5].

In the liquid extraction model, the forces were located along the interface and both components of the polarization forces were significant similar to the bubble deformation case. The volume of fluids models eventually destabilized at the interface which caused a degradation of EHD and surface tension forces, The result was a faster extraction time compared to the interface tracking method due to reduced surface tension. The volume of fluid models were compared to past numerical research [6] for the same geometry it was found that the factor that weighs the advection to the diffusion of the phase parameter is crucial in time dependent models. Increasing this parameter stabilizes the boundary of the fluid but suppresses advection leading to much slower extraction times but when the components are balanced, when large EHD forces are applied the boundary destabilizes. This shows the importance of finding the right value for this parameter in cases that are time dependent and illustrates the variation in time dependent results in volume of fluid models.

The interface tracking model was compared to previous experimental work and with a different interpretation of the experimental results than the original author the results were within the experimental error [7]. The interface tracking method is shown to be the best option for stable models with good time dependent and steady state results. This model's limitation is its inability to experience topological changes to the domains whereas the volume of fluid models were able to reach a steady state solution after the liquid rose and made contact with the electrode. In cases with topological changes during the experiment the volume of fluid methods must be used with much caution taken regarding the phase parameter weighting factor.

TABLE OF CONTENTS

ABSTRACT.....	V
LIST OF FIGURES	X
LIST OF TABLES.....	XV
ACRONYMS, ABBREVIATIONS & NOMENCLATURE	XVII
CHAPTER 1 - INTRODUCTION.....	1
1.1 Heat Transfer Enhancement Techniques.....	1
1.2 Background of EHD.....	5
Flow Redistribution from EHD Force.....	7
1.4 Previous work in EHD Modelling	10
1.5 Research Objective.....	12
CHAPTER 2 - ELECTROHYDRODYNAMIC NUMERICAL MODELLING.....	14
2.1 Introduction to EHD	14
2.2 Electric Body Force Equation	14
2.3 Fundamental Conservation Equations.....	16
Mass and Momentum Conservation.....	16
Electric Field Distribution	17

2.4 Multi-Phase Flow Modelling	17
Moving Mesh Model	18
Level Set Model	21
Phase Field Model	23
CHAPTER 3 - AIR BUBBLE IN FC-72 SIMULATION	26
3.1 Introduction	26
3.2 Numerical Methodology	27
Moving Mesh Method	29
Phase Field and Level Set Method	31
3.3 Results and Comparison	34
Ramp Analysis	34
Initial Interfacial Forces	36
Transient Model	49
Conclusion	55
CHAPTER 4 - LIQUID EXTRACTION	57
4.1 Introduction	57
4.2 Numerical Methodology	59
4.3 Modelling Techniques	62
Moving Mesh Model	62
Phase Field and Level Set Method	63
4.4 Results and Discussion	66

Initial Interfacial Forces.....	66
Liquid Extraction Rising Time	80
Comparison with Previous Works	91
Steady State Result	96
Conclusions	98
CHAPTER 5 - SUMMARY AND CONCLUSIONS.....	99
5.1 Recommendations for Future Work	101
REFERENCES	103
APPENDIX A - INDEPENDENCE TEST FOR BUBBLE DEFORMATION.....	112
Introduction.....	112
Mesh Independence Study	112
APPENDIX B - INDEPENDENCE TESTS FOR LIQUID EXTRACTION MODEL	118
Introduction.....	118
Mesh Independence Study	118
Time Independence Tests.....	123

List of Figures

Figure 1.1: Flow redistribution structures cause by EHD forces.	8
Figure 2.1: Diagram of normal vector on the interface between 2 fluids.	20
Figure 2.2: Bubble during separation that depicts a topological change in the interface.	21
Figure 3.1: 2D axis symmetrical geometry used for EHD two phase flow model. Modified from Di Marco et. al.	28
Figure 3.2: Graph of scaling parameter for the electric potential.	29
Figure 3.3: Height of the highest point on the bubble vs time for a step change in voltage and 0.01 and 0.1 second ramp voltages on the electrode.	35
Figure 3.4: Surface force on the initial bubble shape with an electrode voltage of 20kV for the moving mesh, phase field, and level set models. (a) Interfacial pressure in r-direction (b) Interfacial pressure in z-direction.	38
Figure 3.5: Volume of fluid for the level set and phase field models. Red represents the air and blue represents FC-72. (a) Moving Mesh Model (b) Level Set Model (c) Phase Field Model (d) Phase Field Model after 0.0002s.	40
Figure 3.6: Cut Line across the bubble interface to plot data.	42
Figure 3.7: Volume fraction of air across cut line in Figure 3.6 with different mesh sizes. (a) Phase Field Model (b) Level Set Model.	43
Figure 3.8: Body force magnitude in N/m ³ . Scaled vectors are displayed with their length proportional to the magnitude. (a) Phase Field Model (b) Level Set Model.	44

Figure 3.9: Comparison of EHD force components in different models. T_{sr} is the total radial stress which is the sum of the Dielectrophoretic component (DEP) and Electrostrictive component. (a) Moving Mesh model (b) Phase Field Model.46

Figure 3.10: Electric field in V/m of the Moving Mesh model. Full bubble on left and close up of the top of bubble is shown on the right.47

Figure 3.11: Electric field in V/m of the Phase Field model. Full bubble on left and close up of the top of bubble is shown on the right.48

Figure 3.12: Comparison of bubble height at top of bubble interface as voltage of electrode is ramped from 0 to 20kV using Moving Mesh, Level Set, and Phase Field models.52

Figure 3.13: Bubble shapes for the moving mesh, phase field, and level set model when subjected to a 20kV ramp voltage at various times. (a) bubble position at 0.025s (b) bubble position at 0.05s (c) bubble position at 0.08s.53

Figure 3.14: Bubble shape in the moving mesh model vs the experimental data from Di Marco et al. experiment for a 0.0737mm³ bubble subjected to 20kV.55

Figure 4.1: Geometry used for the models.61

Figure 4.2: Geometry after capillary rise at edge due to surface tension.62

Figure 4.3: Magnitude of EHD body force on the initial domain in N/m³ with different modelling techniques. Proportional force vectors are overlayed. (a) Phase Field, (b) Level Set.68

Figure 4.4: Electrical field of the initial domain of the Level Set model in V/m. (a) full geometry (b) close-up on the center interface.71

Figure 4.5: Electrical field of the initial domain of the Phase Field model in V/m. (a) full geometry (b) close-up on the center interface.72

Figure 4.6: Electrical field of the initial domain of the Moving Mesh model in V/m. (a) full geometry (b) close-up on the center interface.	73
Figure 4.7: Initial interfacial stress comparison with Moving Mesh, Phase Field, and Level Set models.	75
Figure 4.8: Breakdown of the EHD force components in the y-direction.	76
Figure 4.9: Cutline above the liquid-vapour interface where the volume of fluids forces are retrieved from.	77
Figure 4.10: Breakdown of the EHD force into its components with different volume of fluids methods. Data was collected along cutline found in Figure 4.9 (a) Phase Field, (b) Level Set.	79
Figure 4.11: Rising time of the column of fluid being extracted by EHD forces. The base of the electrode is shown with a dotted line.	80
Figure 4.12: Volume fraction of air in the Phase Field model at various times (a) 0ms, (b) 8ms (c) 12ms (d) 15ms (e) 17ms.	83
Figure 4.13: Volume fraction of air in the Level Set model at various times (a) 0ms (b) 8ms (c) 10ms (d) 11ms.	84
Figure 4.14: Shape of the liquid-vapor interface at various times in the Moving Mesh model. ...	86
Figure 4.15: Shape of the liquid-vapor interface at various times in the Phase Field model.	86
Figure 4.16: Shape of the liquid-vapor interface at various times in the Level Set model.	87
Figure 4.17: Comparison of the interface shape across the Moving Mesh, Phase Field, and Level Set models at 8ms.	88
Figure 4.18: Comparison of the interface shape across the Moving Mesh and Phase Field models at 12ms.	89

Figure 4.19: Comparison of the interface shape across the Moving Mesh and Phase Field models at 15ms.	90
Figure 4.20: Comparison of the interface shape across the Moving Mesh and Phase Field models at 17ms.	90
Figure 4.21: Fluid Levels at the center where liquid extraction occurs and at the edge of the domain where the contact angle rises the fluid. Dotted line represents the initial rise from surface tension.	93
Figure 4.22: Data collected by Sadek et al. 2012. (a) mean grey value (b) slope of mean grey value of the interface for different frames. Dotted lines show the ± 2 standard deviations.	94
Figure 4.23: Height of the center of the fluid interface from numerical models performed by Nangle-Smith et al. 2012 [62].	96
Figure 4.24: Results for the Phase Field model at steady state. (a) fluid fraction of vapour (b) body force magnitude in N/m ³ with proportional arrows.	97
Figure A.1: Mesh used for bubble deformation. Example is from maximum grid spacing of 0.008mm. Left is full domain with a close up on the bubble on the right.	113
Figure A.2: Radial and axial interfacial stress of the bubble with various maximum mesh spacings for the Moving Mesh model. (a) Radial Stress Component (b) Axial Stress Component	114
Figure A.3: Radial and axial interfacial stress of the bubble with various maximum mesh spacings for the Phase Field model. (a) Radial Stress Component (b) Axial Stress Component	115
Figure A.4: Radial and axial interfacial stress of the bubble with various maximum mesh spacings for the Level Set model. (a) Radial Stress Component (b) Axial Stress Component	116

Figure B.1: Three meshes that were used to show mesh independence. The maximum node spacing from left to right is 0.1mm, 0.05mm, and 0.02mm.....119

Figure B.2: Comparison of principle stress component with different mesh spacing with the Moving Mesh model.....120

Figure B.3: Comparison of principle stress component with different mesh spacing (a) Phase Field Model (b) Level Set Model.....121

Figure B.4: Comparison of liquid extraction height with different relative tolerances (a) Moving Mesh Model (b) Phase Field Model (c) Level Set Model124

List of Tables

Table 1.1: Heat transfer enhancement techniques, adapted from Bergles, 2011 [11], [13]–[16].	4
Table 3.1: Fluid Properties of liquid FC-72 and air.	27
Table 3.2: Moving Mesh model boundary and solver conditions.	31
Table 3.3: Phase Field and Level Set model boundary and solver conditions. All properties are shared except the last rows labelled with the specific model they are used in.	33
Table 3.4: Comparison of percent overshoot and 2% settling time values for step, 0.01s, and 0.1s ramp voltage on the electrode.	35
Table 3.5: Maximum and minimum surface pressure from initial EHD force on the bubble for each model.	39
Table 4.1: Fluid Properties of liquid and vapour R-134a.	60
Table 4.2: Moving Mesh model boundary and solver conditions.	63
Table 4.3: Phase Field and Level Set model boundary and solver conditions. All properties are shared except the last rows labelled with the specific model they are used in.	65
Table 4.4: Maximum interfacial stress for each model and the percentage compared to the Moving Mesh model.	75
Table 4.5: Maximum EHD stress components for different modelling techniques. Outliers from numerical errors have been excluded.	78
Table 4.6: Liquid extraction times for Moving Mesh, Phase Field, and Level Set models.	81
Table 4.7: Timing for significant events in the Moving Mesh model and the experimental work by Sadek et al., 2012. Sadek corrected row is how many frames after the voltage applied was said to occur.	92

Table A.1: Maximum radial interfacial pressure differences with mesh spacing between the fine mesh, 0.002mm, and the other densities.117

Table A.2: Maximum axial interfacial pressure differences with mesh spacing between the fine mesh, 0.002mm, and the other densities.117

Table B.1: Force differences with mesh spacing between the fine mesh, 0.02mm, and the other densities.122

Table B.2: Liquid extraction timing differences between the low relative error, 0.005 & 0.0025 for Moving Mesh and volume of fluid methods respectively, and the other relative errors.125

Acronyms, Abbreviations & Nomenclature

Acronyms and Abbreviations

AC	Alternating Current
BDF	Backward Differential Formulation
DC	Direct Current
DEP	Dielectrophoretic
EHD	Electrohydrodynamics
GMRES	Generalized Minimal Residual Method
MUMPS	Multifrontal Massively Parallel Sparse Direct Solver
PARDISO	Parallel Direct Solver

Nomenclature

A	Area [m^2]
c_p	Specific heat capacity [$\text{J}/\text{kg}\cdot\text{K}$]
\vec{D}	Electric displacement field [C/m^2]
E	Electric field strength [V/m]
F	Force [N]
h_{\max}	Maximum mesh spacing [m]
h	Heat transfer coefficient [$\text{W}/\text{m}^2\cdot\text{K}$]
I	Identity matrix
k	Thermal conductivity [$\text{W}/\text{m}\cdot\text{K}$]
M_f	Mass flux [kg/m^2]
N_e	Number density of molecules [$1/\text{m}^3$]
\mathbf{n}_i	Normal vector
Q	Total heat transfer rate [W]
q'''	Volumetric heat generation [W/m^3]
P	Pressure [Pa]
T	Stress tensor [N/m^2]
T	Temperature [$^\circ\text{C}$]
t	Time [s]

\mathbf{u} Velocity vector [m/s]

V Voltage [V]

Greek

α_e Molecular polarizability [C.m²/V]

γ Reinitialization parameter/mobility parameter

ε Capillary width/ interface thickness controlling parameter [m]

ε_0 Electrical permittivity of free space (8.85x10⁻¹² N/V²)

ε_r Relative electrical permittivity

λ Mixing energy density

μ Dynamic viscosity [Pa.s]

ρ Density [kg/m³]

ρ_c Volumetric charge density [C/m³]

σ Surface tension coefficient [N/m]

ϕ Level set parameter/phase field parameter

χ Mobility tuning parameter

Subscripts

C Charge

ehd Electrohydrodynamic

ext External

g Gravitational

r Relative

st Surface tension

max Maximum value

mesh Of the mesh node

min Minimum Value

x x-direction

y y-direction

z z-direction

Superscripts

T

Transpose

Chapter 1 - Introduction

Heat transfer enhancement has various advantages including improved efficiency which can decrease the size of heat exchangers, decrease manufacturing or operating costs of cooling systems, or decrease system power consumption to make the system more environmentally friendly. Heat transfer enhancement techniques are crucial in systems where size is important as the traditional method to increase cooling is to make larger heat exchangers. These techniques can also assist in maintaining a heat exchanger performance after efficiency decreases due to fouling occurring. With a decrease in size, there can be reduced pumping requirements or decreasing system weight in vehicles can lead to less energy consumption that can reduce greenhouse gas emission by improving system efficiencies.

In this thesis, high voltages are used to create electric fields in dielectric fluids to improve heat transfer. EHD is predominately used to increase heat transfer in two-phase flow as the discontinuity in the electrical permittivity over the liquid-vapour interface of the fluid results in EHD forces sufficiently large enough to affect the flow. The improvement of heat transfer is due to the creation of different flow patterns in two-phase boiling that can increase turbulence or continue to wet the surface of the heat exchanger that would have otherwise remained dry. This requires minimal energy input (i.e. in mW range [8]) and therefore, Joule heating is not present [9], [10]. However, increased pumping requirements may be required due to electrodes in the fluid path and increased mixing due to EHD flow

1.1 Heat Transfer Enhancement Techniques

There are various techniques that have been created to enhance heat transfer in heat exchangers. The methods can be grouped into two main categories, active and passive strategies

[11]. A passive heat transfer enhancement strategy does not require the input of power and usually involve an additive into the fluid, or a treatment or fin design integrated surface of the heat exchanger in manufacturing. These strategies cannot be turned on and off or change during the heat exchanger's operation. Active strategies, on the other hand, require an input of power. These act to redistribute the flow by introducing an external force. Many of these strategies can be turned on and off or have their intensity varied. Thus, active strategies have the capability to control the amount of heat transfer by changing the heat transfer coefficient.

Some heat transfer enhancement techniques are listed in Table 1.1. These techniques mostly focus on effecting the heat transfer coefficient or the area of heat transfer. Equation 1.1 shows the equation for heat transfer from a surface. It is dependent on the surface area that is in contact with the fluid, the temperature difference between the wall and fluid temperature, and a heat coefficient that is typically empirically determined. The heat transfer coefficient is a conductivity term which shows how well a fluid extracts heat from a surface. High velocity turbulent flows have a higher heat transfer coefficient because the mixing that occurs shrinks the thermal boundary layer. Some techniques, like extended surfaces, act to increase the surface area in contact with the fluid to increase the heat transfer.

$$Q = hA * \Delta T \qquad \text{Equation 1.1}$$

The effectiveness of the heat transfer enhancement methods is dependent on the mode of heat transfer in the system. These methods also tend to increase the pressure drop, so there is typically a tradeoff between increased heat transfer and increased system pressure drop. Careful selection of a heat transfer enhancement technique must be taken to optimize a system. In this thesis, enhancement due to applying high voltages to generate electric fields also known as

electrohydrodynamics (EHD) will be investigated which has various applications in different heat transfer scenarios [12].

Table 1.1: Heat transfer enhancement techniques, adapted from Bergles, 2011 [11], [13]–[16].

Passive Enhancement Techniques	Active Enhancement Techniques
<p style="text-align: center;">Treated Surfaces</p> <p>Alteration of surface finish or coating applied. Used in Boiling and Condensing to create nucleation sites or hydrophobic surfaces. Can erode with flow.</p>	<p style="text-align: center;">Mechanical Aids</p> <p>System implemented to stir or scrape fluid creating mixing or breaking the boundary layer on the walls.</p>
<p style="text-align: center;">Rough Surfaces</p> <p>Random grain roughness on walls to discrete perturbations. Can promote turbulence near wall without large pressure drop occurring.</p>	<p style="text-align: center;">Surface Vibrations</p> <p>Low or high frequency vibration creating mixing. Primarily used in single phase heat transfer.</p>
<p style="text-align: center;">Extended Surfaces</p> <p>Surfaces or fins that are extruded from the wall to increase the surface area.</p>	<p style="text-align: center;">Injection/Suction</p> <p>Supplying or sucking a fluid through a porous surface to improve boiling and condensing. Increases mixing and can shrink boundary layers.</p>
<p style="text-align: center;">Flow Altering Devices</p> <p>Geometric structures within the heat exchanger to create different flow patterns like swirls or vortexes. Promote turbulence and mixing.</p>	<p style="text-align: center;">Jet Impingement</p> <p>Fluid is forced at heat transfer surface minimizing the boundary layer. High heat transfer rates can occur.</p>
<p style="text-align: center;">Surface Tension Devices</p> <p>Grooves or structures on the surface that create capillary flows that can direct fluids in boiling or condensing.</p>	<p style="text-align: center;">Electric Fields</p> <p>Introducing AC or DC electric fields can redistribute fluid in two-phase flows. Increases mixing and surface wetting.</p>
<p style="text-align: center;">Additives</p> <p>Solid, liquid, or gas particles are added to the fluid to create turbulence or change fluid properties.</p>	

1.2 Background of EHD

The addition of an electric field causes a force on the fluid, Equation 1.2 [17], [18]. This additional force can redistribute the phases, cause increased mixing, or replace the effect of gravity in space applications [19], [20]. EHD forces can also be utilized to pump a fluid [21]–[23].

$$F_{EHD} = \rho_c \bar{E} - \frac{1}{2} E^2 \nabla \epsilon + \frac{1}{2} \nabla \rho E^2 \left(\frac{\partial \epsilon}{\partial \rho} \right) \Big|_T \quad \text{Equation 1.2}$$

The equation consists of three terms which are called, from left to right, the Coulomb/Electrophoretic component, the Dielectrophoretic component, and the Electrostriction component. The dielectrophoretic and electrostriction component are also collectively known as the polarization force component.

Coulomb/Electrophoretic Force Component

The Coulomb Force is a force that acts on the free charges or ions in a fluid. The charged particles move along the electric field lines towards the electrode of opposite charge. This can create motion of the fluid which is called “Electroconvection” or “Corona Wind” [24], [25]. In dielectric fluids this force is often neglected as they are non-conductive and therefore there are very little free charges in the system [26]. In some cases, where there is a large electric field strength, charge injection can occur in dielectric fluids and the Coulomb force plays a dominant role affecting fluid motion [27].

Dielectrophoretic Force Component

The dielectrophoretic force arises from inhomogeneity of the electrical permittivity. The change of permittivity can be caused by non-uniform electric fields and temperature or phase gradients in the fluid. This force is significant in multi-phase flows as there is usually an order of magnitude difference between a vapor and liquid phase (For R-134a, the vapor and liquid permittivity are $\epsilon_{\text{vap}} = 1$ and $\epsilon_{\text{liq}} = 9.5$). The large change of permittivity at the interface makes an interfacial stress on the two-phase boundary. The dielectric force will attract the phase with the higher permittivity into the region of high electric field strength. This attraction can cause a resting liquid to be pulled towards an electrode in the vapor domain which has been termed “liquid extraction” [7], [10], [26]. Dielectrophoretic force is also present in single phase systems with large temperature gradients where electrical permittivity can vary at different fluid temperatures.

Electrostrictive Force Component

The electrostriction force is caused by the stretching of the molecules in the dielectric fluid along the field line due to a non-uniform electric field. This can create or enhance dipole moments in the molecule which creates a net force on the molecule. This force is typically neglected in incompressible fluids and thus is only seen in gas and liquid-vapor systems. Electrostriction is present at the interface of two-phase systems as there is a density change between the two phases. This force is not present in temperature gradients as the density gradient is at a constant temperature.

Flow Redistribution from EHD Force

The force introduced from the addition of the electric fields creates a body force on the fluid. New flow structures can occur in the fluid that are not typically seen in flows without EHD. These flow patterns can increase mixing, promote surface wetting, or extract fluid from surfaces [18]. This can increase or decrease the heat transfer by various amounts depending on the direction of the heat flux, the amount of fluid fraction, or the orientation of the system.

Some EHD influenced flow structures are shown in Figure 1.1. These flow structures are found in horizontal annular flow with a concentric electrode which is a commonly used geometry in EHD research [28], [29].

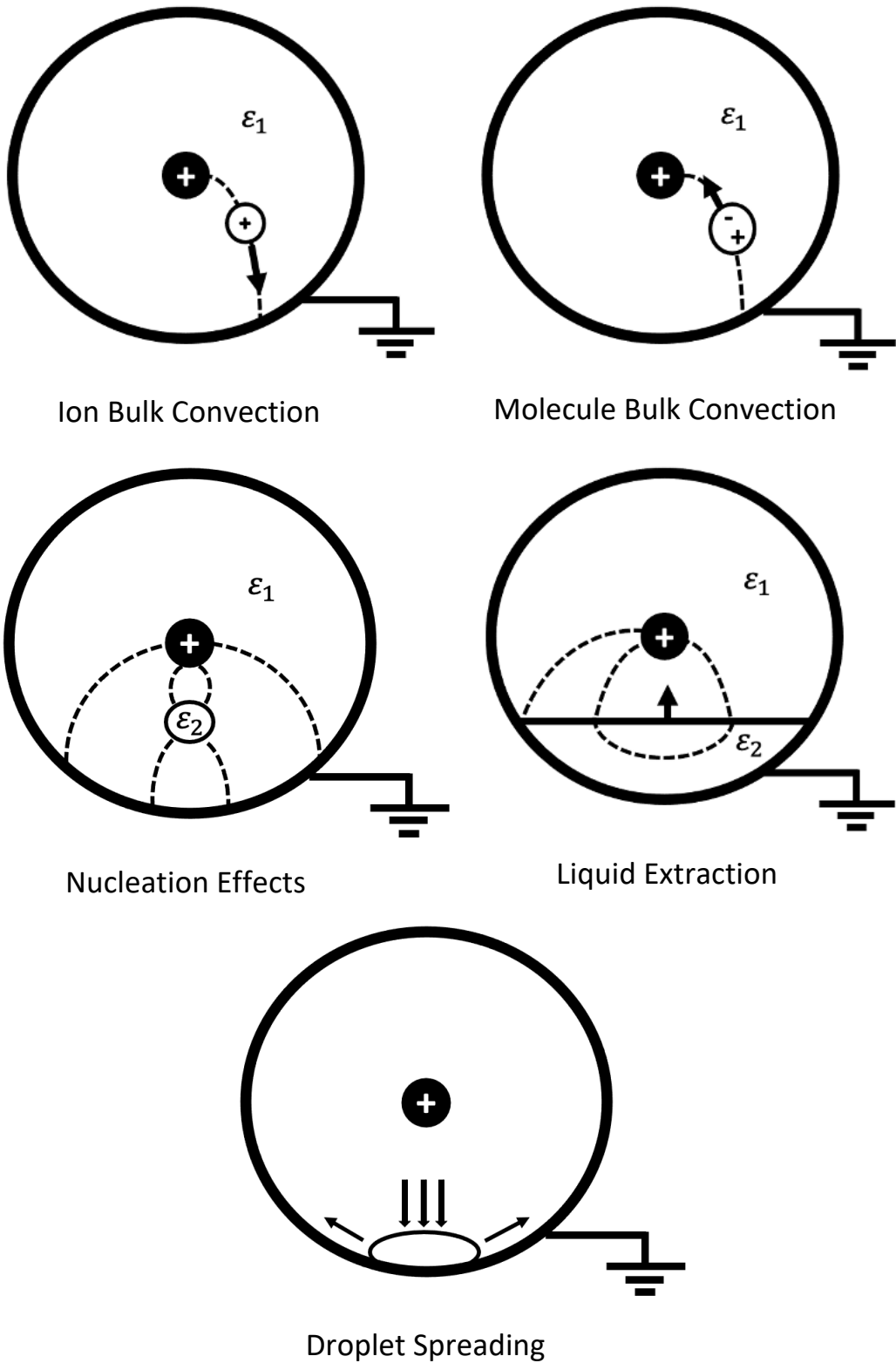


Figure 1.1: Flow redistribution structures cause by EHD forces.

Ion/Molecule Bulk Convection

Occurs from a charged particle or molecule that will have a net force due to its positive or negative charge. The particle will either accept or reject an electron at the electrode depending on the polarity and will move to the oppositely charge surface as a result. A molecule with a dipole moment can orient itself along the field line and experience a net force if there is a gradient of electric field. The motion of the ion or molecule will create a flow as it moves the bulk with it along the electric field lines due to viscous forces [18]. This bulk convection phenomenon is mainly seen in single phase systems with very high voltages [30], [31]. This force is represented in the Coulomb force component of the EHD force equation.

Enhanced Nucleation Effects

When condensing, droplets that are formed on the surface can be pulled away from the wall to allow for more sites for condensation to take place. Bubble formation when boiling can also be affected as the bubble stretches in the direction of the field line which can cause premature bubble separation allowing for open nucleation sites to continue boiling [32]. These effects are caused by the polarization forces from the permittivity difference.

Liquid Extraction

In stratified flows, the difference of permittivity can create an upward force on the liquid surface. The liquid moves towards the region of higher electric field strength, causing a column to form in the center, closest to the electrode. This extraction creates mixing of the fluid and can increase the interfacial area, increasing heat transfer. If an AC is applied, the fluid can oscillate from rising columns to downward flows creating more surface wetting and flow instabilities

[33], [34]. Depending on the orientation of the liquid in the cross section this can take the form of liquid jets or columns from all sides or creating droplets that can be forced into the heat transfer surface [7], [9], [10]. These flows are highly dynamics and provide great heat transfer enhancement and are unique to EHD.

Droplet Spreading

The spreading of a liquid film or small droplet on the surface is caused by a Coulomb pressure. Electrical discharge can cause bulk convection downward causing a forced vapour impingement on the liquid film. This force will act to spread the liquid due to the increased pressure. This spreading affect will allow for more surface area in contact with the fluid and allow for improved heat transfer [35].

1.4 Previous work in EHD Modelling

Modelling of two-phase systems is a complex area of research as the flow is an inherently transient due to large instabilities like bubbles in the liquid interface deformations resulting in dynamic surface wetting. Simple lumped models were made to calculate important system parameters like pressure drop and void fraction in a tube [36]. These models could estimate the point of total evaporation or condensation but did not capture specific physics in how the flow pattern affected local points in the system. These models typically need empirical values and knowledge of two-phase flow patterns to calculate the heat transfer.

Other analytical and numerical models have been developed to attempt to model the interface and interactions between the fluids [37], [38]. These models still use many empirical values but try to model different geometries. Each model still has problems in some applications

as instabilities at the interface are complex especially when additional physics are applied like EHD [39].

Numerous numerical models have been created to simulate two-phase flow patterns with the addition of EHD and have been compared to simple geometry two phase experimental conditions (a single bubble or stationary stratified configuration) but no studies has been performed to compare the difference modelling techniques to test shortcomings. The concern is that certain modelling techniques might be only valid in under specific scenarios such as low EHD forces and are validated with experiments in that range but when used to simulate other scenarios they could breakdown. Having a deep understanding of how each type of model works and the limitations each model possesses is crucial.

There are two main ways to model two-phase flows, interface tracking and volume of fluid methods. Interface tracking methods have a defined interface that changes over time. It has the advantage of having a stable interface and can have an infinitesimally small interface thickness. Volume of fluid methods use a phase parameter that corresponds to the volume fraction of each fluid. The phase parameter is affected by advection and diffusion. The interface is resolved over several nodes so there is a finite interface thickness.

Many previous models were only used to evaluate electric fields and the corresponding EHD force on the boundary [1]–[4]. These models should be very accurate as numerical electric field analysis is simple for most current Multiphysics software packages. Although the models are accurate, the geometries are often simplified and not dynamics and thus cannot predict realistic flow patterns and their transitions. These models do not model two-phase flow, only the electrical permittivity of the two-phases are required to model the EHD force.

Many models neglect the electrostriction term of the EHD force because they state that the system is incompressible [40]–[43]. This force was seen as a compressible effect and is thought to be negligible in most cases, but it is significant across the interface where there is a large permittivity difference and should not be neglected. The inclusion of the electrostrictive force does not increase the complexity of the model, so it can be included in models that it is not significant in without increasing the computational load. In the case it becomes significant in a transient phenomenon, the model will benefit from its inclusion.

Some work has been done in three dimensions and with heat transfer [44], [45]. Without robust validated fluid flow modelling, the added complexities, and multiple sources of error with each added physics module, make it hard to address where and if there are flaws in the system. These models are likely attempting too much without a two-phase flow modelling approach that is trusted.

1.5 Research Objective

In this thesis, a study of different two-phase flow numerical methods will be analyzed and compared when EHD forces are applied. The models developed use fluid flow, two-phase field, and electrostatic modules found in COMSOL Multiphysics with EHD coupling. This work builds on models by Nangle-Smith et al. 2013 [6] and focuses on improving the understanding of the limitations of the current two-phase models with EHD forces implemented.

Experiments conducted by Di Marco et al., 2012 [5], and Sadek et al., 2012 [46], will be simulated using an interface tracking method and two volume of fluid methods and will be compared to experimental data collected. The models will be validated and EHD forces and flow structures will be analyzed to see what limitations each model has in simulating these simplified geometry EHD experiments. The models consist of a bubble deformation case which is a steady

state model that focuses on the balance of EHD, surface tension, and buoyancy forces, and a liquid extraction model that is time dependent and focuses on advection of the fluid caused by EHD.

Chapter 2 - Electrohydrodynamic Numerical Modelling

2.1 Introduction to EHD

EHD convective boiling is a multi-physics problem which couples two phase fluid dynamics, heat transfer, and electrostatics equations. Mass conservation and momentum conservation in each fluid is coupled with a conservation of energy equation and conservation of charge equation are required to define the model. A dielectric fluid like R-134a is subjected to a high voltage and negligible current is seen through the fluid, therefore generating an electric field. If the fluid is polarizable, a magnetic field will have an effect on the fluid but in cases involving dielectric fluids the magnetic forces can be neglected [18]. Different modelling strategies can be used to model the two fluids and their coupling which are moving mesh, phase field volume of fluid, and level set volume of fluid methods. Each method has its own advantages but detailed analysis and comparison on the implementation of the EHD body force has not been completed.

2.2 Electric Body Force Equation

The effect of the electric field in the fluid causes a source in the momentum and energy conservation equations. In the momentum equation a body force is added to the fluid and in the energy equation there is a Joule heating component.

The following assumptions are made about the model:

1. The Joule heating component is typically negligible as the electrical conductivity of the dielectric fluid is very low (i.e. $O(10^{-10} \text{ W}^{-1}\text{m}^{-1})$)[10], [47].
2. The flow is subsonic, and the viscosity is low so we can neglect viscous dissipation from the energy equation.

3. The fluid is Newtonian and is continuous.
4. Magnetic affects can be neglected [7].

The derivation of the EHD body force in an electrostatic field in the presence of dielectrics can be found in “Classical Electricity and Magnetism Second Edition” by Wolfgang K. H. Panofsky and Melba Philips in Chapter 6.6 [17]. The final equation is shown below with the Coulomb force neglected:

$$F_{EHD} = -\frac{1}{2}E^2\nabla\varepsilon + \frac{1}{2}\nabla\rho E^2 \left(\frac{\partial\varepsilon}{\partial\rho}\right)\bigg|_T \quad \text{Equation 2.1}$$

The terms of the EHD force are defined in Chapter 1. When modelling the EHD body force typically one or more components can be neglected. In two-phase systems, the polarization forces are dominant due to the electrical permittivity difference between the phases. Thus, the Coulomb force is neglected. Some two-phase cases may still have a charge injection, so careful consideration of this assumption must be taken before its implementation [24]. In cases with very low charge input is a good indication that the Coulomb force is negligible. In single phase cases with negligible temperature gradients, only the Coulomb force is present as all the fluid has a constant permittivity.

The electrostriction term is often simplified using the Clausius-Mossotti Law [48], shown in Equation 2.2, to make it dependent on only the relative permittivity of the fluid and the electric field.

$$\frac{\varepsilon_r - 1}{\varepsilon_r + 2} = \frac{N_e \alpha_e}{3\varepsilon_0} \quad \text{Equation 2.2}$$

Where: ϵ_r = Relative electrical permittivity
 N_e = Number density of molecules per cubic meter
 α_e = Molecular polarizability
 ϵ_0 = Electrical permittivity of free space

2.3 Fundamental Conservation Equations

Mass and Momentum Conservation

The following conservation equations are used to model the fluid flow and heat transfer in the system. They represent the conservation of mass, momentum, and energy. As the flow has low Reynolds numbers, subsonic with Mach number below $Ma = 0.2$, incompressible assumptions are applied to the equations. The fluid is also assumed to be Newtonian and act as a continuum.

$$\frac{\partial \rho}{\partial t} + \rho \nabla \cdot (\mathbf{u}) = 0 \quad \text{Equation 2.3}$$

$$\rho \frac{\partial \mathbf{u}}{\partial t} + \rho (\mathbf{u} \cdot \Delta) \mathbf{u} = -\nabla p + \mu \nabla^2 \mathbf{u} + F_g + F_{st} + F_{ext} \quad \text{Equation 2.4}$$

$$\rho c_p \frac{\partial T}{\partial t} + \rho c_p (\mathbf{u} \cdot \nabla T) = k \nabla^2 T + q''' \quad \text{Equation 2.5}$$

In Equation 2.4, the body forces denoted by F_g , F_{st} , and F_{ext} are body forces that represent gravity, surface tension, and other external forces respectively. The EHD force is added as an external force as part of F_{ext} .

The presence of an electrical current can cause a heat generation through the fluid in the conservation of energy equation. This heat generation would be in the q''' component but as the current through the fluid remains low due to being non-conductive, this heat generation is often negligible.

Electric Field Distribution

The electric field strength is found using Gauss' Law which is shown below:

$$\nabla \cdot \vec{D} \stackrel{\text{def}}{=} \nabla \cdot (\epsilon \vec{E}) = \rho_c \quad \text{Equation 2.6}$$

Where: \vec{D} = Electric displacement field
 ρ_c = volumetric charge density

When there are no free charges in the system the volumetric charge density is equal to zero. The electric field is also related to the voltage potential via the following equation:

$$\vec{E} \stackrel{\text{def}}{=} -\nabla V \quad \text{Equation 2.7}$$

Using Equations 2.6 and 2.7, the voltage potential and electric field can be calculated, and the electric field strength can be used to find the EHD body force resulting from such field.

2.4 Multi-Phase Flow Modelling

An important detail in modelling EHD flow is modelling the two phases and the interaction between them. COMSOL is a multi-physics software that allows to model different types of problems and has the flexibility to couple the different physics modules as the user may need. In the EHD flow case, a coupling between a multiphase flow model and an electrostatic model is required. The coupling that takes place is through the EHD force shown above and is significant near the interface between the two phases. Due to the force being larger at the interface, the multiphase model must have good interface tracking and the interface must be very stable as the additional force can act to destabilize the multiphase numerics. There are two

commonly used types of phase tracking methods are used in the COMSOL software which are interface tracking models and volume of fluid modelling [6], [42].

Interface tracking modelling calculates how the interface deforms and then treats the phases as separate fluids within each domain with the interface as a boundary condition for both fluids. This model allows for transfer of properties between the phases but is unable to handle diffusion of the phases. The interface model that is used is called the Moving Mesh model which stretches the mesh to deform the domains and move the interface. The Moving Mesh model also is not capable of undergoing topological changes to the fluid domains. A topological change is any deformation of a domain that adds or removes new shapes. This can be when a bubble that attaches to a wall necks and the interfaces touch or when an interface touches any boundary.

Volume of fluid methods use a phase parameter to define the mass or volume fraction of one of the fluids. This phase parameter is subjected to advection to move around the fluid domain. These models are capable of modelling diffusion of the phase parameter which in the case of EHD allows the interface thickness to grow due to the force. The volume of fluid methods are more robust as they allow for topological changes but diffusion can hinder the accuracy. Two volume of fluids models are used which are the Level Set and the Phase Field model. The Level Set model neglects diffusion of the phases but uses the diffusive term to keep the interface as small as possible whereas the Phase Field model has a diffusion term and attempts to model the physics of diffusion.

Moving Mesh Model

The Moving Mesh model couples a single-phase flow model and a moving mesh interface to evaluate the flow field within each fluid domain and determine the interface between

the fluids using deforming mesh domains. This implementation of the interface ensures an infinitesimal boundary between the two fluids which keeps the electrostatic analysis and the EHD forces accurate. As surface tension force is also dependent on the gradient of the interface, this model can also better predict the surface tension force.

The deformation of the mesh is calculated from the velocity of the fluid element adjacent to the interface that is normal to the mesh. The normal component of the velocity is calculated, and that velocity is given to the node of the mesh which moves with time. A mass flux can also be prescribed to allow for mass to move across the interface but can be neglected in adiabatic models. Equation 2.8 shows the formula used to give the interfacial node a velocity for its deformation and Figure 2.1 shows a diagram of the normal vector, \mathbf{n}_i .

$$\mathbf{u}_{mesh} = \left(\mathbf{u}_1 \cdot \mathbf{n}_i - \frac{M_f}{\rho_1} \right) \mathbf{n}_i \quad \text{Equation 2.8}$$

Where: \mathbf{u}_{mesh} = Velocity vector of interfacial mesh node
 \mathbf{u}_1 = Velocity vector of fluid 1 element adjacent to the interface
 \mathbf{n}_i = Normal vector to the interface
 M_f = Mass flux
 ρ_1 = Density of fluid 1

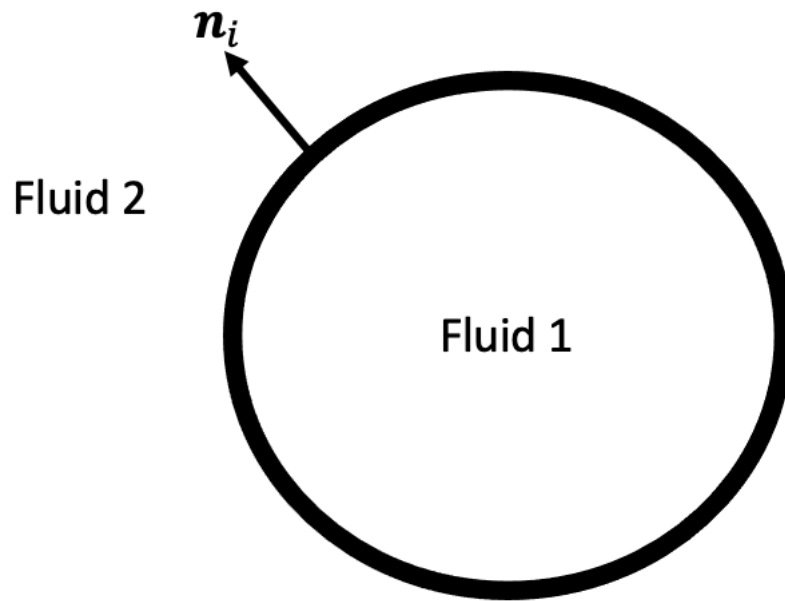


Figure 2.1: Diagram of normal vector on the interface between 2 fluids.

After the interface is deformed, the rest of the mesh is stretched to the new geometry. The drawback of this model is with large deformations the mesh can stretch in a way that greatly increases the skewness, expansion ratio, and aspect ratio. This can be mitigated by setting remeshing conditions such that when a metric exceeds a tolerance that is defined by the user the deformed geometry is remeshed with the initial meshing conditions. Remeshing can be computationally expensive and can cause numerical instability when the model attempts to reinitialize the variables being solved. Remeshing also makes mesh independence testing difficult as the new mesh can reduce in size making refinement studies similar to the initial study. Finer meshes also remesh sooner as the smaller control volumes deform more in areas where greater force is concentrated.

Another drawback of the moving mesh model is that it cannot withstand topological change. If the interface approaches a boundary or another interface the model will fail. In the event of the interface approaching a boundary, two nodes can collapse into a single point making

the numerics unsolvable or the interface node can travel past the domain creating a negative control volume which also fails the model physically and numerically. This drawback cannot be prevented at this time and therefore this model is case dependent and only works in cases that are appropriate or during the time before geometrical change in unsuitable models. Figure 2.2 shows a bubble approaching separation, where necking occurs. When the interfacial nodes touch the model will stop and issue an error.

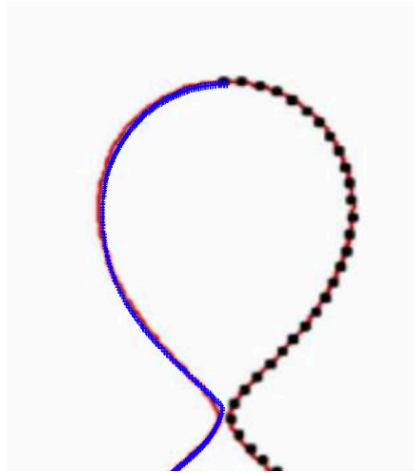


Figure 2.2: Bubble during separation that depicts a topological change in the interface.

Level Set Model

The Level Set method uses a level set parameter, Φ , to define different fluids and their properties. The goal of this method is to use advection to move the level set line where $\Phi = 0.5$ and then reinitialize the boundary between the two fluids to maintain the boundary thickness [49].

$$\frac{\partial \phi}{\partial t} + \mathbf{u} \cdot \nabla \phi = \gamma \nabla \cdot \left(\varepsilon \nabla \phi - \phi(1 - \phi) \frac{\nabla \phi}{|\nabla \phi|} \right) \quad \text{Equation 2.9}$$

Where: ϕ = level set parameter
 γ = reinitialization parameter
 ε = interface thickness controlling parameter

The left side of the equation has the change in level set parameter and the advection term and on the right side is the reinitialization function to maintain the thickness of the boundary. Level Set models prior to 1900 did not consider the right side of the equation and therefore do not have any way to shrink the boundary if it starts to diffuse. This would create problems with EHD forces applied but some previous works have continued to use this older method [50]. The reinitialization parameter controls the strength of the reinitialization function in relation to the advection and the interface thickness controlling parameter is the thickness the reinitialization attempts to achieve on the new formed boundary [51]. The default values are set to 1 for the reinitialization parameter and $h_{\max}/2$ for the interface thickness controlling parameter where h_{\max} is the maximum element size in the entire component. The properties of the fluids are given by a weighted fraction between the two fluids using the level set parameter as shown below.

$$\rho = \rho_1 + (\rho_2 - \rho_1)\phi \quad \text{Equation 2.10}$$

$$\mu = \mu_1 + (\mu_2 - \mu_1)\phi \quad \text{Equation 2.11}$$

Due to having a parameter that controls the volume fraction at the boundary is discrete and therefore the thickness of the boundary is important. The dielectrophoretic forces are dependent on the gradient between the two fluids because the electric field is calculated using the volume fraction of the fluids to determine the electrical permittivity of each control volume. Therefore, the size of the interface must be refined so that the EHD forces are accurate. The size

of the boundary is controlled mainly by the mesh sizing so small mesh sizing near the initial boundaries as well as in locations the interface will go are important.

Diffusion is not captured in this model which is beneficial in the case of EHD where the force applied to the free surface can tend to broaden the gradient. As the force acts on the gradient between the two fluids, this force acts as a body force instead of a surface pressure like in the moving mesh model. This body force is either localized in a single node when the gradient is steep or can be distributed over a few nodes if the boundary spreads. The boundary smearing can be worsened by the body force which causes a degradation of the boundary. Then with a larger boundary gradient the free surface forces which include surface tension and the EHD force also degrade. This can cause detachment of the bubble if surface tension decreases too much. In the Level Set method, the reinitialization attempts to counteract the expanding boundary to reduce the interface thickness to the desired width.

Phase Field Model

The Phase Field model tracks the interface between the two fluids using diffusion equations. This model uses a phase parameter which specifies the volume fraction of the node. This model has been used previously as it is simple to implement and captures the most physics of the volume of fluid methods [52]. The equations to model the movement of this parameter are as follows:

$$\frac{\partial \phi}{\partial t} + \mathbf{u} \cdot \nabla \phi = \nabla \cdot \frac{\gamma \lambda}{\varepsilon^2} \nabla \Psi \quad \text{Equation 2.12}$$

$$\Psi = -\nabla \cdot \varepsilon^2 \nabla \phi + (\phi^2 - 1)\phi + \left(\frac{\varepsilon^2}{\lambda} \right) \frac{\partial f_{ext}}{\partial \phi} \quad \text{Equation 2.13}$$

$$\sigma = \frac{2\sqrt{2} \lambda}{3 \varepsilon} \quad \text{Equation 2.14}$$

$$\gamma = \chi \varepsilon^2 \quad \text{Equation 2.15}$$

Where: ϕ = phase field variable
 λ = mixing energy density
 γ = mobility parameter
 ε = capillary width
 σ = surface tension coefficient
 χ = mobility tuning parameter

Equations 2.12 and 2.13 are the transport equations for the phase parameter. These equations come from the Cahn-Hilliard equation for diffusion. The left side of the equation shows the advection of the phase field, and the right side is the diffusion. This method attempts to minimize the free energy in the system which is made up of mixing, bulk distortion, and anchoring energy [51].

The mixing energy density and capillary width are related to the surface tension coefficient through Equation 2.14 and mixing energy density is changed via the mobility parameter which is shown in Equation 2.15. The mobility tuning parameter may be changed to vary the weighting between the advection and diffusion in Equation 2.12.

With the coupling of EHD forces to the phase field, the boundary thickness is important similar to the Level Set method. A large gradient will impact the electric fields around the boundary and reduce the electric field strength which will reduce the electrohydrodynamic force. It is essential to try to refine the boundary and ensure it does not diffuse. The mobility tuning parameter plays a role in trying to maintain a fine boundary, but care must be taken to ensure the physics is captured properly. Setting the parameter too low will make the boundary too large and

make the EHD forces not accurate and raising it too high will dampen the advection and restrict movement of the fluid.

This model captures more physics than the Level Set method as it has diffusion equations but with the implementation of EHD force there are many forces acting on the boundary. The forces on the boundary now include advection, diffusion, surface tension, and EHD force. Having all these forces on the boundary act to destabilize the boundary and can lead to excessive diffusion and large gradients. As the force acting to keep the boundary fine is mainly surface tension which diminishes as the gradient widens, if the boundary begins to widen there is no force to shrink the boundary and the model will fail or display unphysical results. The Phase Field model is only applicable in some EHD cases where it remains stable as diffusion is usually not significant and the fluid mixing is limited.

Chapter 3 - Air Bubble in FC-72 Simulation

3.1 Introduction

When an electric field is applied to an air bubble in a dielectric fluid, the bubble's shape can be deformed. The level of deformation is related to the geometry of the electrodes and the strength of the electric field. This affect can help enhance boiling heat transfer by removing the bubble prematurely to allow for better surface rewetting reducing the amount of air, acting as a insulative layer, near the heat transfer surface. This affect can also be reversed to push the air bubble to the wall making a larger of air layer that insulates the heat transfer surface and reduces heat transfer. Being able to vary the voltage and change the polarity of the electrode, the rate of heat transfer from the surface should be able to be controlled to an extent. Various studies have looked at an electric field's influence on the shape of bubbles and heat transfer in boiling scenarios as boiling is a common two-phase case [5], [48], [53], [54].

An experiment was done by Di Marco et al., 2013 [5], to show the deformation of a single bubble exposed to an electric field. In this experiment, they inject air into FC-72 from an orifice of a grounded plate at the bottom of the container and capture the shape of the bubble with a high-resolution camera. Once a specified volume is reached (0.0737 mm^3 and 0.384 mm^3), a voltage of 20kV DC is applied to an axis symmetric washer-shaped electrode to create the electric field above the bubble.

A volume of fluid method was used to model this experiment by the investigator, but only an earlier interface tracking model has been attempted [6]. Having a simple 2D axis symmetric geometry makes this case ideal for testing the different models within COMSOL. The Moving Mesh, Level Set, and Phase Field models will be verified and compared using published

experimental data of a two-phase bubble in FC-72 which is deformed with an electric field. The models will be 2D axis-symmetric, adiabatic and use the properties of FC-72 and air.

3.2 Numerical Methodology

Three numerical methods for modelling bubble distortion will be used and compared including: a fully coupled two-phase fluid Moving Mesh approach, a segregated Phase Field volume of fluid approach, and a segregated Level Set volume of fluid approach. The fully coupled method is used to solve all the variables at the same time whereas the segregated solver solves the electrostatics, flow field, and two-phase parameter sequentially. The fully coupled solver is more stable and can solve smaller systems more quickly but slows down significantly when using a high number of parameters with a dense mesh. The volume of fluids approach uses extra parameters to solve the phase field than the Moving Mesh model, so the segregated solver was utilized to reduce the computational cost. The models used was 2D axis symmetric, adiabatic and use FC-72 as the liquid with an air bubble submersed. It is assumed that the properties of the materials remain constant and are shown in Table 3.1 and that there are no free charges in the system and therefore the Coulomb component of the EHD force may be neglected.

Table 3.1: *Fluid Properties of liquid FC-72 and air.*

Material Property	Value
Surface Tension	0.0107 N/m
Vapor Permittivity	1
Liquid Permittivity	1.74
Liquid Density	1672 kg/m ³
Vapor Density	1.19 kg/m ³
Liquid Viscosity	0.000614 Pa*s
Vapor Viscosity	0.0000182 Pa*s

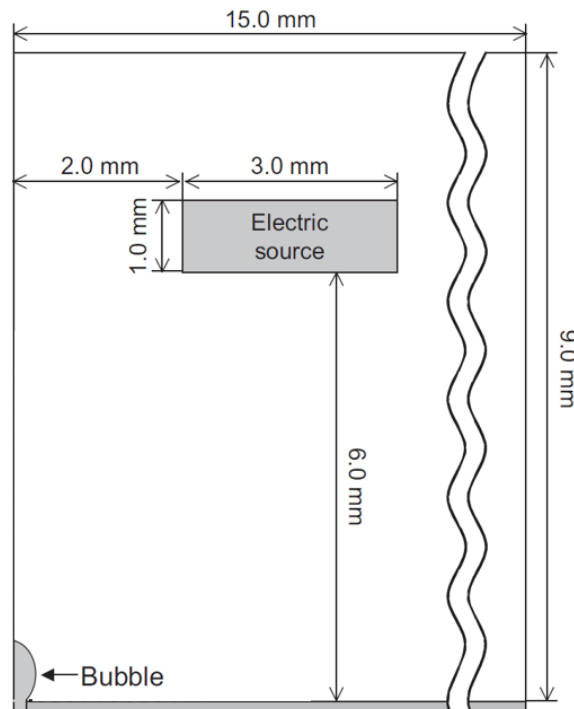


Figure 3.1: 2D axis symmetrical geometry used for EHD two phase flow model. Modified from Di Marco et. al.

The bubble was injected from an orifice in the bottom of a grounded plate and a washer shaped electrode with a voltage potential of 20 kV was suspended in the FC-72. The voltage potential was increased linearly from 0 to 20 kV over 0.01 seconds to ensure that the bubble did not detach from the wall from the momentum of the initial deformation. The geometry in Figure 3-1 was used to match Di Marco et. al., 2013 [5], experimental set up and the initial bubble shape was taken as the steady state bubble without EHD obtained by a Moving Mesh steady state analysis and verified by Di Marco et. al., 2013, experiment without EHD with a volume of 0.0737mm^3 . The models include forces from surface tension, gravity, and the dielectrophoretic and electrostrictive components of the EHD force. Due to the orifice that the bubble is attached to, the contact angle was varied until an angle that matched the experiment was found. This was required because the plate was modelled without an orifice and therefore the contact angle that

would be located on the edge of the orifice could reflect any angle before detachment. There has shown to be effects on the contact angle due to EHD but such affects were not modelled in this study [55]. Mesh independence and time step independence tests were completed and can be found in Appendix A.

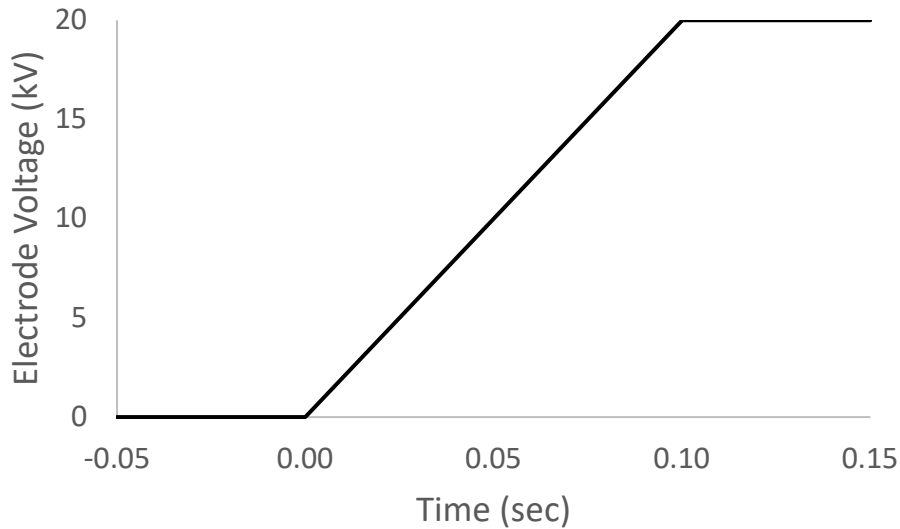


Figure 3.2: Graph of scaling parameter for the electric potential.

Moving Mesh Method

The Moving Mesh method uses conservation of mass and momentum in two domains, one being the liquid and the other the vapour. The model treats both as a single phase but then allows for the boundary between the two domains to move depending on interfacial forces. These forces include gravity, hydrodynamic pressure, surface tension, and EHD force in this case. The movement of the mesh is done via mesh deformation. The EHD force is implemented as a surface pressure along the liquid-gas interface boundary with an r and z component. This surface pressure is taken from the Maxwell stress tensor with an added Electrostriction term, shown in Equation 3.1.

$$T_{ehd} = (\varepsilon_0 \varepsilon_r \bar{E}) E^T - \frac{1}{2} \varepsilon_0 E^2 \left(\varepsilon_r - \rho \left(\frac{\partial \varepsilon_r}{\partial \rho} \right)_T \right) I \quad \text{Equation 3.1}$$

Equation 3.1 is transformed using the Clausius Mossotti Law, Equation 3.2, to make the electrostriction term a function of the electric field and the relative permittivity only. This creates the final form of the stress tensor applied to the interface as shown in Equation 3.3.

$$\rho \frac{\partial \varepsilon}{\partial \rho} = \frac{\varepsilon_0 (\varepsilon_r - 1) (\varepsilon_r + 2)}{3} \quad \text{Equation 3.2}$$

$$T_{ehd} = (\varepsilon_0 \varepsilon_r \bar{E}) E^T - \frac{1}{2} \varepsilon_0 E^2 \left(\varepsilon_r - \frac{\varepsilon_0 (\varepsilon_r - 1) (\varepsilon_r + 2)}{3} \right) I \quad \text{Equation 3.3}$$

Other parameters for the Moving Mesh model are shown in Table 3.2. The contact angle chosen was found by a study with a parameter sweep of contact angles. The contact angle is able to change due to being attached to an orifice. The orifice was not modelled in this study, so the corresponding contact angle was found via the parameter sweep. This study used an implicit time dependent solver, so no time steps were specified but tolerances are instead used to make an adaptive time step.

Table 3.2: *Moving Mesh model boundary and solver conditions.*

Laminar Flow	Contact angle with wetted walls	42°
	Pressure point-constraint (top right corner)	0 Pa
	Surface Force	Tx, Ty
Electrostatics	Bottom plate voltage	0 V
	Electrode voltage	Ramp from 0 to 20kV
	Axial Symmetry	On Centerline
Mesh Deformation	Symmetry/Roller	On Centerline
	Mesh Smoothing Type	Yeoh
	Stiffening Factor	10
Time Dependent Solver	Time Stepping Method	BDF free
	Relative Tolerance	0.005
	Absolute Tolerance	0.05
	Time-Dependent Solver Type	Direct Fully Coupled
	Direct Solver	MUMPS

Phase Field and Level Set Method

The models incorporate the same forces as the Moving Mesh model which include buoyancy, surface tension, hydrodynamic pressure, and EHD force. The EHD force is modelled as a body force on the fluid domain. The stress form of the EHD body force equation from Equation 3.3 is transformed to a body force by taking the divergence of the stress tensor, shown in Equation 3.4.

$$F_{EHD} = \nabla \cdot T_{EHD} \quad \text{Equation 3.4}$$

The volume of fluid models use a phase parameter subjected to advection and diffusion that represents the volume fraction of each fluid. Surface tension is modelled based on the

gradient of the phase parameter in the interface, so keeping a sharp interface is important for the model. This means that the volume of fluid methods requires a fine mesh to resolve the interface sharply.

Due to the inclusion of another parameter field and the finer mesh requirement, the volume of fluids methods are 10 to 50 times more computationally expensive than the Moving Mesh model. Due to the increased complexity, a segregated solver was used to reduce the computational load and make convergence faster and more stable.

The segregated solver process works in the following order:

- 1) Solves for the phase field with direct solver
- 2) Attributes an electrical permittivity to the control volumes equal to their volume fraction
- 3) Solves for the electric field with direct solver
- 4) Calculates body forces with the electric field and relative permittivity of the fluid
- 5) Solves for velocity and pressure using a multi-grid solving method
- 6) Velocity is given to advection term of phase field solver and order starts again

Table 3.3: Phase Field and Level Set model boundary and solver conditions. All properties are shared except the last rows labelled with the specific model they are used in.

Two-Phase Flow	Contact angle with wetted walls	42°
	Interface thickness	Half of Mesh Spacing
	Pressure point-constraint (top right corner)	0 Pa
	Volumetric Force	F _x , F _y
Electrostatics	Bottom plate voltage	0 V
	Electrode voltage	Ramp from 0 to 20kV
	Axial Symmetry	On Centerline
Time Dependent Solver	Method	BDF free
	Relative Tolerance	0.005
	Absolute Tolerance	0.01
	Time-Dependent Solver Type	Segregated
	Direct Solver	PARDISO
	AMG Solver	GMRES
Phase Field	Mobility Tuning Parameter	4
Level Set	Reinitialization Parameter	1

Table 3.3 shows the parameters used in the models. Most of the parameters are shared in the volume of fluids models but each model uses an individual weighting parameter to balance the phase advection and diffusion discussed in Chapter 2. Numerical models were conducted by increasing the value of these parameters to stabilize the interface until the bubble showed a change in its dynamics signaling advection suppression.

3.3 Results and Comparison

Ramp Analysis

In preliminary testing, many numerical instabilities arose which caused bubble detachment, unsuccessful convergences, and large bubble oscillations. Bubble oscillations were seen in other time dependent cases so this affect is likely due to the large change in forces when a step voltage is applied [56]. These issues caused more computational time for a steady state solution or model failure. One solution to prevent these issues is to ramp the voltage of the electrode so that the force balance between the buoyancy, surface tension, and EHD force is not as unbalanced and therefore the bubble has less acceleration.

The Moving Mesh model had better convergence than the two volume of fluids models as it never ran into bubble detachment or model failure. The Moving Mesh model also could use a coarser mesh then the volume of fluid models and had faster modelling times. Therefore, it is the best model to test different ramp cases. The step voltage change was compared to a 0.01 and 0.1 second ramp voltage and the height of the maximum point on the bubble was recorded to compare the oscillations the bubble underwent. The amount of overshoot shows the instability of the model as the higher the bubble reaches the more likely it is to detach from the momentum. The time to reach steady state affects the computational time as it takes longer to reach steady state and more movement from the bubble increases the computation effort to reach a steady state in each time step.

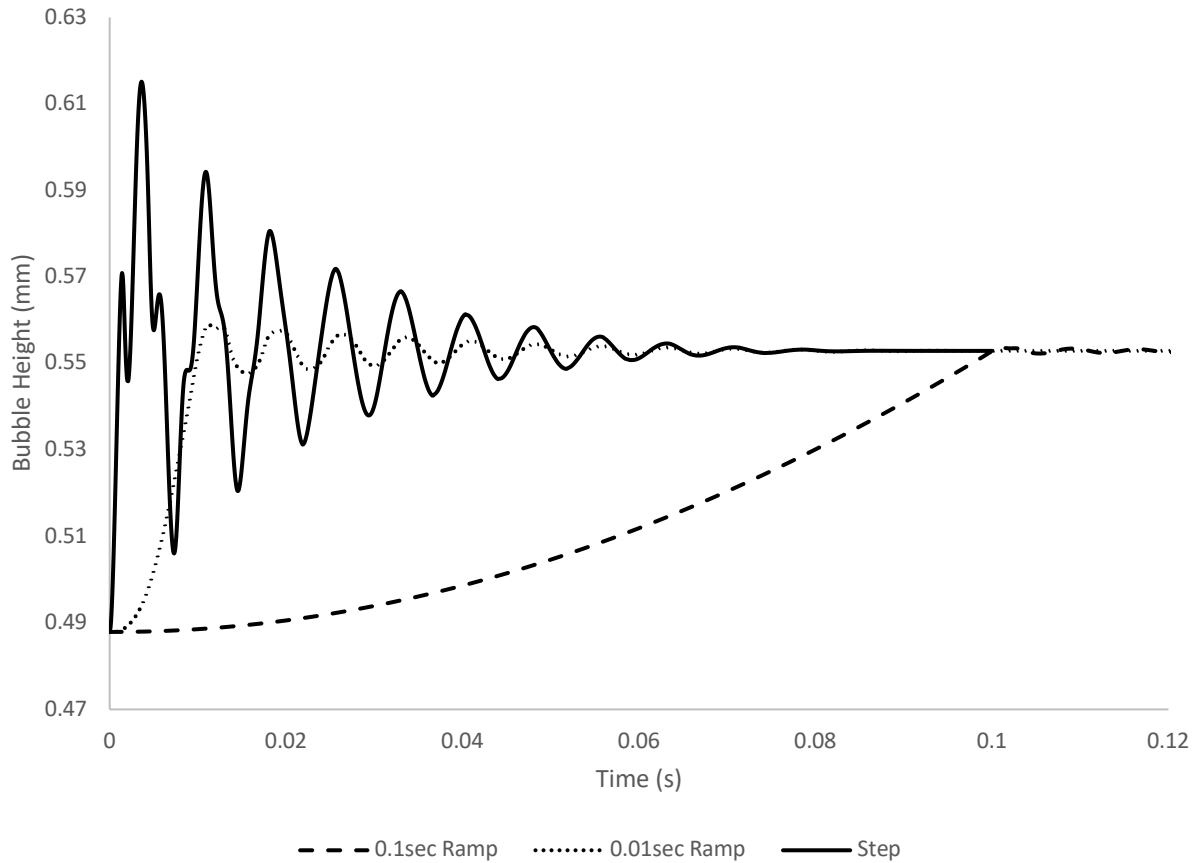


Figure 3.3: Height of the highest point on the bubble vs time for a step change in voltage and 0.01 and 0.1 second ramp voltages on the electrode.

$$\text{Percent Overshoot} = \frac{\text{Max Height} - \text{Steady State Height}}{\text{Steady State Height}} * 100\%$$

Table 3.4: Comparison of percent overshoot and 2% settling time values for step, 0.01s, and 0.1s ramp voltage on the electrode.

Model	Percent Overshoot	2% Settling time
Step	95.8%	0.064s
0.01s Ramp	8.8%	0.053s
0.1s Ramp	1.0%	0.100s

Figure 3.3 shows the results of the ramp study and Table 3.4 shows a list of the data extracted from Figure 3.3 including percent overshoot and 2% settling time values. The step case had a large percent overshoot at 95.8% compared to the ramp cases which were 8.8% and 1.0%

for the 0.01s and 0.1s ramp respectively. This shows that the addition of a ramp stabilizes the model and removes the momentum causing large overshoots. Comparing the ramp cases, the steep 0.01s ramp had a higher overshoot but took less time to settle to below 2% error. The 0.01s ramp took 0.43s to settle after the voltage remained constant whereas the 0.1s ramp had below 2% error when it finished the ramp, so no additional time was necessary to be within 2% error.

The best case for convergence and reduced computation effort is the 0.1s ramp because the small overshoot is the most stable case, and the slow increase of height means that each time step will be able to converge faster as there is less movement than the oscillations in the 0.01s ramp. The 0.1s ramp will need to be simulated for more time because it takes more time to achieve steady state but because of there being less oscillations the timesteps will be able to be larger as the speed of the bubble movement will be less so they will take a similar amount of time. For the rest of the simulations, a 0.1s ramp will be used for all the models. The step model will be employed when looking at values that affect the initial shape of the bubble like the initial stress on the bubble. This will ensure that all the bubbles are the exact same shape when looking at this data.

Initial Interfacial Forces

To compare the different models, the initial interfacial stress is used. The initial stress is used so that there are no variations due to the time dependent numerics and so that the force is taken on the exact same line between all the models. To have interfacial forces, the ramp study results could not be used as the initial forces are zero, so the electrode was set to 20kV, and the electrostatics and two-phase field equations were solved for the first timestep. The electric field and phase field are required to calculate the body forces caused by EHD on the bubble, but the

fluid flow conservation equations are only needed after the force is applied to show the resulting motion. The pressure in the r-direction and z-direction can be found along the initial interface line and are shown in Figure 3.4.

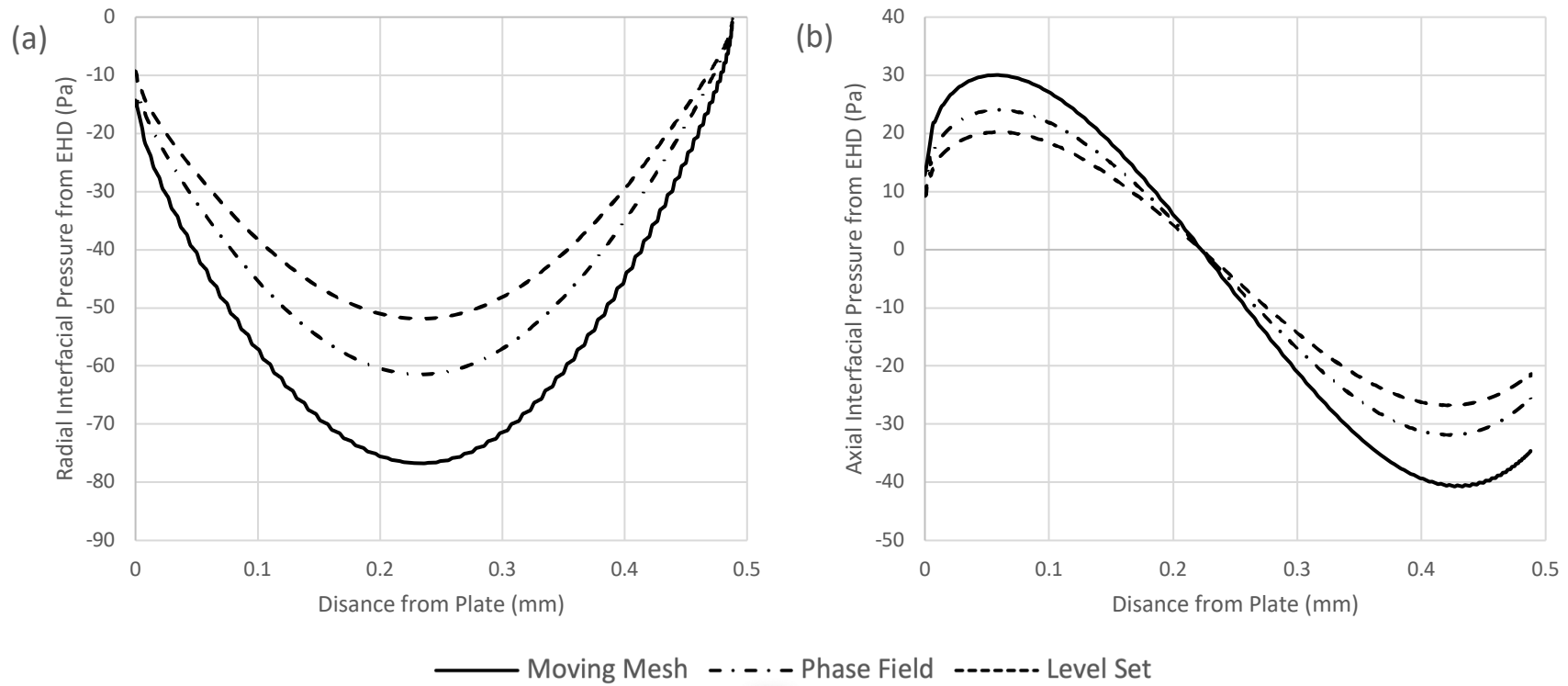


Figure 3.4: Surface force on the initial bubble shape with an electrode voltage of 20kV for the moving mesh, phase field, and level set models. (a) Interfacial pressure in r-direction (b) Interfacial pressure in z-direction.

From Figure 3.4 it is shown that the force of the Moving Mesh model is larger than the two volume of fluid models. The Moving Mesh model's force is about 1.5 times larger than the Level Set model and 1.3 times larger than the Phase Field model as seen in Table 3.5. This is due to the interface tracking method having a sharp interface and the volume of fluids methods having a discrete interface that is resolved over a few nodes.

The difference between the forces of the level set and phase field model is due to how many nodes the interface is resolved in. Figure 3.5 (a) to (c) show the volume fraction of air across the interface. The Moving Mesh model has a sharp transition from air to liquid FC-72 as the phase parameter is not needed but Level Set and Phase Field models have a gradient.

Table 3.5: Maximum and minimum surface pressure from initial EHD force on the bubble for each model.

Model	$T_{r,min}$ (Pa)	$T_{z,max}$ (Pa)	$T_{z,max}$ (Pa)
Moving Mesh	-76.7	30.0	-40.7
Phase Field	-61.4	24.1	-26.8
Level Set	-51.9	20.2	-26.8

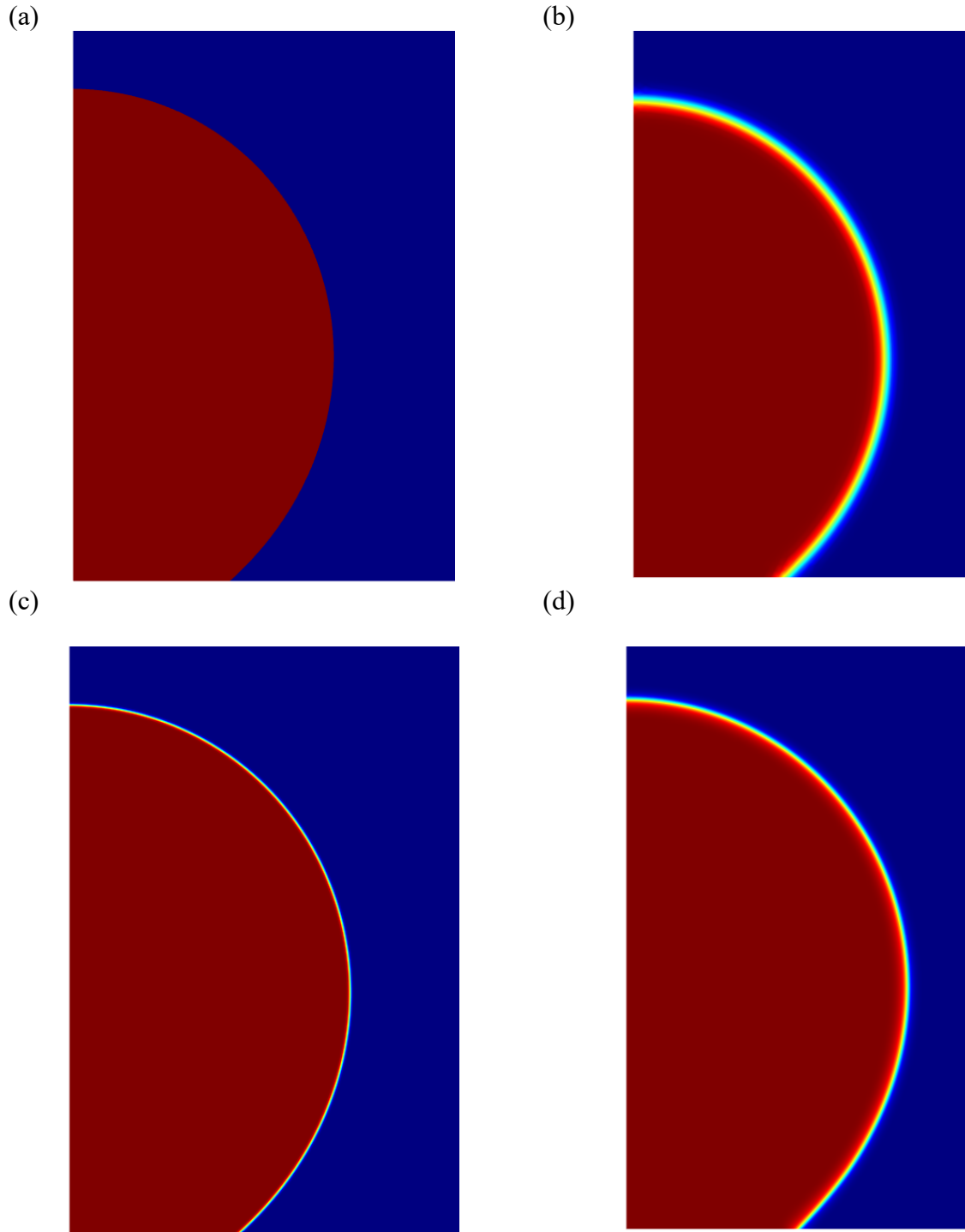


Figure 3.5: Volume of fluid for the level set and phase field models. Red represents the air and blue represents FC-72. (a) Moving Mesh Model (b) Level Set Model (c) Phase Field Model (d) Phase Field Model after 0.0002s.

To look at the interface, a cut line is made as shown in Figure 3.6. The cut line is 0.04mm long crossing the bubble 0.225mm from the bottom plate, at the largest radius. The distance starts at the green vector and distance increases in the direction of the red vector. The volume of fluid which is equivalent to the phase parameter is graphed on the cut line in Figure 3.7. The edge of the control volumes are seen where there is a change in slope of the volume fraction. In the Phase Field model graph, Figure 3.7 (a), the entire interface is resolved over 3 control volumes for the two finer meshes to reach 99% of the fluid whereas the Level Set model takes 5 control volumes, seen in Figure 3.7 (b). Also, the middle control volume of the Phase Field model has a steeper gradient than the same control volume in the Level Set model.

Due to the Level Set model using more nodes to resolve the boundary, the force is lower than that of the Phase Field model. Without the capability to shrink the interface more, the largest gradient located on the center node is shallower in the Level Set model which in turn reduces the EHD force dependent on that gradient.

This effect is independent of the mesh size due to the gradient across the interface not completely changing phase. The Phase Field model goes from a volume fraction of 0.1 to 0.9 over the middle interface whereas the Level Set model going from 0.15 to 0.85 which leads to the reduced force. When the mesh size is reduced, the interface is smaller but due to the numerics in the models not being able to capture the complete change of phase, there will be a shallower gradient. The body force created at the interface will be increased but it will also act on a smaller volume and create the same interfacial pressure. This effect shows that the volume of fluid methods will always underpredict the interfacial pressure unless the interface can be captured within one node like the Moving Mesh model.

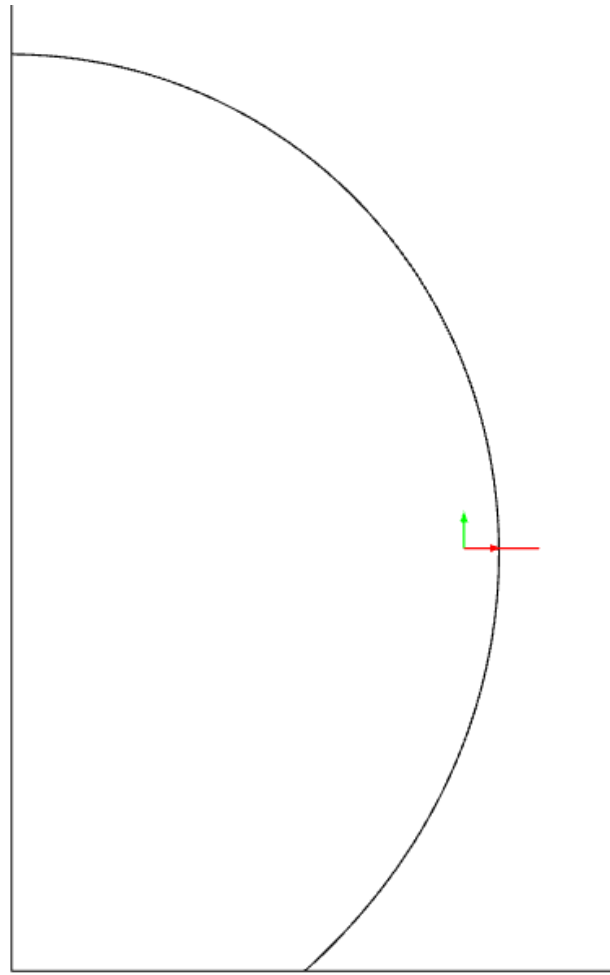
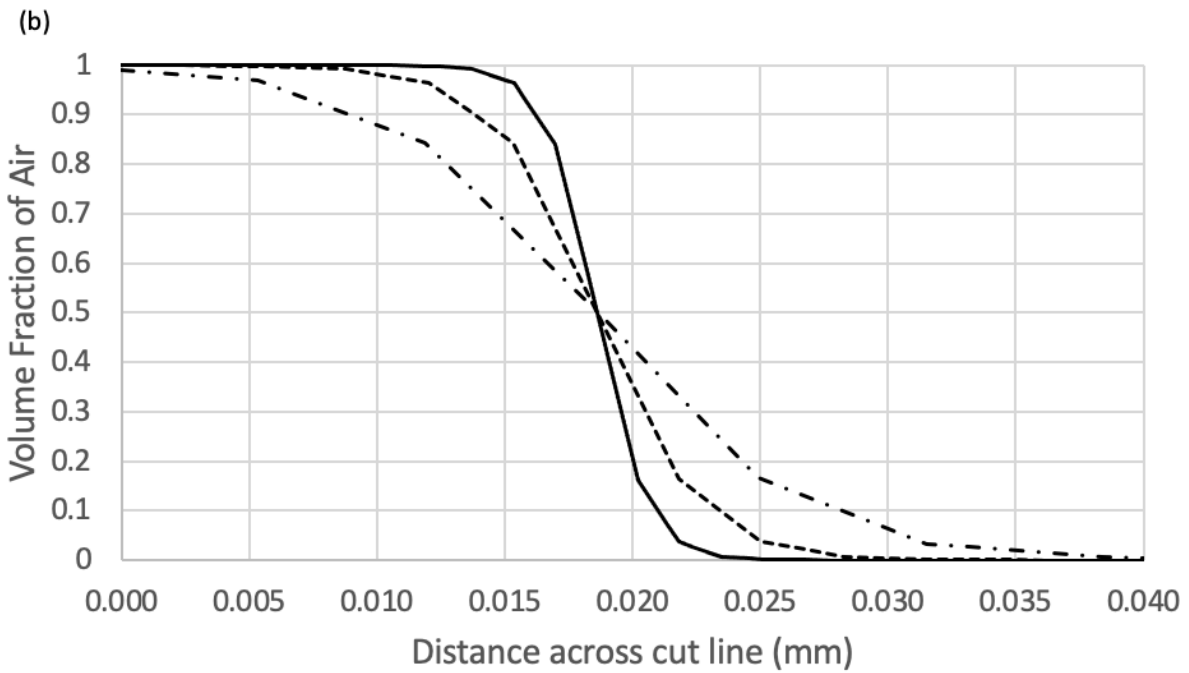
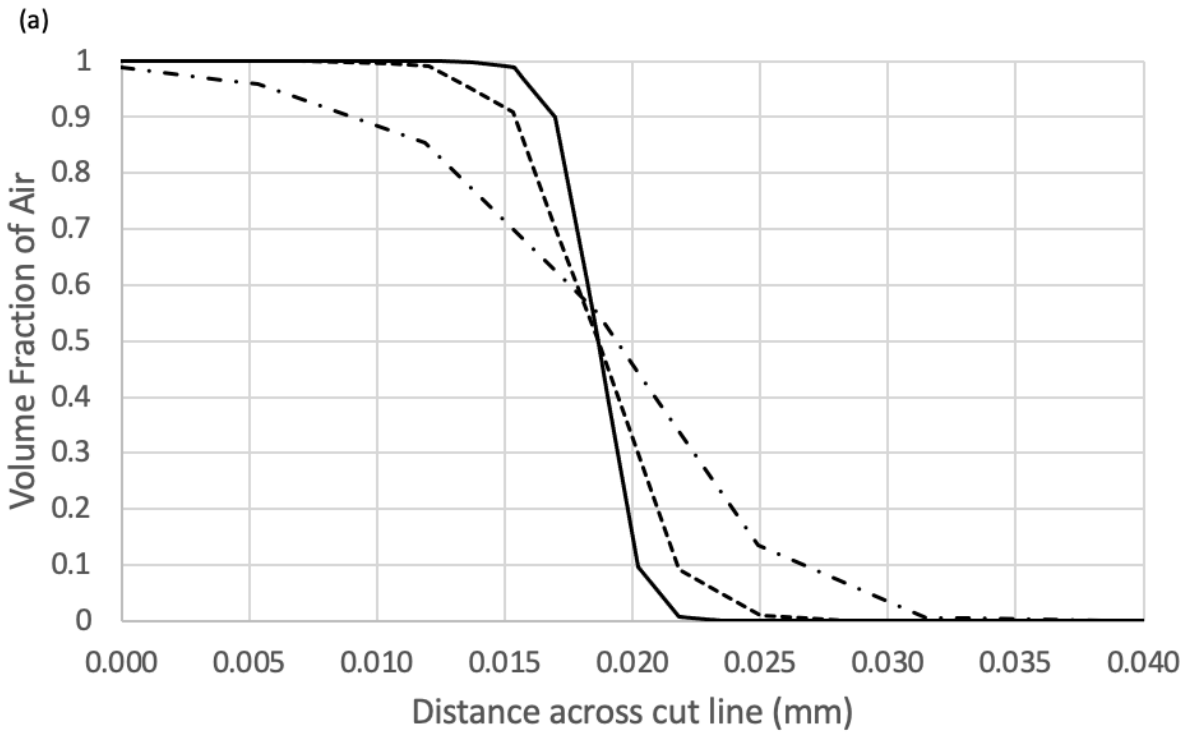


Figure 3.6: Cut Line across the bubble interface to plot data.



— 0.002mm - - - 0.004mm - · - 0.008mm

Figure 3.7: Volume fraction of air across cut line in Figure 3.6 with different mesh sizes. (a) Phase Field Model (b) Level Set Model.

The Phase Field volume of fluid model is incapable of maintaining the initial boundary so there is an expansion of interface distance shown by comparing Figure 3.5 (c) and (d). After a few timesteps, the interface is larger, but the expansion stops when it hits an equilibrium shown in Figure 3.5 (d). This equilibrium point occurs when the outward and inward diffusive components are equal. Higher surface tension cases will tend to have smaller interfaces. The Level Set model can also have expanding boundaries but as there are no outward diffusion modelled, it is due to advection.

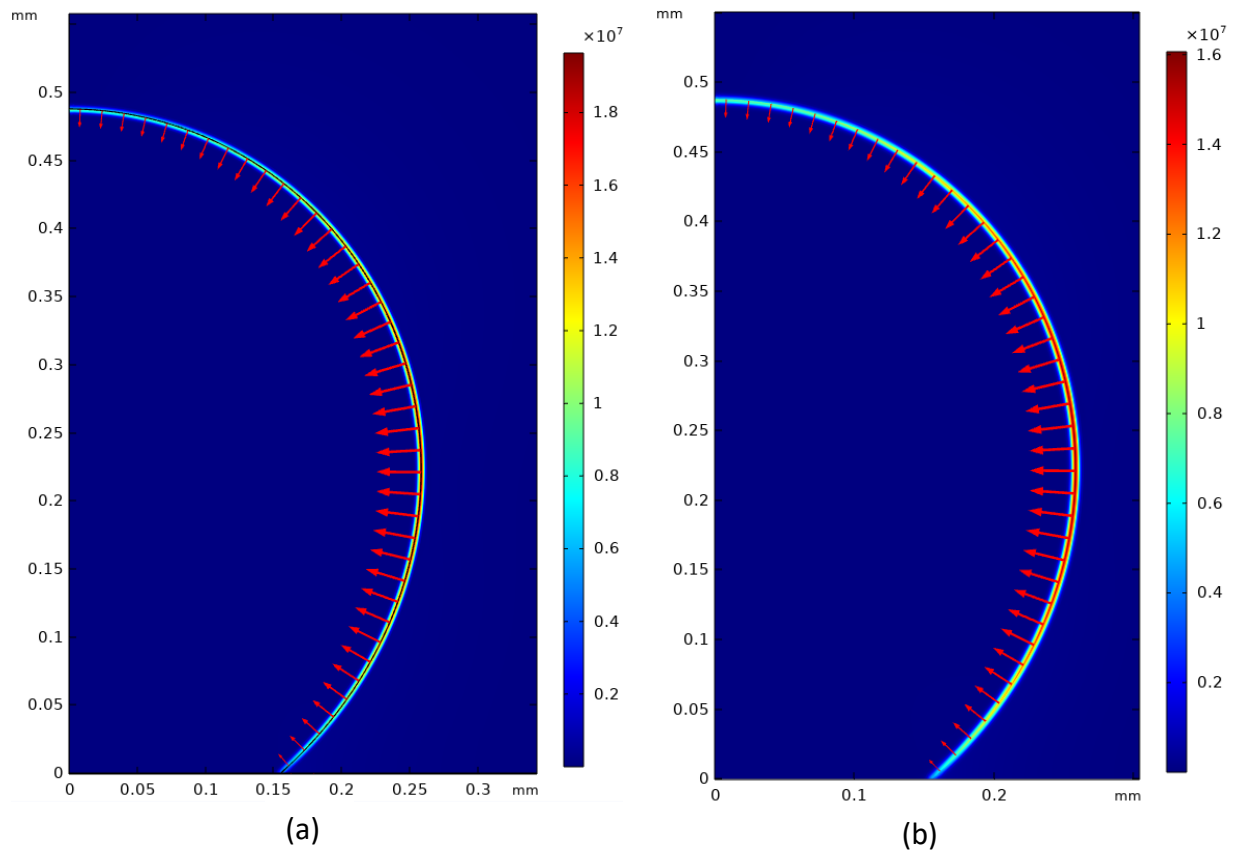


Figure 3.8: Body force magnitude in N/m^3 . Scaled vectors are displayed with their length proportional to the magnitude. (a) Phase Field Model (b) Level Set Model.

Examination of the forces as a two-dimensional surface it is seen, in Figure 3.8, the EHD force is only present on the interface as expected from the dielectrophoretic and electrostrictive forces that are modelled. The direction of the EHD force on the bubble is in the inward direction with the force in the r-direction being greater than the force in the z-direction. This will cause the bubble to deform and become thinner radially and rise axially. From Figure 3.8, the forces in the Level Set model are less than the Phase Field model seen by the differing scales in the surface graphs.

Figure 3.9 shows the different components of the EHD force that is modelled. From this it is seen that the dielectrophoretic force and the electrostriction force are similar in magnitude, and both are in the same direction. This is interesting as previously stated, electrostrictive forces in EHD have been neglected in past works but are very important in this case. The electrostriction force is slightly higher than the dielectrophoretic force. This differs from Di Marco et al., 2013, numerical model but the case used to compare the EHD force components was a larger bubble and the results could be different than found here [5]. This shows that in similar cases the importance of electrostriction may vary with small changes in geometry.

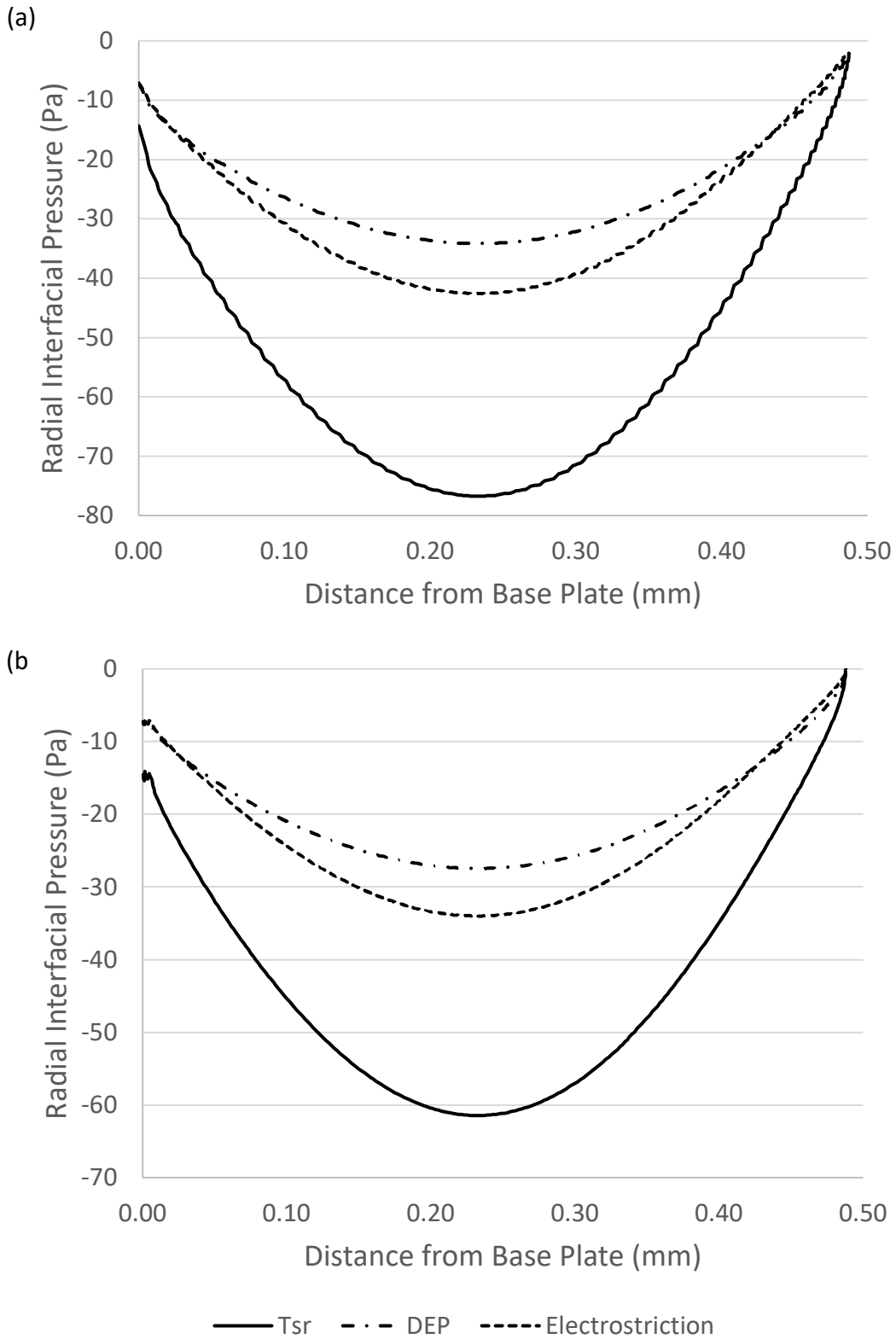


Figure 3.9: Comparison of EHD force components in different models. Tsr is the total radial stress which is the sum of the Dielectrophoretic component (DEP) and Electrostrictive component. (a) Moving Mesh model (b) Phase Field Model.

The electric field created by the electrode is shown in Figure 3.10 and 3.11. In the Moving Mesh model there is a sharp change in the electric field strength due to the infinitesimal interface whereas in the volume of fluid models (Phase Field model shown in Figure 3.11), a gradient of electric field strength is seen. This highlights one of the issues that reduces EHD force as the gradient of electric field is what causes the dielectrophoretic and electrostriction forces. Having a finite gradient instead of the step change seen in the Moving Mesh model can cause the reduction in the polarization forces.

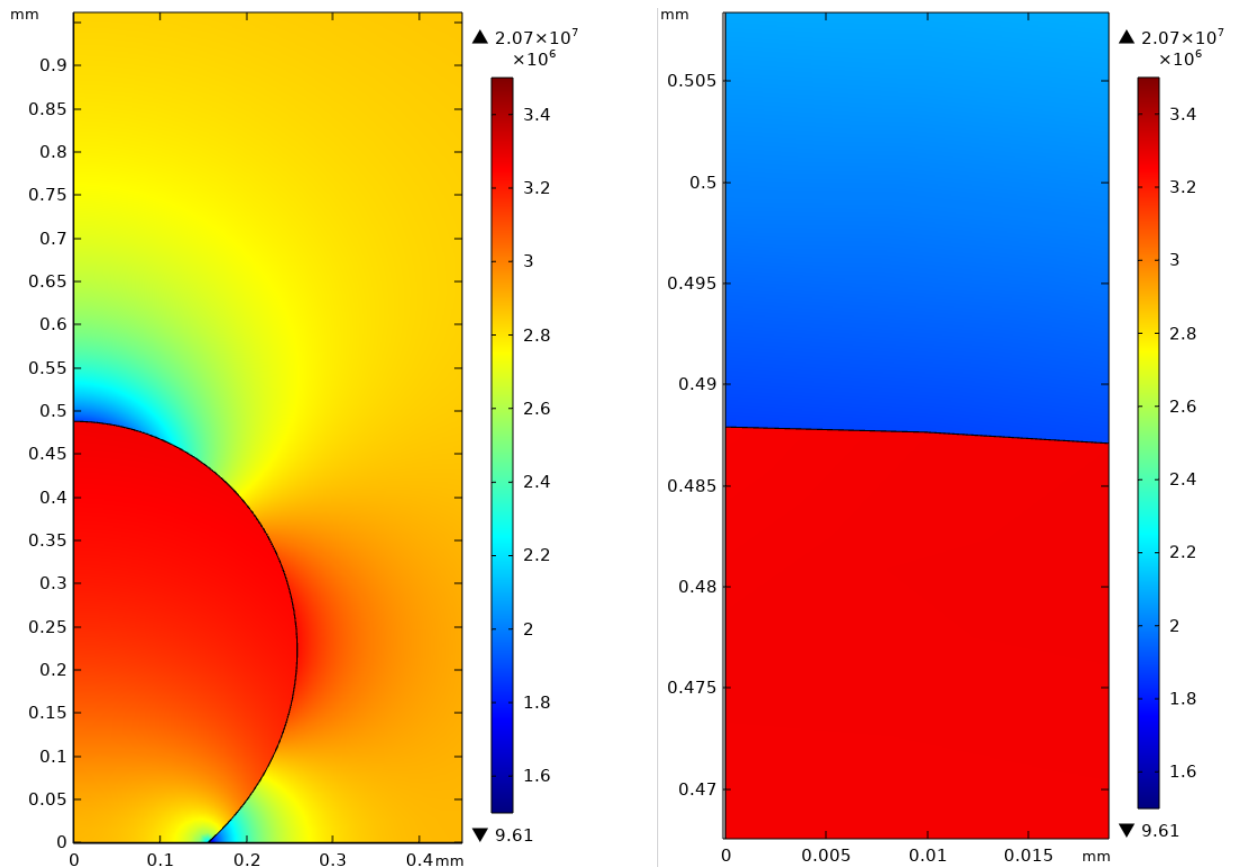


Figure 3.10: Electric field in V/m of the Moving Mesh model. Full bubble on left and close up of the top of bubble is shown on the right.

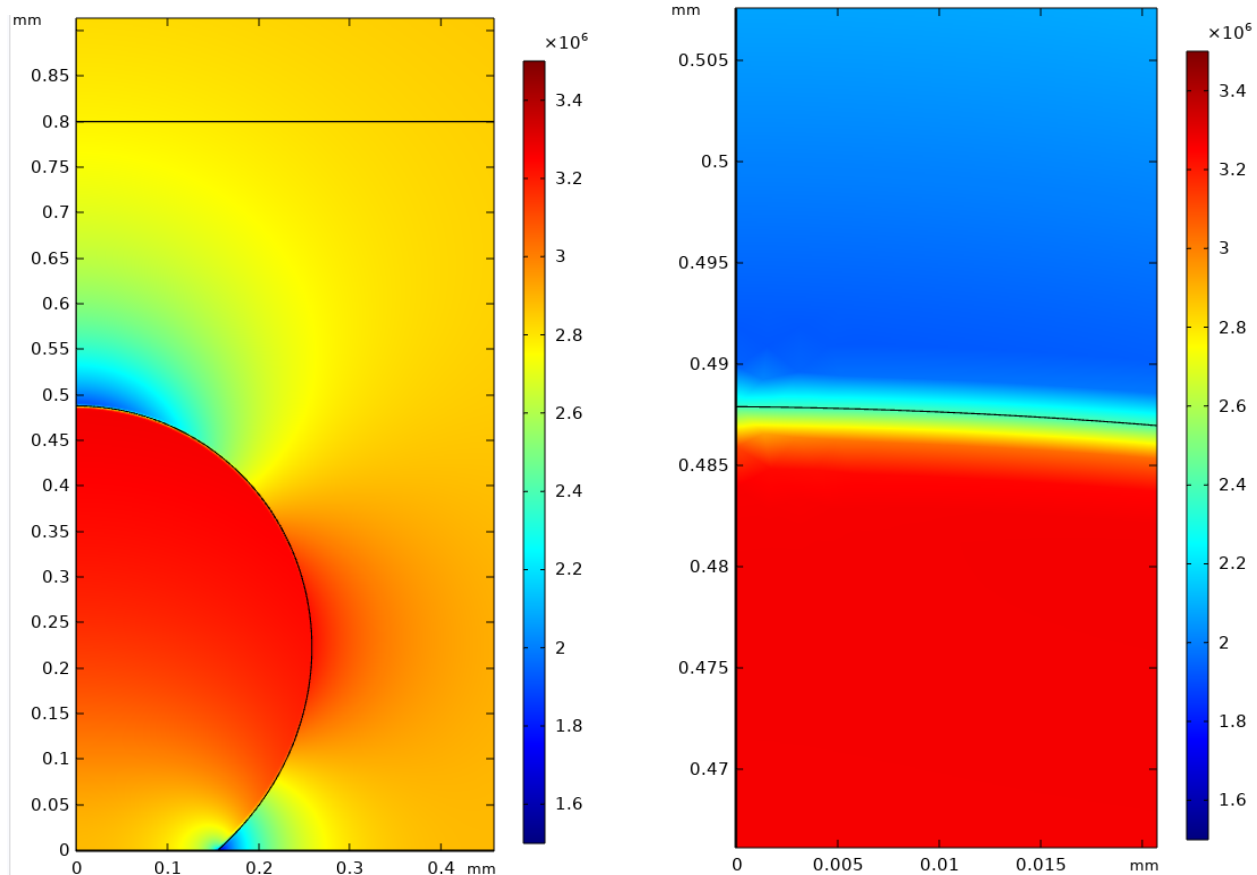


Figure 3.11: Electric field in V/m of the Phase Field model. Full bubble on left and close up of the top of bubble is shown on the right.

The gradient seen in Figure 3.11, not only reduces the force on the interface, but it also creates a variable body force in the entire volume of the gradient instead of a pressure on only the interface line. This variable volume force can have a negative impact on transient cases because differing forces in the interface will give the control volume different velocities affecting advection. If the advection component pushes the phase parameter away from the center and the diffusion cannot shrink the interface the model can fail. Some of these failures include interface growth causing reduced surface tension and bubble detachment, phase infiltrating across the interface causing phase mixing, or general deterioration of the interface (i.e., wavy interfaces) causing unphysical bubble shapes. As the EHD coupling is not native to

the COMSOL software, the implementation of EHD force destabilizes the interface equations without numerics to restabilize the boundary.

Transient Model

For the transient model, the ramp voltage of 0.1 seconds was employed to stabilize the bubble oscillations. The models were run for 0.12 seconds to achieve a steady state. The models were solved using an implicit Backward Differentiation Formula (BDF) method for time stepping with data taken at every 0.001 seconds. The BDF method adapts the time steps to achieve a specified relative tolerance and therefore timestep independence testing was done by adjusting the relative tolerance. This time stepping method has been used in previous models involving two-phase flow with EHD as it is the main time stepping method in COMSOL [57].

To compare the results between the Moving Mesh and volume of fluids models, bubble height is taken where the phase parameter indicates half of each volume is each phase. As the bubbles experience a compressive force from all sides but a larger pressure radially inwards, the bubble will get thinner radially and rise axially. This axial rise will be used to compare the bubbles through time.

Figure 3.12 shows the height of the maximum part of the bubble with time for the three models. The Moving Mesh model shows a steady rise in height with the ramp of voltage. This height rise is parabolic which is consistent as the EHD body force equation being proportional to the square of the electric field. As the voltage, and therefore the electric field, is being increased linearly, it is expected the force is increasing parabolically which is seen in Figure 3.12. After the ramp, there are some oscillations until the bubble hits steady state due to the momentum the bubble has from its motion, but it is quickly dissipated.

The volume of fluid methods had their interface breakdown causing the interface to expand causing the surface tension force to deteriorate and cause phase infiltration and detachment of the bubble. This was due to the large EHD force on the interface which the models were unable to stabilize. The bubble shapes are shown in Figure 3.13. They are seen to have the same shape at 0.025 seconds when the applied voltage is at 5kV but differences are seen in the following times.

In Figure 3.12, the Phase Field model is close to the Moving Mesh model in the initial 0.03 seconds but then departs and the height diverges off the graph. At low electric fields this model is comparable to the Moving Mesh model as seen in Figure 3.13 (a), but slowly departs in Figure 3.13 (b) and (c). This slow departure is caused by the degradation of the interface seen in the expansion noted in Figure 3.5 (d). As the interface starts to expand, the forces that are dependent on the interface gradient are reduced. These forces include surface tension and EHD force. The surface tension force is the only force opposing the bubble departure so when it is reduced the bubble starts to detach.

The Level Set model also diverged from the moving mesh model at a similar voltage but after a sharp rise the bubble experienced a recovery at 0.05 seconds. The interface breakdown seen in the Phase Field model was also present in the Level Set model which caused the bubble to begin to detach as the surface tension force deteriorated. The Level Set model had a recovery because the growing interface caused the inward diffusion to become larger resulting in better control of the interface size. The difference between the Phase Field model and Level Set models is the Phase Field model uses Hillard-Cahn diffusion, where the diffusion is based on physical properties instead of the Level Set using a false diffusion term to shrink the boundary. The model was almost able to recover to Moving Mesh model but experienced some phase infiltration at the

symmetry line which caused the model to diverge. This phase infiltration occurred during the recovery of the interface, and it caused a large numerical error as the model continued. The reasoning behind the instability increasing is not understood and could be due to the numerics in the 2D axis-symmetry having no volume along the center line and artificially increasing the fluid due to this singularity.

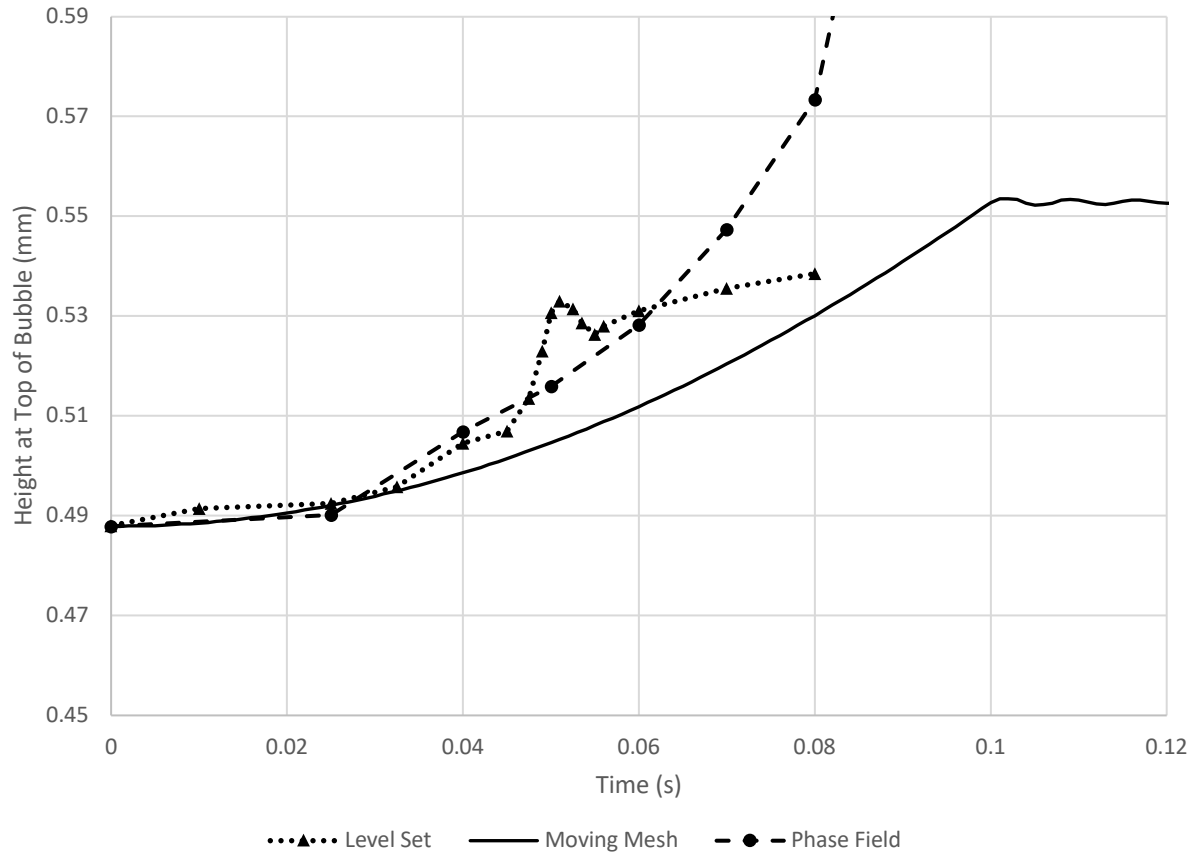


Figure 3.12: Comparison of bubble height at top of bubble interface as voltage of electrode is ramped from 0 to 20kV using Moving Mesh, Level Set, and Phase Field models.

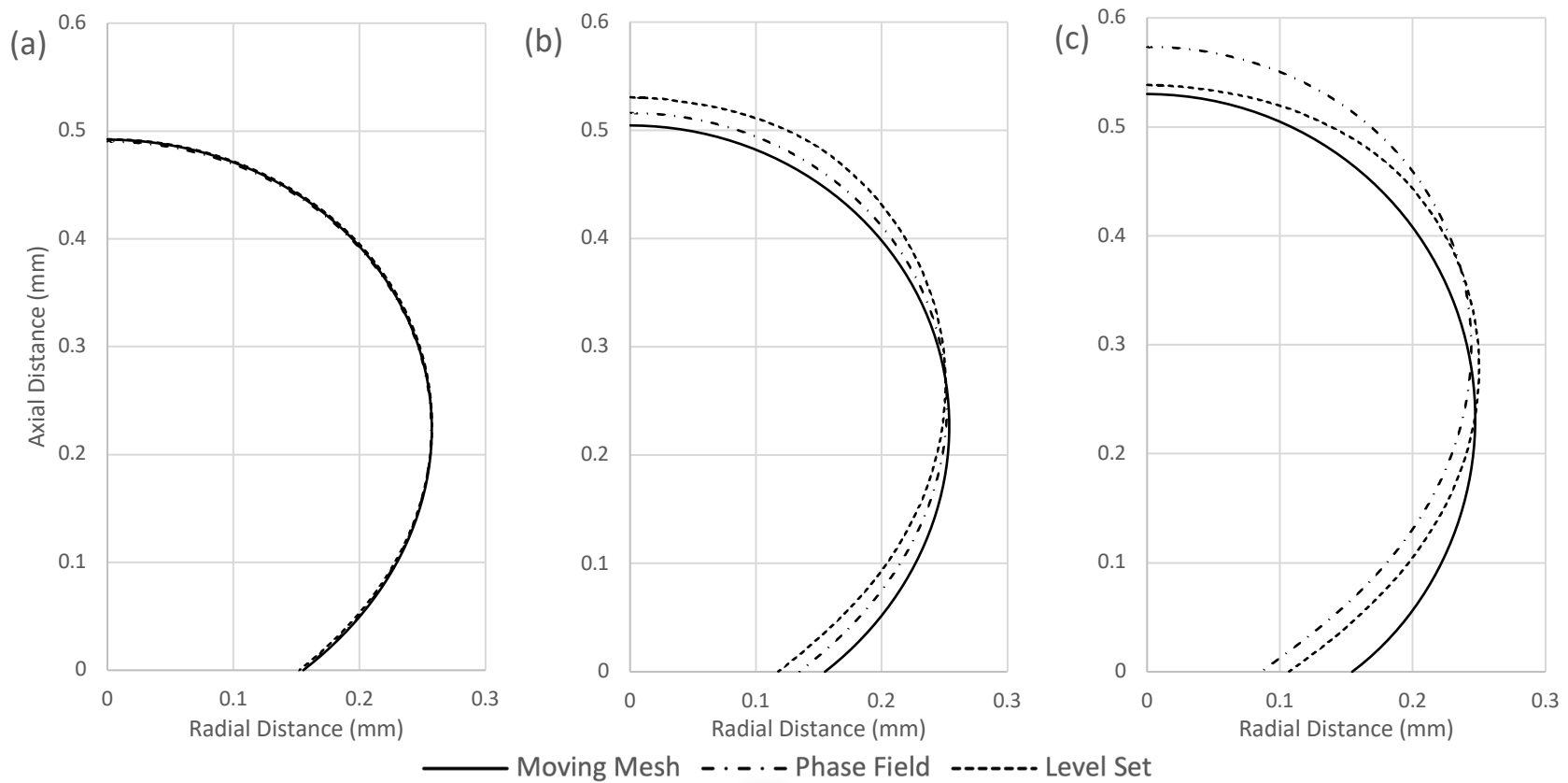


Figure 3.13: Bubble shapes for the moving mesh, phase field, and level set model when subjected to a 20kV ramp voltage at various times. (a) bubble position at 0.025s (b) bubble position at 0.05s (c) bubble position at 0.08s.

The moving mesh model was run until steady state was reached and had good agreement with the experimental results done by Di Marco et al., 2013 [5]. Figure 3.14 shows the final bubble shape in the moving mesh model compared with the shape obtained from a photograph of the experiment. The data from the photograph was scaled with radius of the orifice which was 0.15mm. The largest deviation from the experiment and numerical model was 0.007mm. This validation shows that the Moving Mesh model accurately depicts buoyancy vs surface tension from the initial bubble condition and accurately shows the EHD forces applied.

The other volume of fluid models were unable to reach a steady state and therefore they cannot accurately model the balance of forces in this EHD case but for low electrode voltages they were close to the Moving Mesh model so they can be useful with lower electric fields. The volume of fluid models are still an important model to use and improve as other cases with topological changes cannot be modelled with the Moving Mesh model.

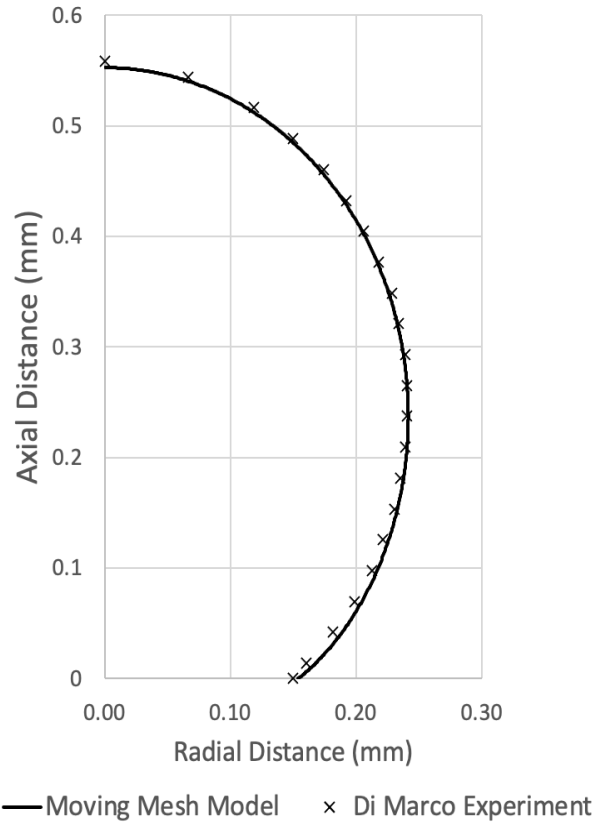


Figure 3.14: Bubble shape in the moving mesh model vs the experimental data from Di Marco et al. experiment for a 0.0737mm³ bubble subjected to 20kV.

Conclusion

A 2D axis-symmetric model was simulated and compared with experimental work done by Di Marco et. al., 2013. Two segregated volume of fluids methods, Phase Field and Level Set models, and one coupled interface tracking method, Moving Mesh model, were used to simulated bubble deformation in the presence of an electric field.

The Moving Mesh model was validated against experimental work and showed agreement within 5%. The Phase Field and Moving Mesh models have lower EHD force from the phase gradient along the interface and are unstable in transient cases and cannot be validated against the steady state data. In lower electric fields, the volume of fluids models are consistent with the validated Moving Mesh model and can be accurate in such cases. In cases with no

topological changes, the Moving Mesh model should always be used but for such cases the volume of fluids models should be improved to add more stability at the interface.

Chapter 4 - Liquid Extraction

4.1 Introduction

An EHD force can be applied in a two-phase heat exchanger to enhance or decrease heat transfer. This can control the heat transfer coefficient and can help improve the heat exchanger design. One important component of a horizontal two-phase heat exchanger is called dryout. Gravity can cause the liquid volume to drop to the bottom and vapour flows along the top in a stratified flow. The surface of the heat exchanger touching the liquid phase has better heat transfer due to liquid having a higher thermal conductivity and the capability to continue to boil and absorb latent heat in its transformation of phase. There can be intermittent wetting of the top surface but if there is not any fluid reaching the top surface, the temperature of the surface will rise. Due to the limited heat transfer to the vapour, the heat exchanger also has poorer effectiveness in this region.

EHD forces can allow for flow redistribution that can act to rewet surfaces that were dry in the case without EHD. The interface between the two fluids has a permittivity difference which will allow for dielectrophoretic and electrostrictive forces to be present. These forces can agitate the flow and cause it to increase mixing and wet the top surface.

One common heat exchanger that EHD is added to is the coaxial heat exchanger. An electrode is introduced into the center of an inner circular pipe with the inner pipe grounded. One flow pattern seen when an EHD force is introduced is called liquid extraction [26], [47]. This is when a liquid column extends from the surface of the liquid up to the electrode.

An experiment was performed by Sadek et al., 2008, there was a partially filled pipe with the fluid at rest and an electrode through the center was set to 3kV. The initial distance of the liquid to the electrode was 1.5mm. A high-speed camera visualized the liquid extraction, and it

was found that the time for the liquid column to reach the electrode was 6.5 ± 0.5 ms. This experiment used pixel greyness and change in greyness to approximate the start time of the electrode step voltage. This method could be ineffective if the initial rise is very slow as the pixels above the initial interface line may not darken dramatically at the start of the voltage and anything blocking the center of the fluid can make the start time delayed.

A model was performed by Sadek et al., 2008, which had results of 6ms extraction times that fit the data. The model was a quasi-static numerical approach where the electric field was solved and then EHD interfacial pressure was calculated and given to the interface. This model excluded surface tension which would have slowed the liquid extraction.

Numerical models of this situation were improved by Nangle-Smith et al., 2016. The model used the Moving Mesh model to track the interface of the fluid and the Phase Field model in COMSOL Multiphysics. The circular geometry was unable to be used as the Moving Mesh model at the time, so a square domain was used with the electrode gap maintained. The rise time was compared between the models in this geometry and as seen with the volume of fluids methods, the reduction in force from the discrete interface caused the Moving Mesh model to raise faster than the Level Set model. Numerical models with the true geometry were conducted and a factor was used to compensate for the reduction of force caused by the Level Set model. The rise timing for the Moving Mesh in the square domain was found to be 17.5ms and adjusting the Level Set model resulted in an approximated 11ms rise time.

This phenomenon is a three-dimensional case as the fluid is moving perpendicular to the cross section, but the geometry is simplified into a two-dimensional cross section as the numerical models used computationally expensive. Further work on three-dimensional effects in this case can improve the current understanding of this phenomenon as well.

The simplified two-dimensional model will be modelled using the Moving Mesh, Phase Field, and Level Set methods in COMSOL Multiphysics with EHD coupling to model the liquid extraction phenomenon. The models will be adiabatic and include gravitational force, surface tension, and dielectrophoretic and electrostrictive components of the EHD force. As shown in Chapter 4, these models include interface tracking methods with an infinitesimal interface and volume of fluids methods that have a finite interface thickness with the Moving Mesh model being validated against Di Marco et al., 2013.

4.2 Numerical Methodology

Three two-phase flow models are implemented to model the liquid extraction including the fully coupled Moving Mesh, segregated Phase Field, and segregated Level Set models. The fully coupled model is typically more stable than a segregated approach but can take a long time when there are many nodes. The domain in this model is much smaller than that of the Chapter 3 Bubble Deformation, but a finer mesh is required to solve for the interface, so the volume of fluid methods still require the segregated method. The fully coupled method solves all the equations simultaneously which can reduce oscillations in numerical errors in the different physic modules. Such oscillations can result from the phase field moving too far in a timestep which creates a lower force from the electric field and on the second iteration the force is less in the phase field solution making the movement reduced and increasing the force for the next iteration. With relaxation the solution will eventually settle but if it is very unstable, enough iterations might pass to trigger an error that the solution could not converge.

The model is adiabatic and uses the simplified geometry seen in Figure 4.1. This geometry is the cross section of the inside of the pipe of diameter 10.2mm with an electrode

down the center of diameter 3.18mm. The fluid is R-134a which is in the annulus between the pipe and the electrode. The initial surface of fluid is defined as 1.5 mm from the bottom of the electrode. Surface tension for R134a at 25°C is 0.008 N/m [58] and the contact angle is assumed to be 35 degrees [59]. The properties of liquid and vapour R-134a remain constant and are found in Table 4.1. It is assumed that there are no free charges and therefore Coulomb force is neglected.

Table 4.1: Fluid Properties of liquid and vapour R-134a.

Material Property	Value
Surface Tension	0.008 N/m
Contact Angle	35°
Vapor Permittivity	1
Liquid Permittivity	9.5
Liquid Density	1206 kg/m ³
Vapor Density	5.3 kg/m ³
Liquid Viscosity	0.000022 Pa*s
Vapor Viscosity	0.000012 Pa*s

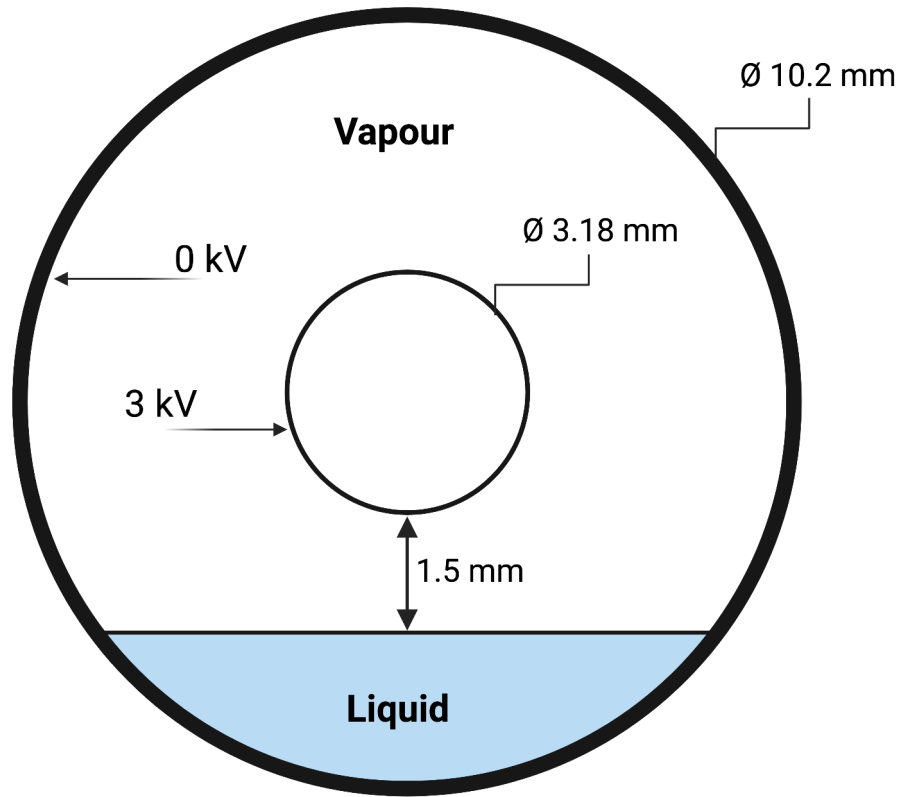


Figure 4.1: Geometry used for the models.

This initial condition is not the true initial state as the contact angle with the edge of the domain is not correct. The model is run using the Moving Mesh model to achieve a steady state where there is a capillary rise at the edges from surface tension. The final geometry, shown in Figure 4.2, is the steady state initial condition without EHD that will be used for the rest of the models. The electrode will be set to 3kV, and the outside pipe is grounded. Mesh and timestep independence testing were conducted with results shown in Appendix B.

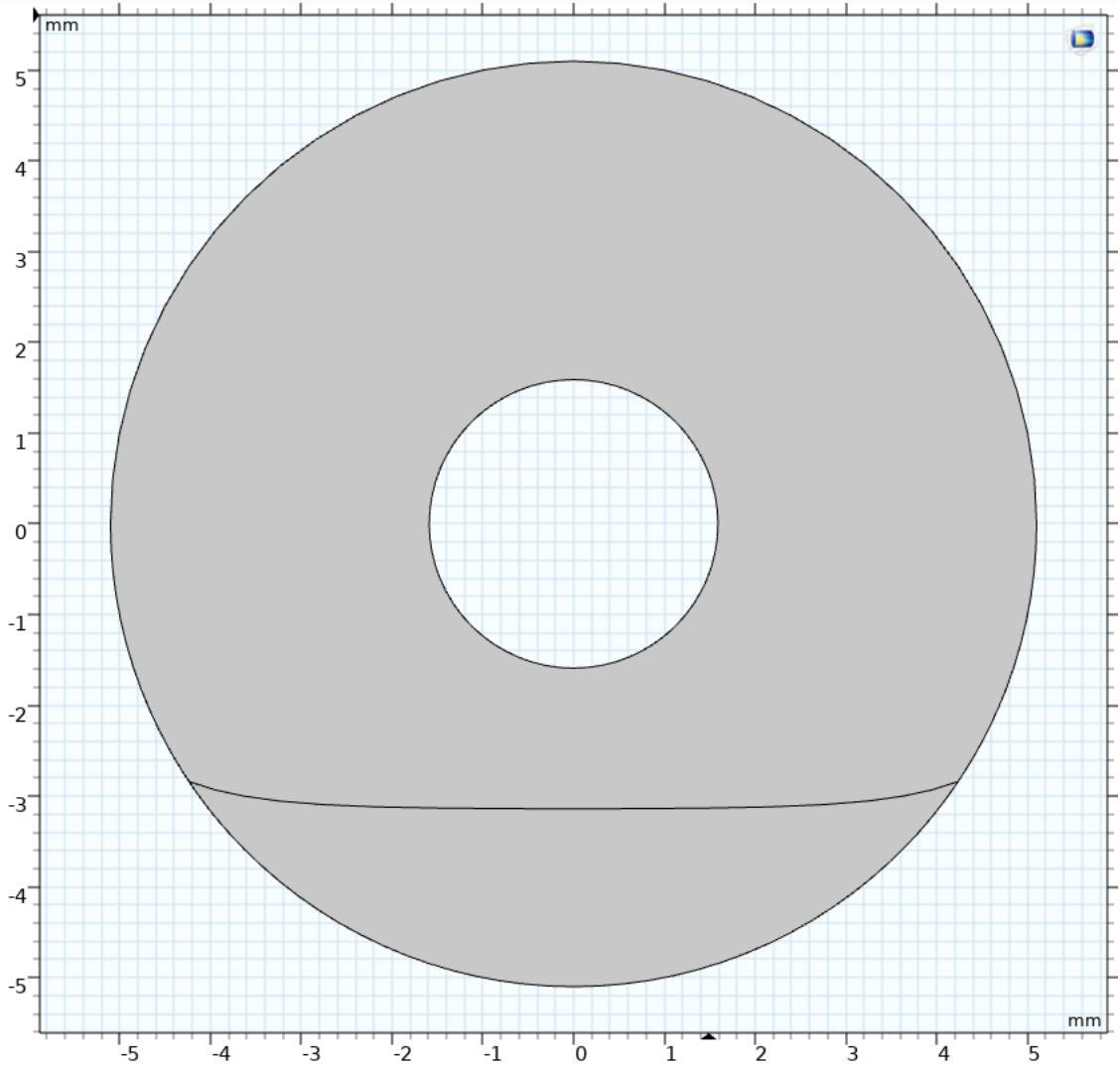


Figure 4.2: Geometry after capillary rise at edge due to surface tension.

4.3 Modelling Techniques

Moving Mesh Model

The Moving Mesh model works the same as when it was implemented in Chapter 3. The EHD force is applied to the interface between the two phases and takes the form of the stress tensor in Equation 3.3. Although there is symmetry between the left and right side of the model, initial testing experienced problems with the interface on the symmetry line of the Moving Mesh model. Therefore, symmetry was not used in this model.

The other parameters that relate to the solver and mesh deformation are kept consistent with the Bubble Deformation study as they were validated and can be seen in Table 4.2. Pressure was defined on the left most point of the outer pipe and was defined at 0 Pa. In previous studies, automatic remeshing was used to reduce skewness when deformation occurs but it reduces the trustworthiness of mesh refinement studies so it will be omitted in this study [6].

Table 4.2: *Moving Mesh model boundary and solver conditions.*

Laminar Flow	Contact angle with wetted walls	35°
	Pressure point-constraint (left of outer pipe)	0 Pa
	Surface Force	Tx, Ty
Electrostatics	Outer pipe voltage	0 V
	Electrode voltage	3kV
Mesh Deformation	Mesh Smoothing Type	Yeoh
	Stiffening Factor	10
Time Dependent Solver	Time Stepping Method	BDF free
	Relative Tolerance	0.005
	Absolute Tolerance	0.05
	Time-Dependent Solver Type	Direct Fully Coupled
	Direct Solver	MUMPS

Phase Field and Level Set Method

Both of the volume of fluid models are modelled the same as in Chapter 3 like the Moving Mesh model. The EHD force is modelled as a body force term shown in Equation 3.4. The volume of fluid methods are able to use a symmetry boundary down the center of the domain so the domain is halved to reduce the computational load. Due to the smaller geometry,

the multigrid method used to solve for the fluid flow field in the bubble deformation case is not required and can be replaced with a direct solver.

Table 4.3 shows the solver settings input into the model. The weighting parameters, mobility tuning and reinitialization parameter, that scale the advection and diffusion of the phase parameter are the only difference between the settings for the two volume of fluids methods. The mobility tuning parameter is set to its default of 1 because the boundary did not have excessive diffusion at the beginning of the model like the bubble deformation case. This might be because the interface has motion unlike in the Bubble Deformation case where the bubble is stationary. This reduction will make the interface less stable, but the dynamics of the liquid extraction will be displayed better as the advection term will not be suppressed.

The segregated solver works in the same order as shown in Chapter 3, so the process steps are similar, but the multi-grid solver is not utilized. The steps are shown below:

- 1) Solves for the phase field with direct solver
- 2) Attributes an electrical permittivity to the control volumes equal to their volume fraction
- 3) Solves for the electric field with direct solver
- 4) Calculates body forces with the electric field and relative permittivity of the fluid
- 5) Solves for velocity and pressure using a direct solver
- 6) Velocity is given to advection term of phase field solver and order starts again

Table 4.3: Phase Field and Level Set model boundary and solver conditions. All properties are shared except the last rows labelled with the specific model they are used in.

Two-Phase Flow	Contact angle with wetted walls	42°
	Interface thickness	Half of Mesh Spacing (Level Set) Mesh Spacing (Phase Field)
	Pressure point-constraint (left of outer pipe)	0 Pa
	Volumetric Force	Fx, Fy
Electrostatics	Outer pipe voltage	0 V
	Electrode voltage	3kV
	Axial Symmetry	On Centerline
Time Dependent Solver	Method	BDF free
	Relative Tolerance	0.005
	Absolute Tolerance	0.01
	Time-Dependent Solver Type	Segregated
	Direct Solver	PARDISO
Phase Field	Mobility Tuning Parameter	1
Level Set	Reinitialization Parameter	1

4.4 Results and Discussion

Initial Interfacial Forces

The initial force on the Bubble in Chapter 3 showed a reduction in interfacial pressure for the volume of fluid methods cases. This force reduction is inevitable as the phase transition is discrete so there is not a sharp gradient like the interface tracking method.

Figure 4.3 shows a surface with the body force plotted for the Phase Field and Level Set models. The largest body force is located just above the initial interface which contrasts the Bubble Deformation model that had the body force line on the interface. This means that the body force term is experienced in the area with a volume fraction that's higher in vapour content. This can cause increasing interface thickness as the advection is high in the high vapour volume fraction fluid which can separate from the lower vapour volume fraction fluid that does not have a body force.

The highest force is in the center where the liquid surface is closest to the electrode. This upward force is what will make a column of liquid rise. Along the entire interface there are upward forces but to preserve mass equality there the fluid must drop away from the center to allow for the column to form. Unlike the Bubble Deformation case, the Level Set model experiences higher forces. This is due to the interface thickness in the phase field being set to the mesh spacing as it was unstable in cases with half mesh spacing.

There is one node that experiences a higher force than the surrounding nodes that is after the black line signaling the change of domains. This is due to the different mesh in the liquid extraction region than the outside. The middle region has a lot of movement of the interface and requires a very fine mesh, but the outside domain is mostly still. Where the domains intersect

with the interface, there is a change in mesh uniformity which creates this numerical error. A diagram of the mesh can be seen in Figure B.1.

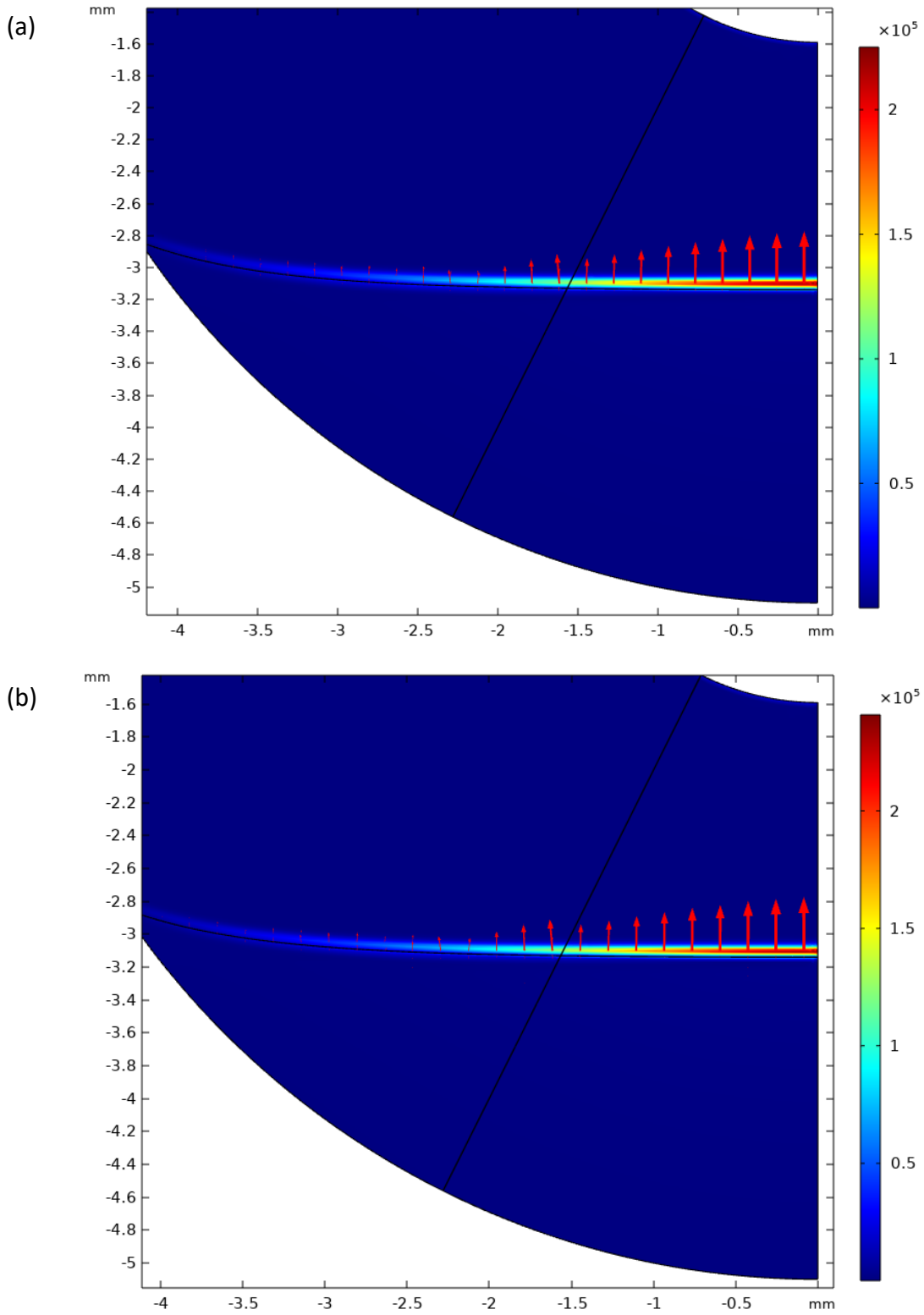


Figure 4.3: Magnitude of EHD body force on the initial domain in N/m^3 with different modelling techniques. Proportional force vectors are overlaid. (a) Phase Field, (b) Level Set.

The electric fields are shown in Figures 4.4 and 4.6. The volume of fluid models have a similar electric field to one another as they have almost the same phase field. There is a large difference in the comparison between the volume of fluid models and the Moving Mesh model in this case. The electric field reduces significantly as it approaches the interface in the Phase Field and Level Set model whereas it remains high until it hits the interface and drops in the Moving Mesh case. This is different than the case in Chapter 3 where the electric field decreased over the interface line and better reflected the Moving Mesh model.

The difference between these two cases is the relative permittivity of the liquid. In the previous study, the permittivity of the liquid was 1.74 and, in this case, the liquid permittivity was 9.5. The large difference in electrical permittivity in this case increases how well the electric potential can permeate the boundary. The fluid has a high permittivity so the potential field can pass through the liquid well and as it is in contact with the outer pipe the liquid acts as though it is grounded. With the high differences of electrical permittivity, even a low volume fraction of liquid would create a relatively higher permittivity than the vapour above it and act grounded like the liquid.

The higher level of grounded fluid seen in the volume of fluid method cases is what causes the interfacial force to be located above the boundary instead of in the center like the previous case. This deflection of the electric field is not physical as the interface should be infinitesimal and it would not affect the field but in modelling it will be present. One method that could reduce this affect is having stepwise properties where all properties on one side of the phase parameter act as liquid, and the other as vapour. This can lead to other numerical errors like non-uniform boundaries as each node in a boundary could oscillate between the parameter threshold for the step function. This would create a jagged boundary and would affect the electric

field. This study does not take into consideration the effect of stepwise properties. Other approaches have been explored to better represent better methods to solve for the electric field but they are shown to not be accurate with large permittivity differences like in this case [60], [61].

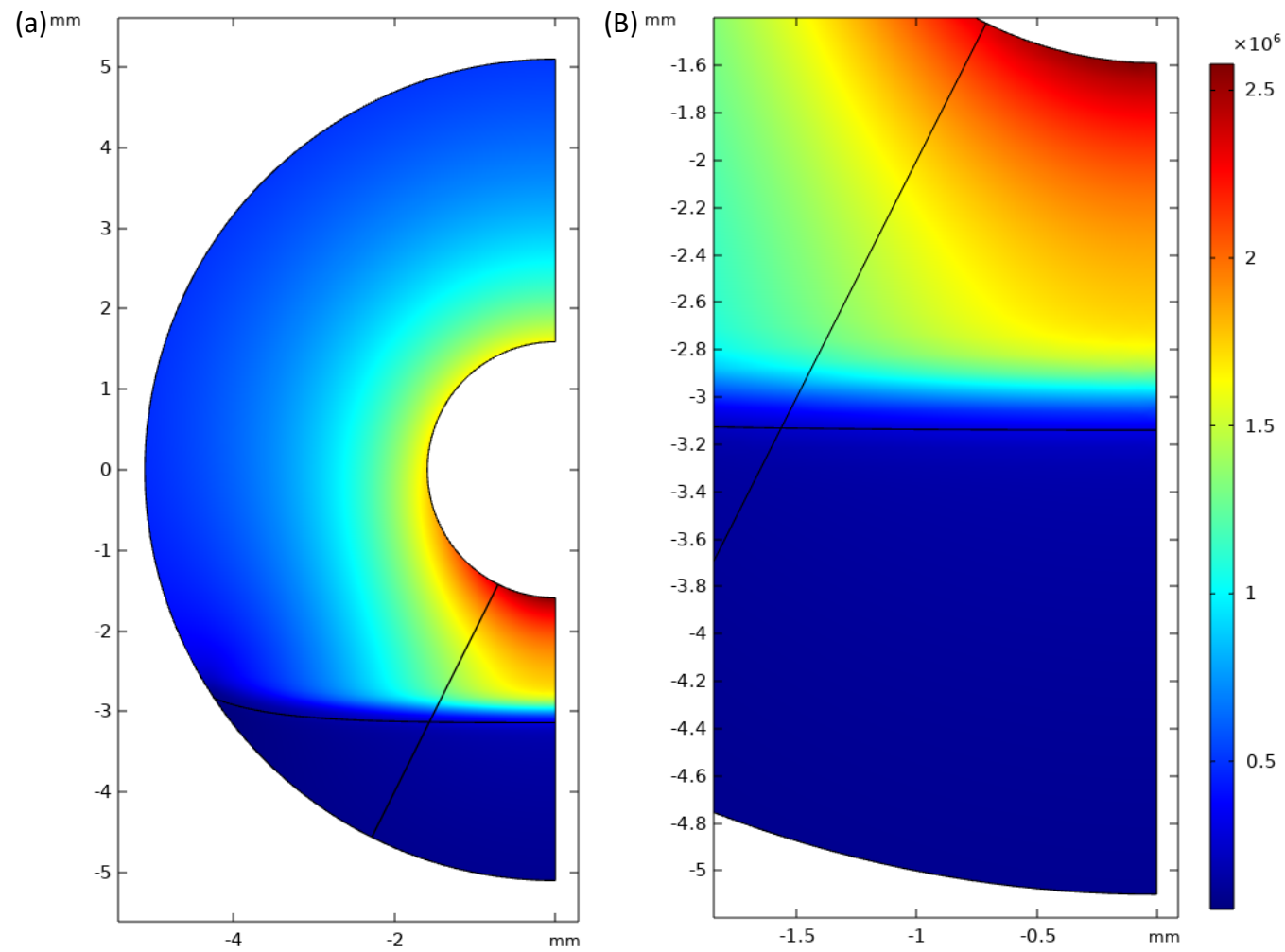


Figure 4.4: Electrical field of the initial domain of the Level Set model in V/m. (a) full geometry (b) close-up on the center interface.

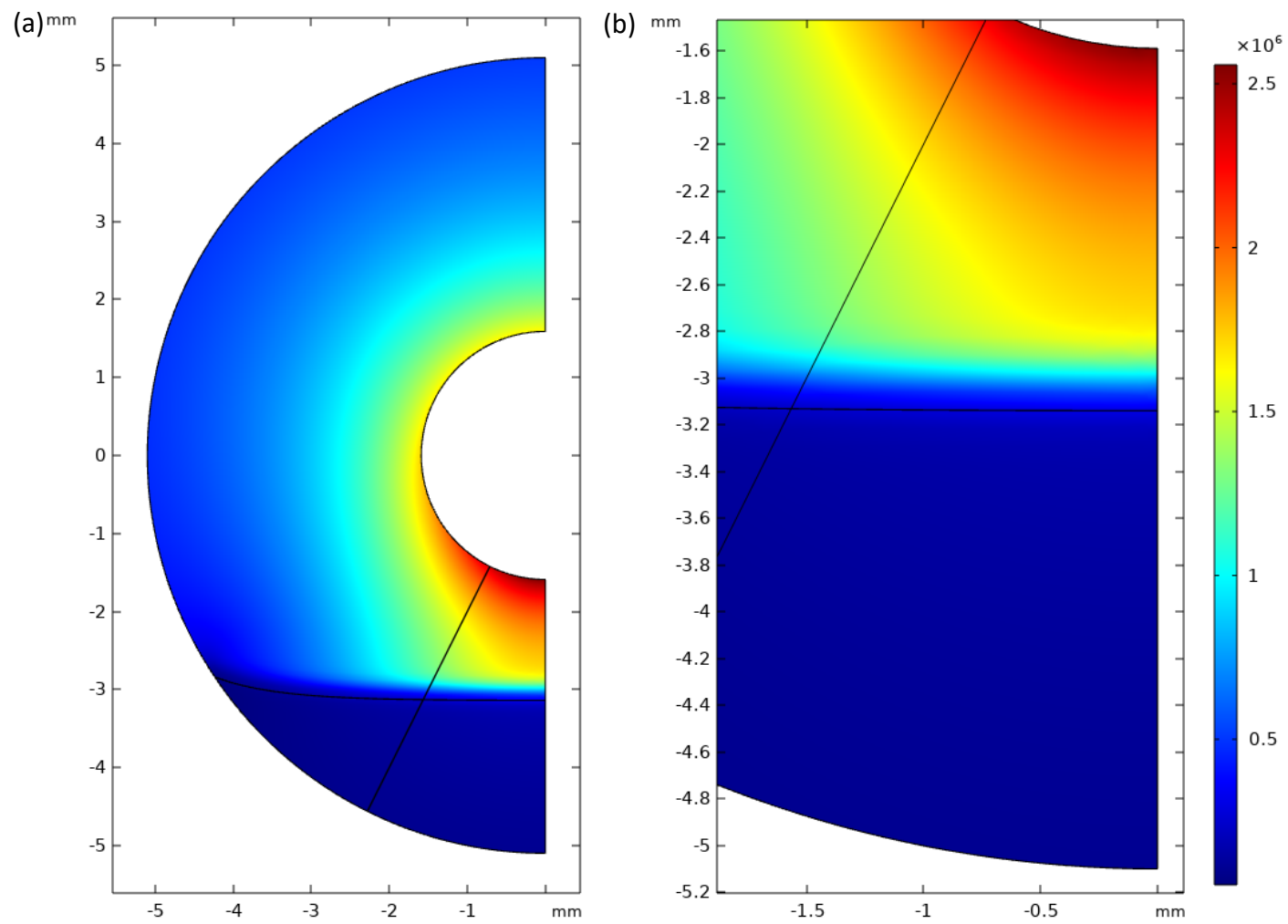


Figure 4.5: Electrical field of the initial domain of the Phase Field model in V/m. (a) full geometry (b) close-up on the center interface.

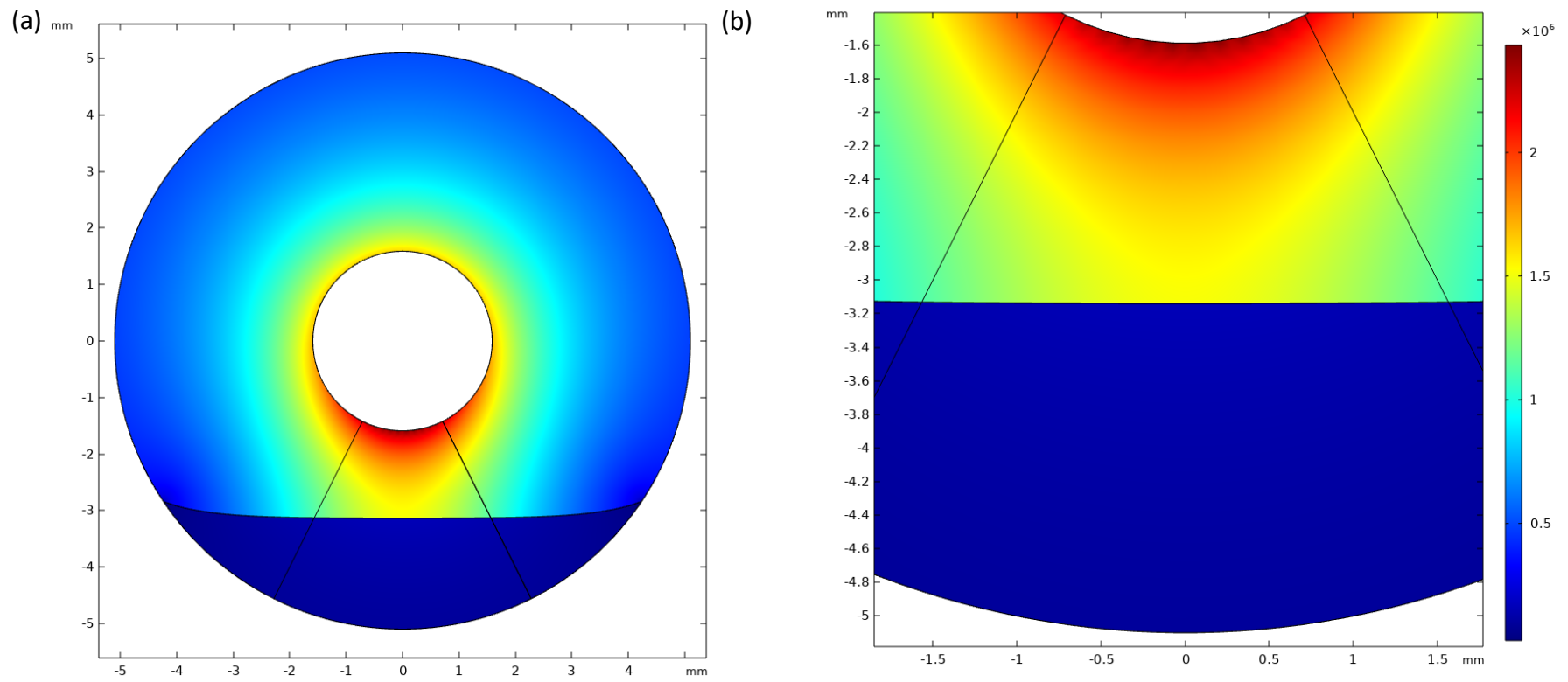


Figure 4.6: Electrical field of the initial domain of the Moving Mesh model in V/m. (a) full geometry (b) close-up on the center interface.

In order to plot the forces for the volume of fluids methods, the maximum force at each horizontal location was taken. The Moving Mesh model had the force applied directly on the interface so the pressure could be taken from the interface line. The interfacial stresses were plotted in Figure 4.7. The plot shows that the largest pressure is in the center where the fluid is closest to the electrode and the Moving Mesh model has the largest force followed by the Level Set and then Phase Field models. The maximum interfacial pressure from each of the models is shown in Table 4. There is a 16% lower interfacial pressure estimated by the Level Set model compared to the Moving Mesh model and 24% in the Phase Field. This shows that the volume of fluids method undercalculates the interfacial pressure which is consistent with the Bubble Deformation experiment in Chapter 3. This shows a large improvement of the volume of fluid models compared to the previous work by Nangle-Smith et al. It was previously reported that the initial interfacial stress was 5 times higher in the Moving Mesh model than the Level Set model compared to a factor of 1.2 times higher for the Moving Mesh model over the Level Set model [6]. This deviation could be from mesh spacing or an increased interface thickness.

This again shows that the initial phase field condition in which the Level Set model was able to utilize a smaller interfacial thickness without destabilizing allowed the force to be larger than the Phase Field. In the study with the Phase Field using a lower interface thickness, the interface became wavy due to the destabilization. These initial force calculations are not going to keep the same trends throughout a time dependent study as the interfaces will tend to expand and reduce the body force. The numerics for the Level Set model will likely expand more as it typically takes more nodes to resolve the boundary as seen in the previous Bubble Deformation study. This will cause the Phase Field model to eventually have a larger force than the Level Set model after some time steps.

Table 4.4: Maximum interfacial stress for each model and the percentage compared to the Moving Mesh model.

Model	$T_{y,max}$ (Pa)	Percent of Moving Mesh
Moving Mesh	12.8	-
Phase Field	9.7	76%
Level Set	10.7	84%

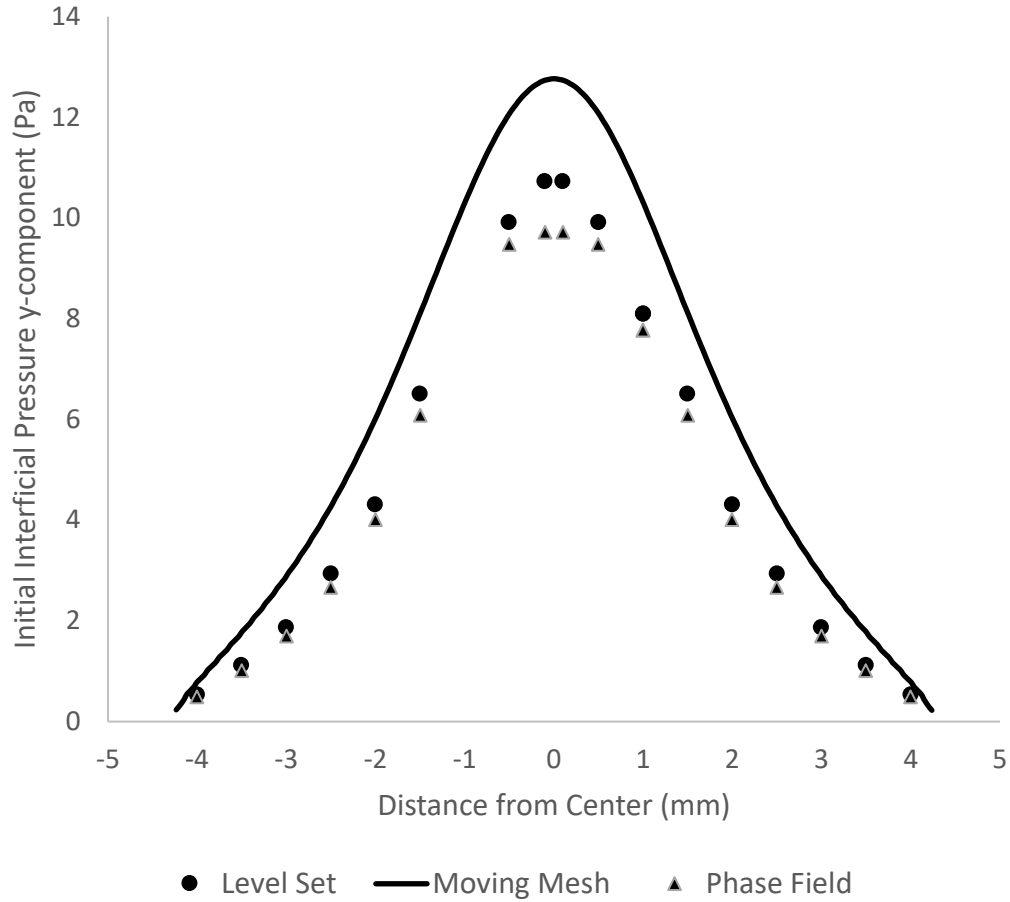


Figure 4.7: Initial interfacial stress comparison with Moving Mesh, Phase Field, and Level Set models.

Breaking up the EHD stress into the dielectrophoretic and electrostriction components in the Moving Mesh model can show the significance of each in this model. The components of the EHD force are shown in Figure 4.8 with the total EHD stress in the y-direction, T_{sy} . In this case

the dielectrophoretic component is larger than the electrostriction component by a factor of 2.5. This shows that both forces are significant to the overall EHD stress. The two components are also in the same direction so they both contribute to liquid extraction.

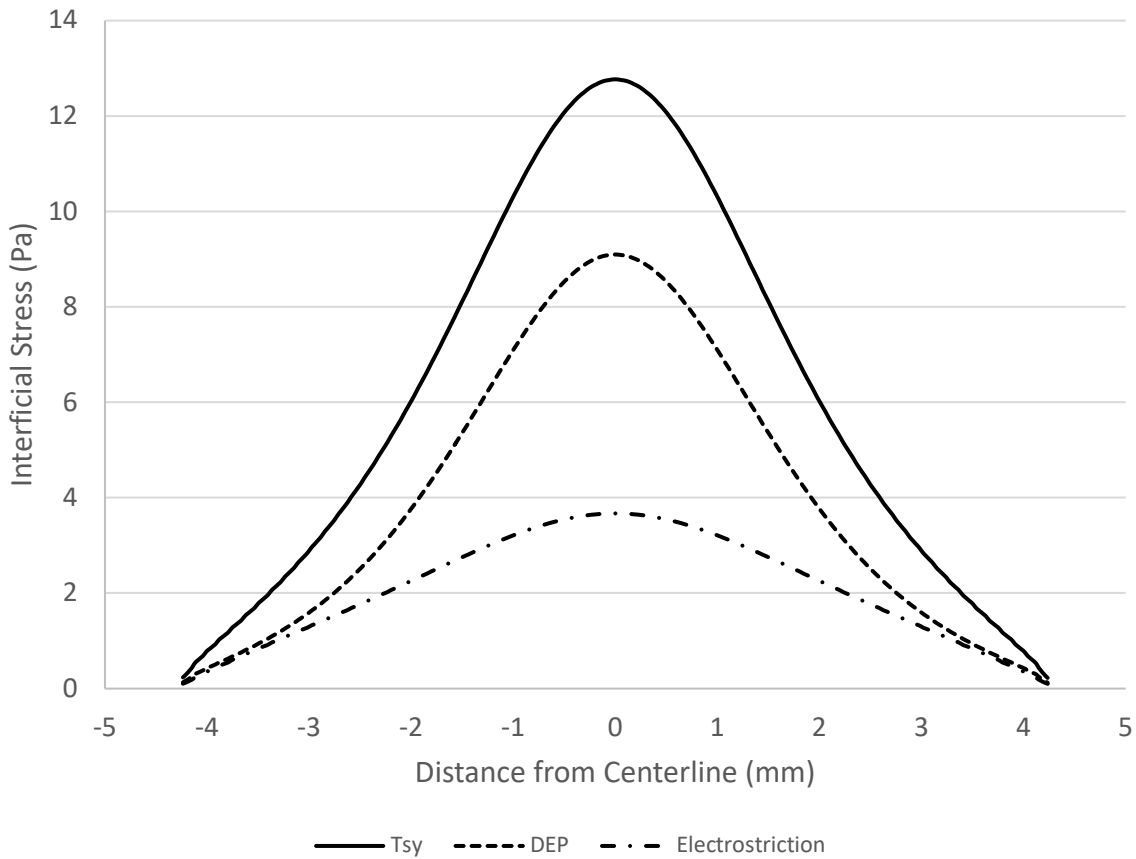


Figure 4.8: Breakdown of the EHD force components in the y-direction.

For the volume of fluids methods, the forces are calculated over a cut line shown in Figure 4.9. This is due to the force being highest above the initial interface and because the center of the domain, where the liquid extraction occurs, is of the most interest in this case. By positioning the cutline at the location of maximum stress in the center, the values are more accurate to what was found in Figure 4.8, but more points can be observed more efficiently. The cutline is at -3.1mm in the y-axis and extends from 0 to -1.4mm in the x-axis. The farther from

the centerline, the more deviation there will be from the true maximum force as the cut line does not conform to the interface and maximum stress location.

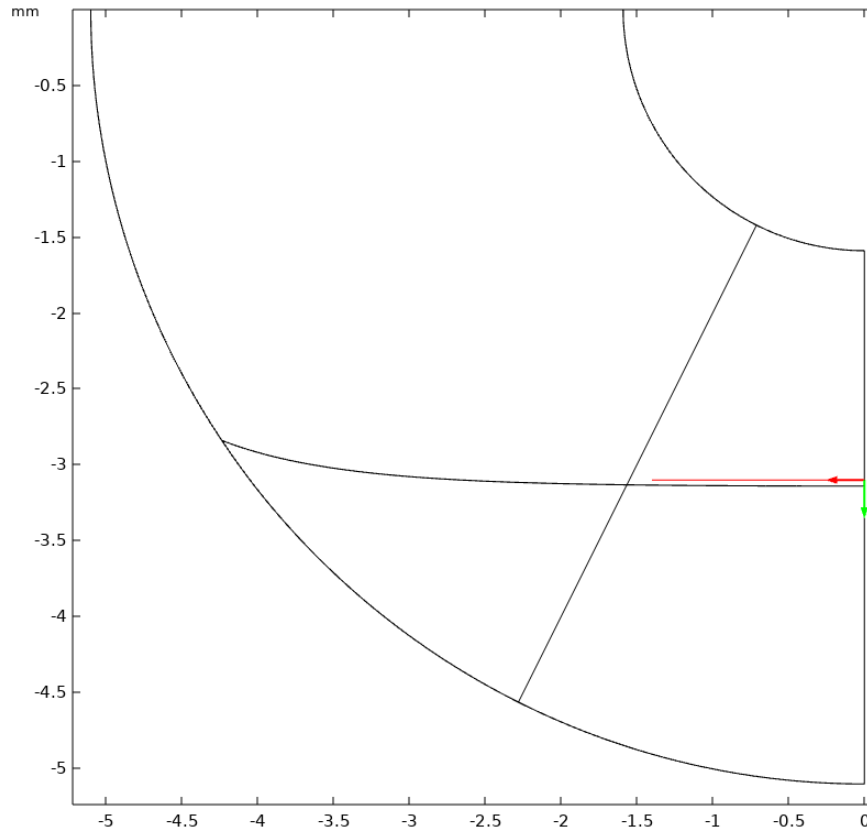


Figure 4.9: Cutline above the liquid-vapour interface where the volume of fluids forces are retrieved from.

Figure 4.10 shows the components of the force for the volume of fluids methods along the cutline. The dielectrophoretic force is larger than the electrostriction force in these cases as well but by less than the difference seen in the Moving Mesh model. The volume of fluid models show a comparable electrostriction force to that of the Moving Mesh model, but the main difference is that the dielectrophoretic force is lower. The cause of this can be attributed to the deformed electric field caused by the interface gradient. The electric field is skewed towards the vapour which means the interface will experience a smaller electric field difference on the

boundary and therefore less dielectrophoretic force. The values of the maximum force components are seen in Table 4.5. The center of the domain has some additional numerical error from the changing mesh elements to meet the center of the domain. The outlier points are not used in Table 4.5.

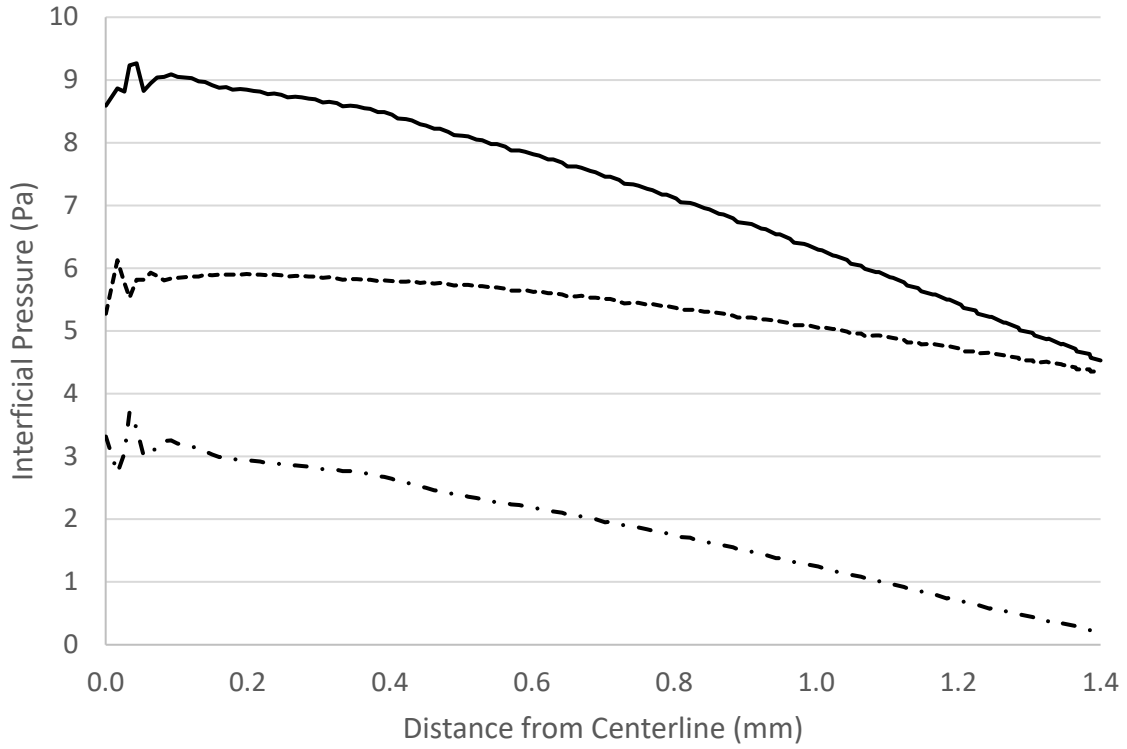
Table 4.5: Maximum EHD stress components for different modelling techniques. Outliers from numerical errors have been excluded.

Model	DEP (Pa)	Electrostriction (Pa)
Moving Mesh	9.0	3.6
Phase Field	5.8	3.2
Level Set	6.0	3.7

It is interesting to note that the electrostriction force in the Level Set model is higher than the Moving Mesh model. This is likely due to electrostriction pressure only present in the liquid portion of the domain due to the Clausius-Mossotti relationship having the term $(\epsilon_r - 1)$ which goes to zero in vapour as $\epsilon_r = 1$. In the volume of fluids cases, the fluid above the interface does not have a relative permittivity of 1 as it is a mixture of the two fluids and thus if the electric field gradient is higher in a region above the middle line, electrostriction can be larger.

This means that the region where the force is largest is likely due to trade-off between the two forces. As the region goes higher there is a higher gradient of electric field, but as electrical permittivity reaches 1 the electrostriction reduces. Considering that the electrostrictive force should not be in the vapour region at all this is not a physical result and means that the volume of fluids models will have some error associated with the force location.

(a)



(b)

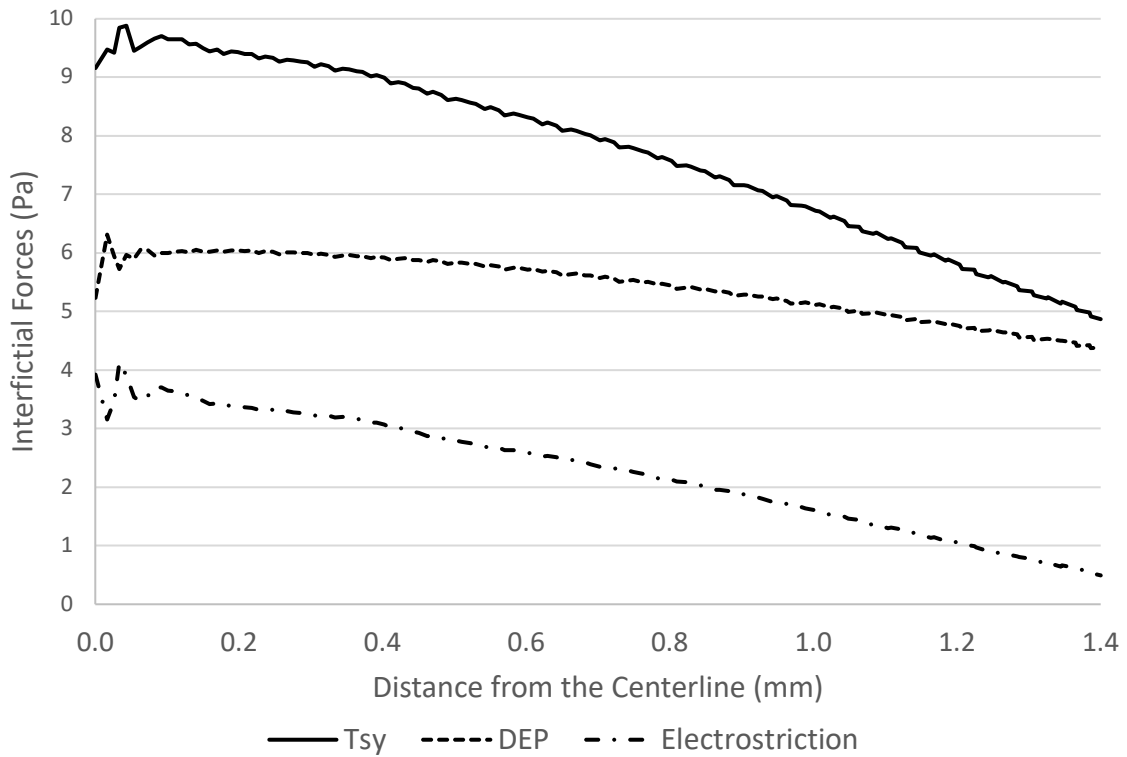


Figure 4.10: Breakdown of the EHD force into its components with different volume of fluids methods. Data was collected along outline found in Figure 4.9 (a) Phase Field, (b) Level Set.

Liquid Extraction Rising Time

The Moving Mesh, Phase Field, and Level Set models were set to run for 0.1 seconds as previous models concluded with a rise time of under 20ms. The Moving Mesh model, being unable to change its topology, was run until a failure occurred which was when the liquid column approached the electrode. The height of the volume of fluid models is said to be where the phase parameter is equal to a half. This represents an area where half the control volume is liquid, and the other half is vapour. The top of the liquid column's height is plotted versus time to see the rise time for the liquid extraction seen in Figure 4.11.

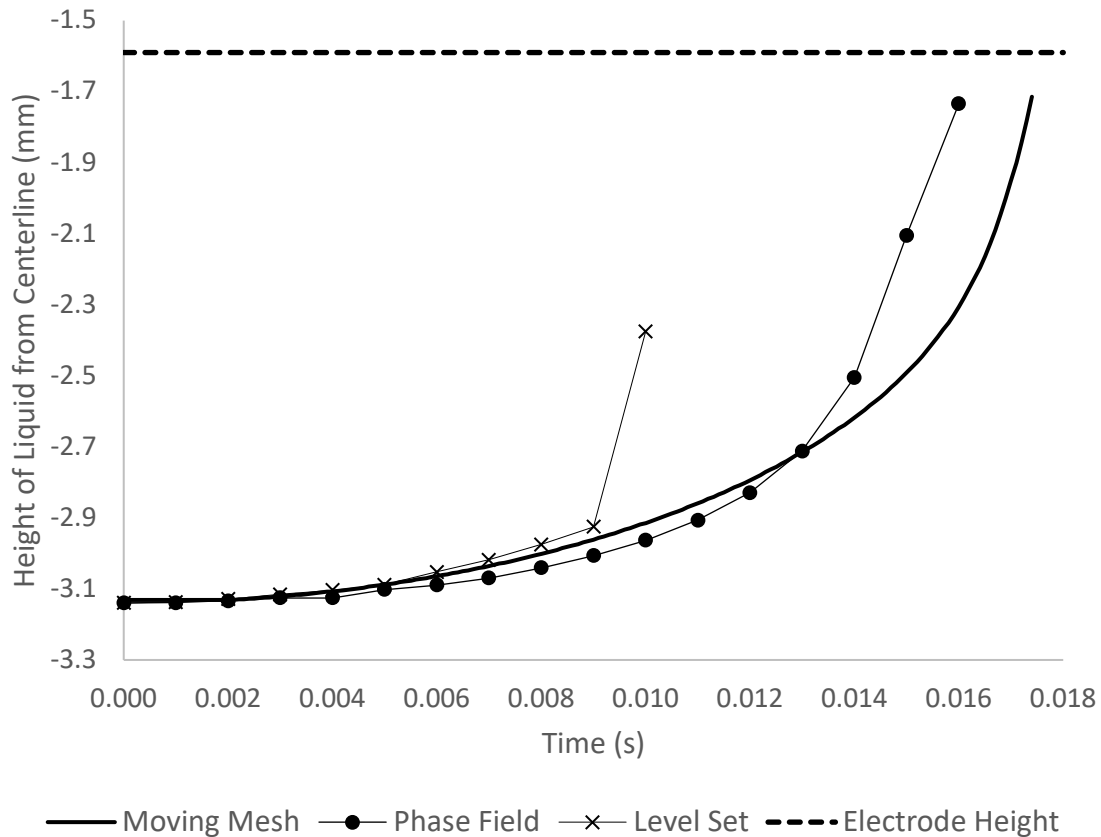


Figure 4.11: Rising time of the column of fluid being extracted by EHD forces. The base of the electrode is shown with a dotted line.

Table 4.6: *Liquid extraction times for Moving Mesh, Phase Field, and Level Set models.*

Model	Liquid Extraction Time (ms)
Moving Mesh	17.5
Phase Field	16.4
Level Set	10.5

The final liquid extraction times for all the models are shown above in Table 4.6.

Although the forces on the volume of fluid models were less than the Moving Mesh model, they had extraction times that were faster. This is due to the expansion of the interface reducing gradient forces including EHD and surface tension force. Figures 4.12 & 4.13 show the volume fraction of fluid in the Phase Field and Level Set model at various times. In Figure 4.12 (b), there is a region of above the interface that has a liquid component in it. This comes from the boundary expanding as the column rises. This may be caused by the body force being above the interface as seen in Figure 4.3.

The Phase Field model starts by underpredicting the column height before 12ms, but then rises faster than the Moving Mesh model. This is because, at first, the force is less than the Moving Mesh model, so it does not rise as quickly. After the interface expansion, the surface tension degrades, and it no longer holds the fluid down. The EHD force being applied to the interface causes the destabilization like in the Bubble Deformation study and causes a degradation of all forces that depend on the interface gradient.

The Level Set model performs similar to that of the Phase Field model except in the first region it slightly over predicts the column height. This is due to the reduction in interface compared to the Phase Field and the force being applied above the interface resulting in higher electrostrictive forces. Just after 9ms, surface tension completely breaks causing a jet of fluid to

rise to the interface in less than 2ms. This model's flow pattern is completely different than the other two and is not accurate to what would happen in this case.

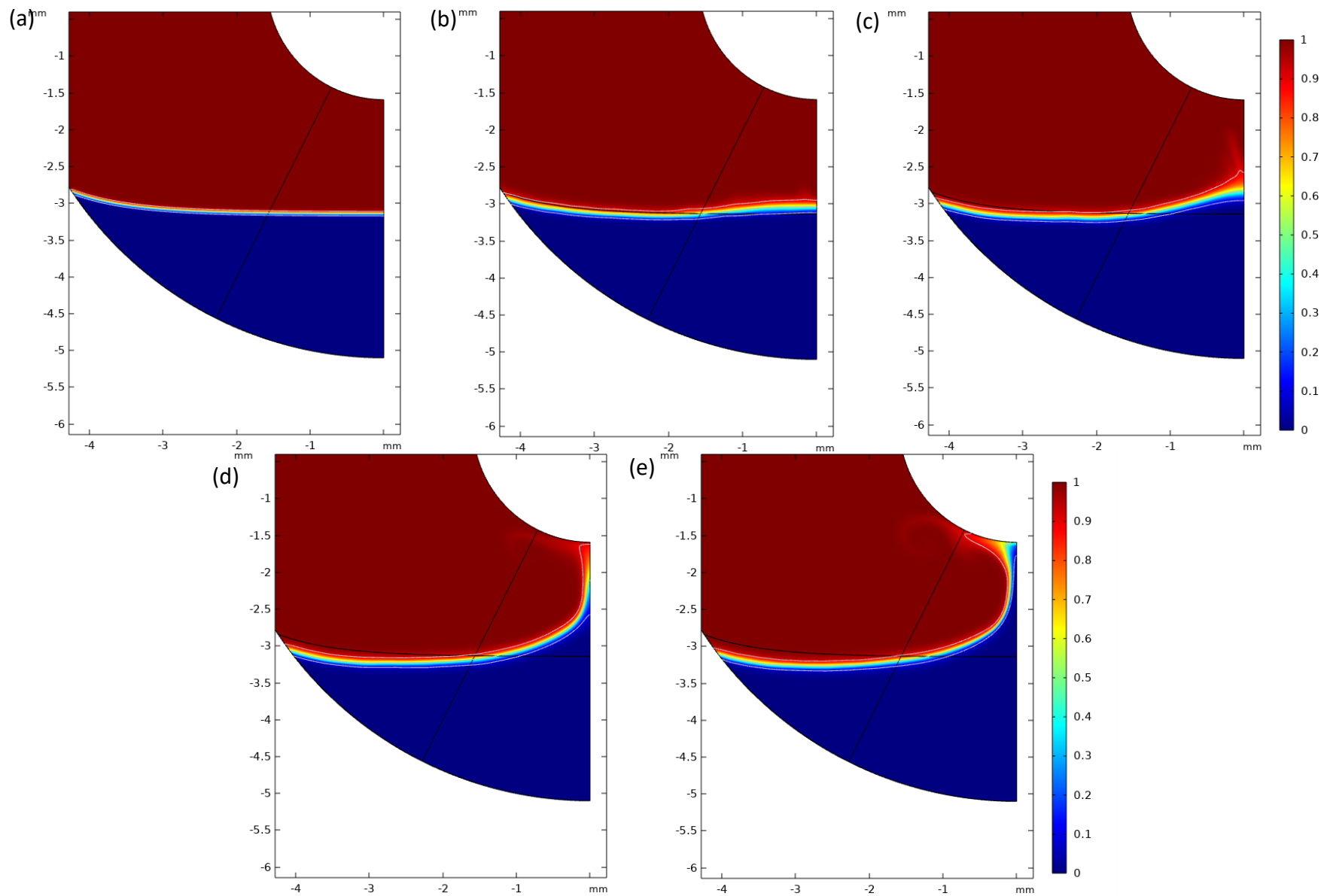


Figure 4.12: Volume fraction of air in the Phase Field model at various times (a) 0ms, (b) 8ms (c) 12ms (d) 15ms (e) 17ms.

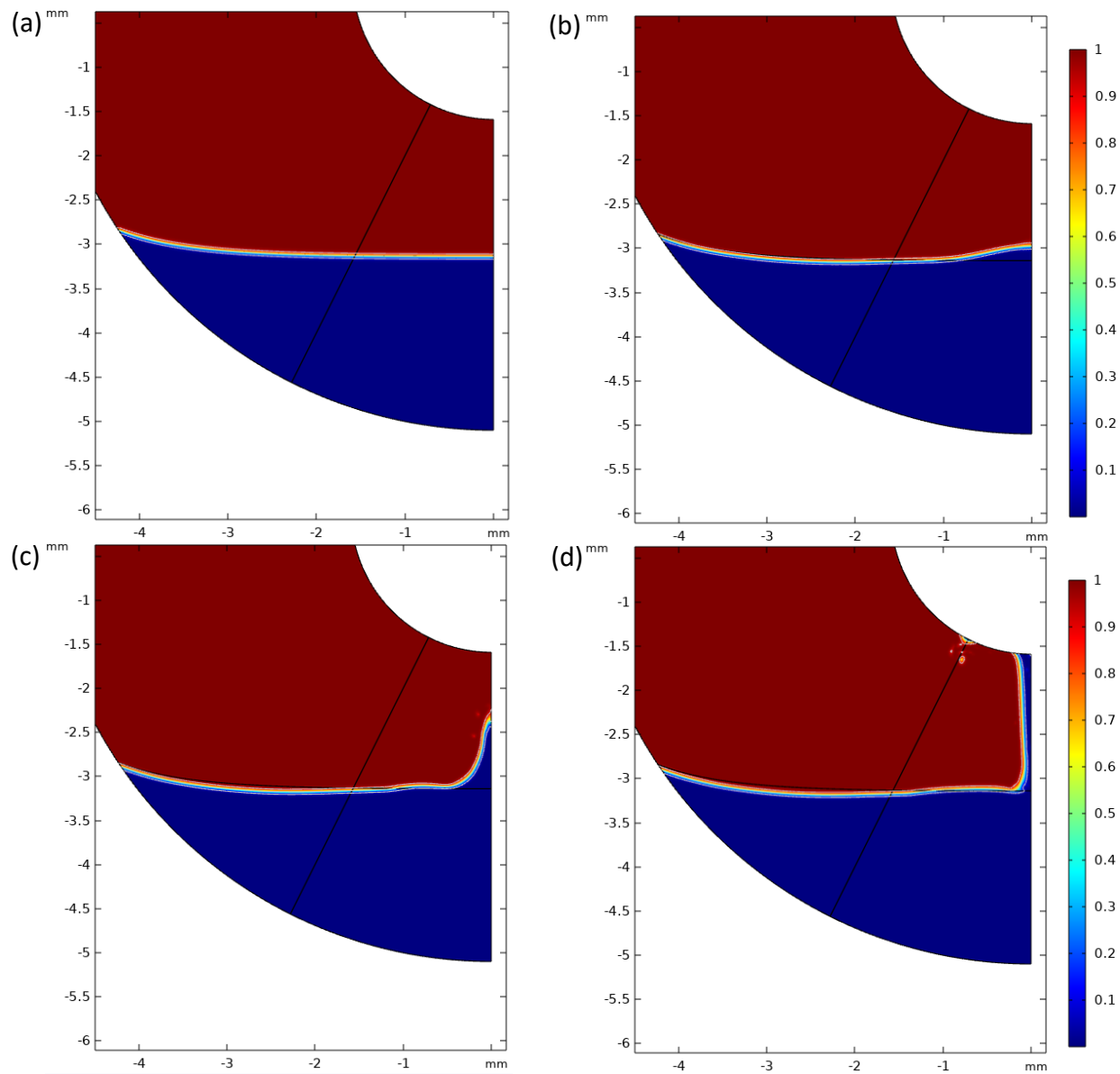


Figure 4.13: Volume fraction of air in the Level Set model at various times (a) 0ms (b) 8ms (c) 10ms (d) 11ms.

In Figure 4.13 (c) & (d), the boundary does not expand as much as in the Phase Field model, but surface tension is still lost. The Phase Field model had a reduction of both the EHD force and surface tension due to interface expansion whereas the Level Set model was able to continue the EHD force while the surface tension began to degrade. Because both models had force degradation, they have a lot of numerical error associated with them and thus cannot be completely trusted.

Although the forces are not comparable to the Moving Mesh model, the flow structure can be looked at to see if they are similar. Figures 4.14 and 4.15 show the interface of each modelling technique at different times. These graphs are expanded in the y-direction so that the lines are more separated. In Figures 4.14 and 4.15 the columns take a similar shape where there is a decrease in surface level on the outside as the peak rises in the center. At the final time the Phase Field model is higher and is touching the electrode, but the general shape is consistent.

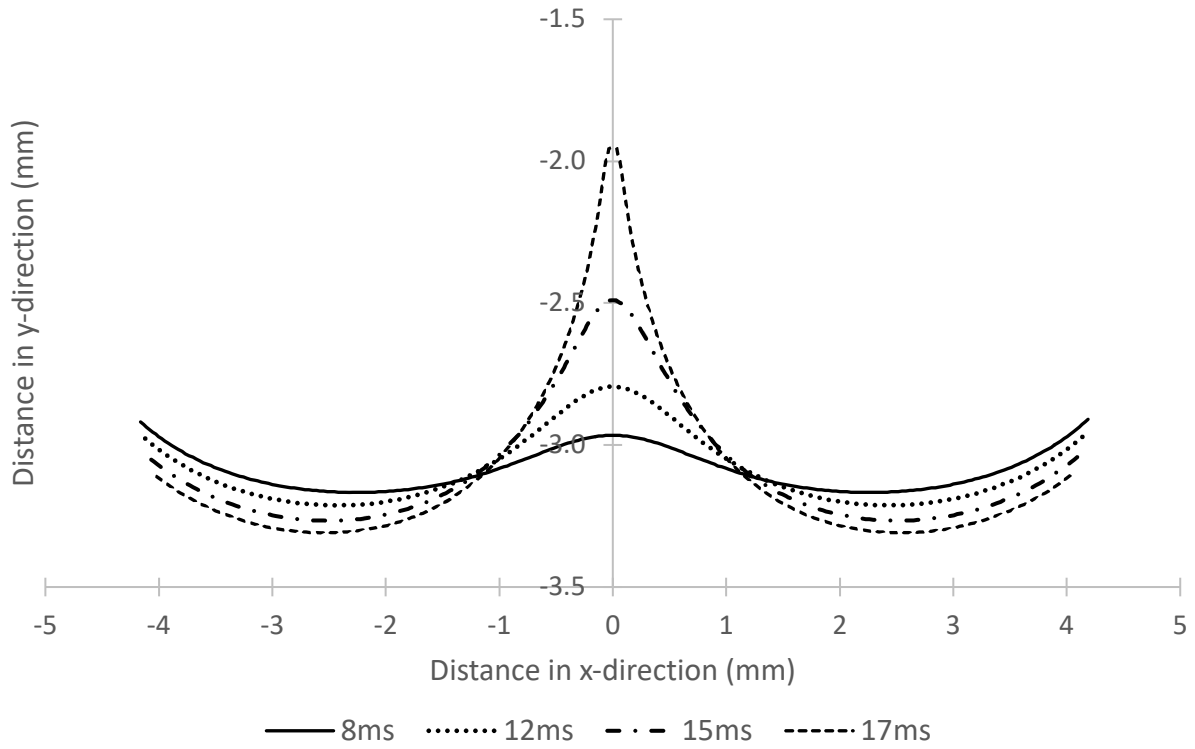


Figure 4.14: Shape of the liquid-vapor interface at various times in the Moving Mesh model.

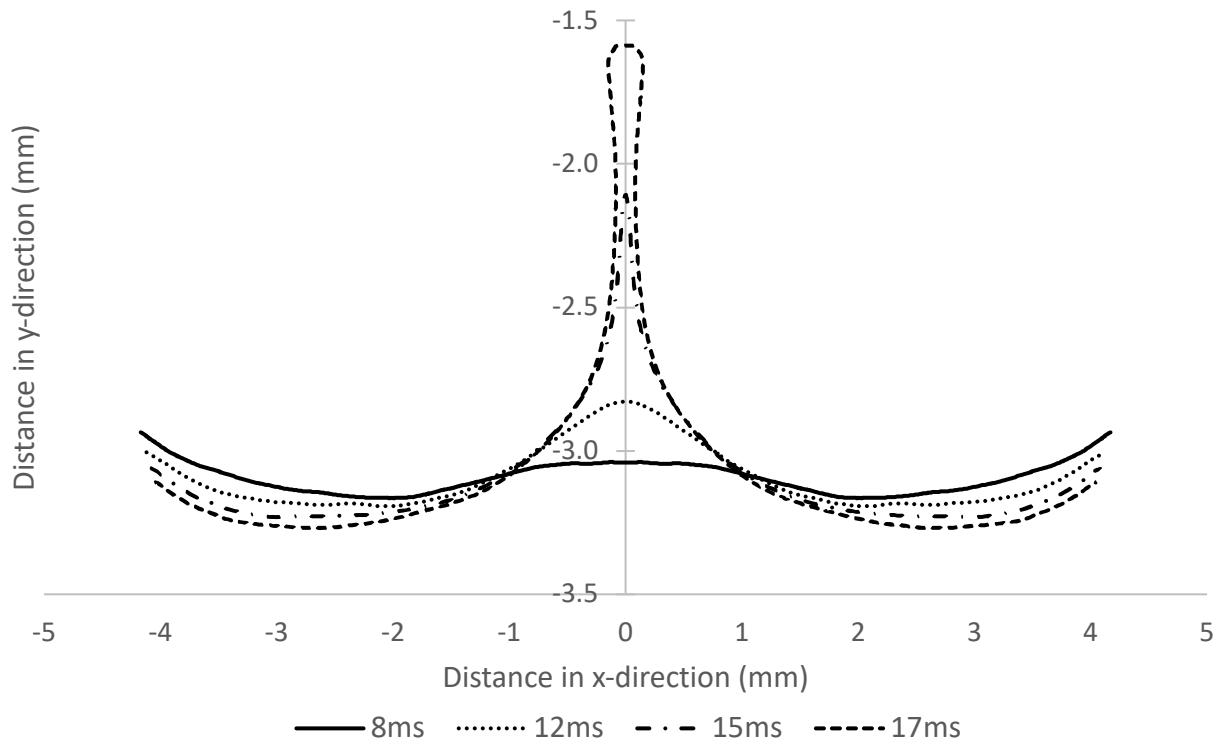


Figure 4.15: Shape of the liquid-vapor interface at various times in the Phase Field model.

Figure 4.16 is much different than the other two patterns. The outside fluid level barely lowers as the column rises and there is an inflection point on the 10ms and 12ms contour in the center. The surface of the fluid stays low until it gets to the column and then rises quickly instead of a smooth rise all the way from the outside seen in the other models. The Level Set model does not pull fluid to the center and up the column like the other cases, it makes a very narrow column with only the fluid in close proximity.

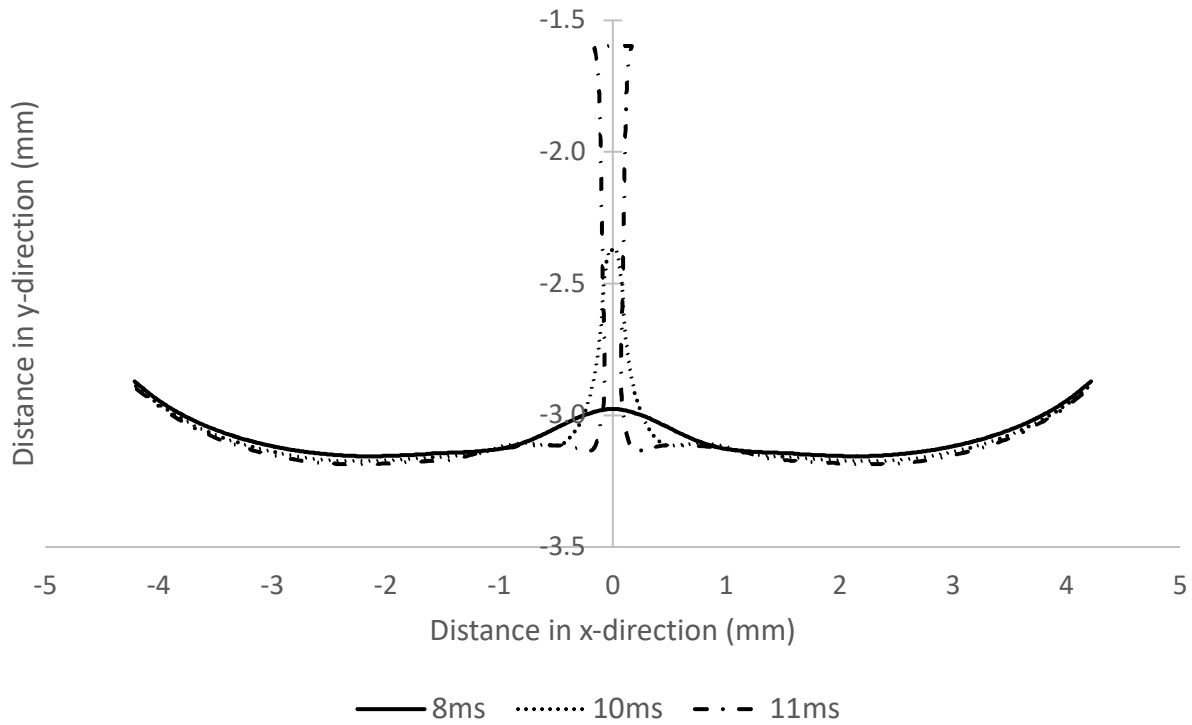


Figure 4.16: Shape of the liquid-vapor interface at various times in the Level Set model.

Comparing the shape of the interfaces at the same time is shown in Figures 4.17 to 4.20. The y-axis scale varies greatly in each of the graphs to show the small changes at each time. Not much movement is made in the first 8ms, so the first shape is taken at the 8ms time shown in Figure 4.17. The peak in the center is not very high but it shows that the Phase Field has a lower peak in the center, but the rest of the surface is similar. The difference is only 0.08mm but it

shows the interface is rounder than the Moving Mesh model. The Level Set model has a thin column already and the surface tension has broken down and has degraded to be insignificant. The full extraction only takes 10.5ms so this is the last time that it remains similar to the other models. The Level Set model is not included with the next graphs as it has already fully extracted.

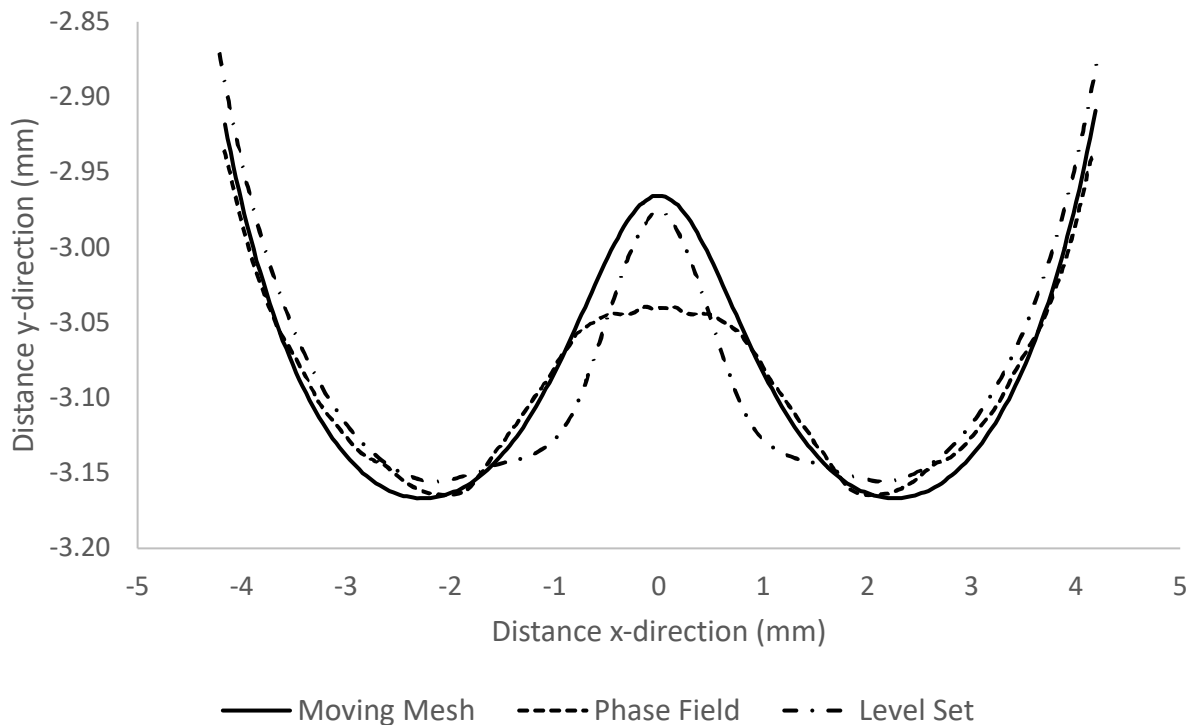


Figure 4.17: Comparison of the interface shape across the Moving Mesh, Phase Field, and Level Set models at 8ms.

At 12ms, the shape of the surface is similar in shape between the Moving Mesh and Phase Field models. The Phase Field is still slightly behind the Moving Mesh model with the outer regions being higher and the center being slightly lower than the moving mesh model. The thickness of the column is about the same between the models. At this point, the surface tension

and EHD force are reduced by approximately the same amount making the model rise similarly to the Moving Mesh model.

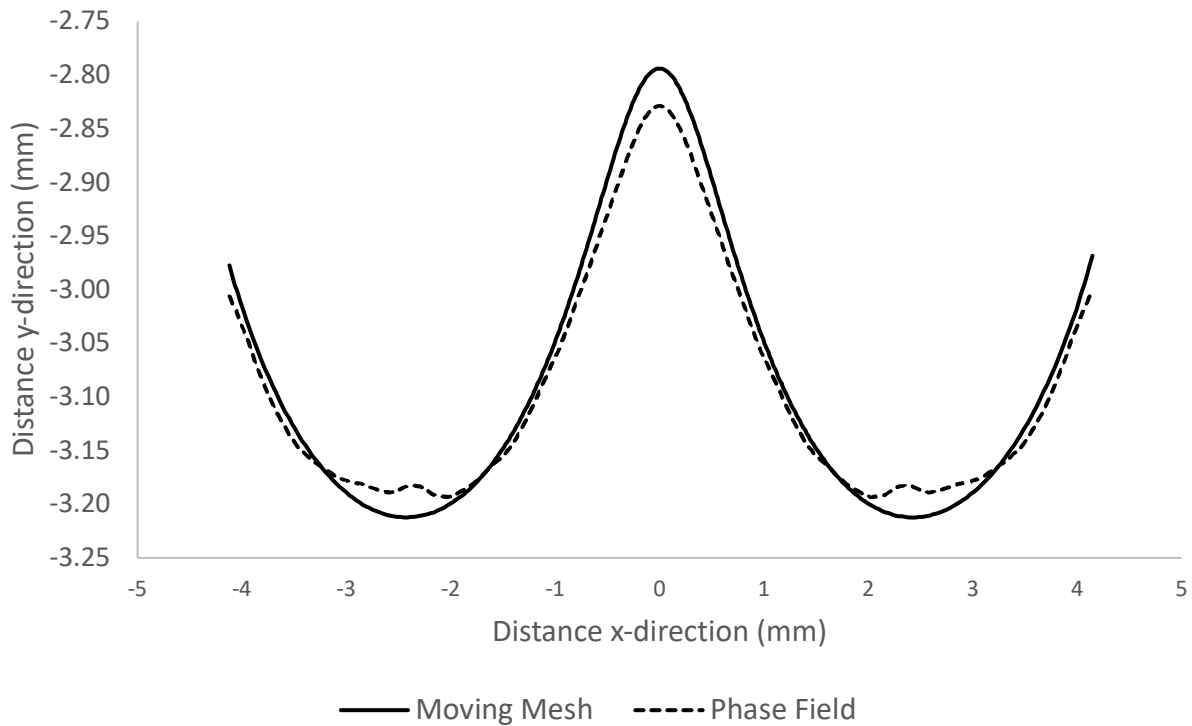


Figure 4.18: Comparison of the interface shape across the Moving Mesh and Phase Field models at 12ms.

Figures 4.19 & 4.20 show the departure of the two models at 15ms and 17ms. The Phase Field column is thinner than the Moving Mesh model. In Figure 4.14, the column in the Moving Mesh model does not get thinner as it rises, the thinning of the column is where the surface tension is degraded more than the EHD force. The Phase Field model's column grows thinner than the Moving Mesh model like the Level Set model before surface tension degraded. In Figure 4.20, the Phase Field model has already hit the electrode, so the top shape of the column is caused by the attachment to the electrode surface.

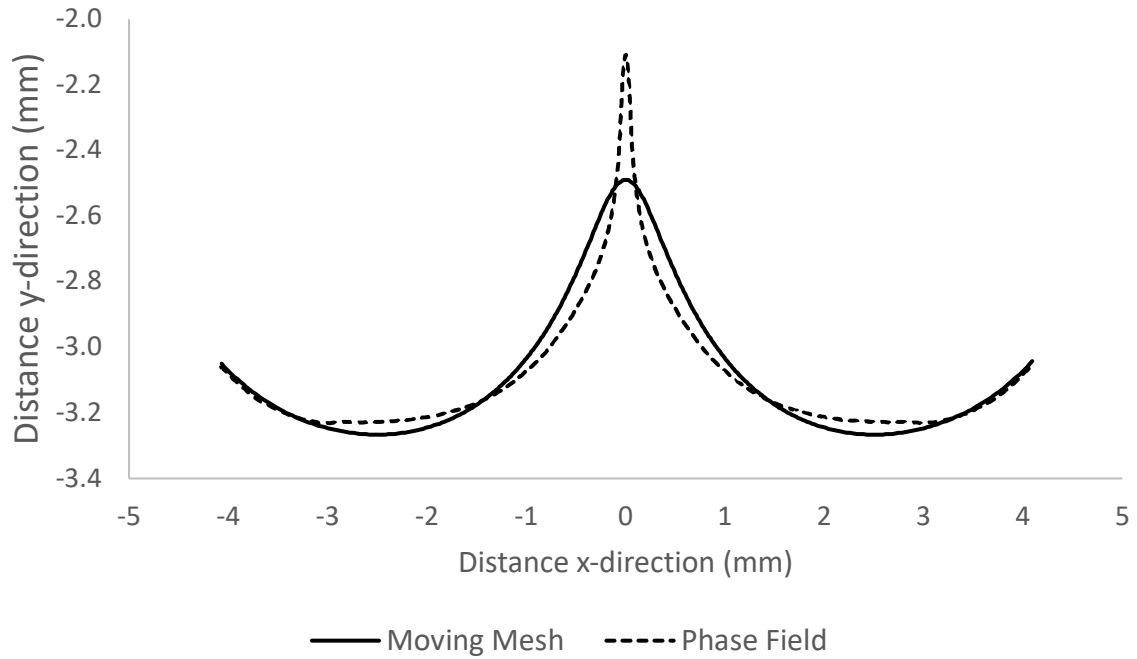


Figure 4.19: Comparison of the interface shape across the Moving Mesh and Phase Field models at 15ms.

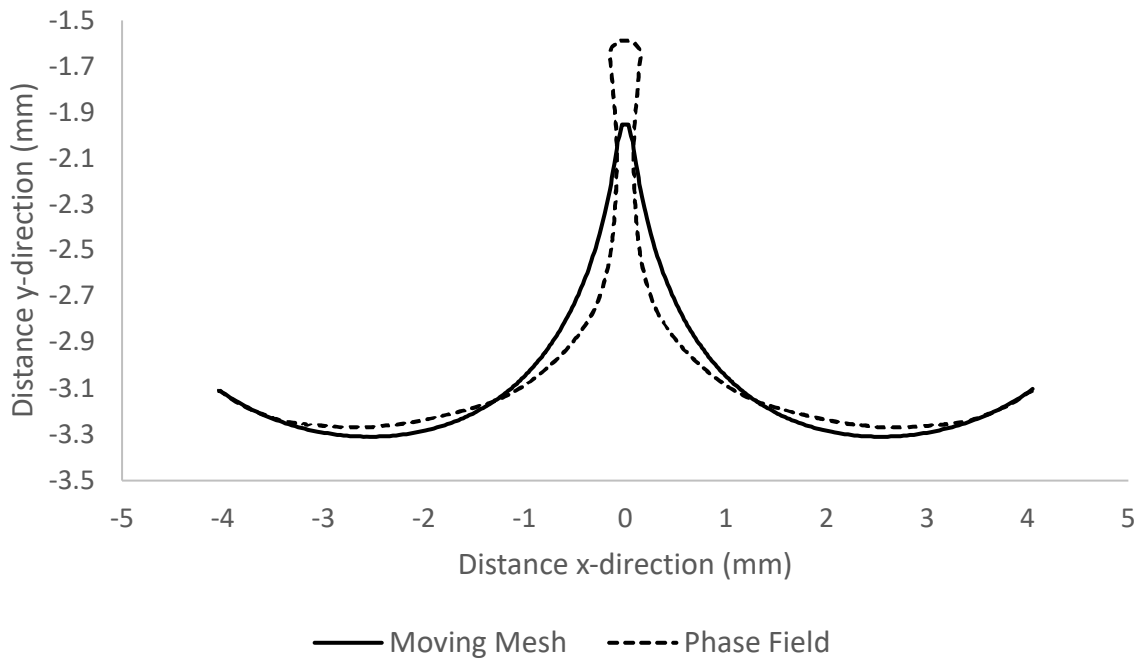


Figure 4.20: Comparison of the interface shape across the Moving Mesh and Phase Field models at 17ms.

Comparison with Previous Works

Experiments done by Sadek et al., 2012, showed that the liquid extraction timing was filmed to be 6.5 ± 0.5 ms. As previously stated in the introduction, this time used a method to determine the start of the electrode voltage that may be prone to unforeseen errors. The method to determine the start of the experiment was an image processing routine. This routine would have a defined interface line, and sample the mean grey pixel colour, 2 pixels above the interface line. The slope is also taken from the previous value to determine the change in pixel greyness. When the value passed 2 standard deviations of mean grey value and slope of mean grey value, the extraction is said to have begun.

The issue that arises is that the interface is captured from the side of a clear pipe and, in the models of the liquid extraction shown in this chapter, there is a rise at the edge making the center lower than that at the pipe wall due to the initial capillary rise caused by surface tension. This means that the column that is beginning to rise will be blocked from view and there will not be a change in gray value until the center exceeds the initial interface. Figure 4.21 shows the rise of the center column compared to the highest point at the edge of the pipe. If the initial interface line is defined from where the fluid is seen from a side view, the line will be at the height of the dotted line. If the experiment is said to have started at this time, 11.3ms, the rise time would be 6.2ms, which falls in the uncertainty of the camera.

Looking at the pixel data that Sadek et al. retrieved from the experiment, Figure 4.22, a decrease in mean grey occurred before the start was triggered. Two specific areas are of interest, one being the significant reduction in grey value at frames 34 to 40, and the other is the significant negative slope of grey value at frame 21.

The significantly negative values could be an indication of where the outside edge and the center column are at the same height. This is when the level seen from the side is at the lowest. The best frame to represent this point would be the lowest grey value seen on frame 39. The surface heights intersect in Figure 4.21 at 9.9ms. The significant negative slope of grey value could be the actual start time of the experiment as the edge starts to lower. The start of the experiment would cause a reduction in mean grey and the initial departure could have a significant slope. If you use frame 21 as the actual start time, then the lowest grey value is after 18 frames or 9ms which accounting for the error due to the 2000fps of the camera on both the start and stop comes to a minimum grey value at 9 ± 1 ms which the numerical result predicted was 9.9ms. Also, the time to the observable start would be 24 frames which is 12 ± 1 ms which also fits with the numerical model which predicts 11.3ms. Data is collected in Table 4.7.

Table 4.7: Timing for significant events in the Moving Mesh model and the experimental work by Sadek et al., 2012. Sadek corrected row is how many frames after the voltage applied was said to occur.

Experiment	Center Rises Past Initial	Lowest Fluid Point	Voltage Applied
Sadek	Frame 45	Frame 39	Frame 21
Moving Mesh model	11.3ms	9.9 ms	0ms
Sadek corrected	24 frames / 12 ± 1 ms	18 frames / 9 ± 1 ms	0

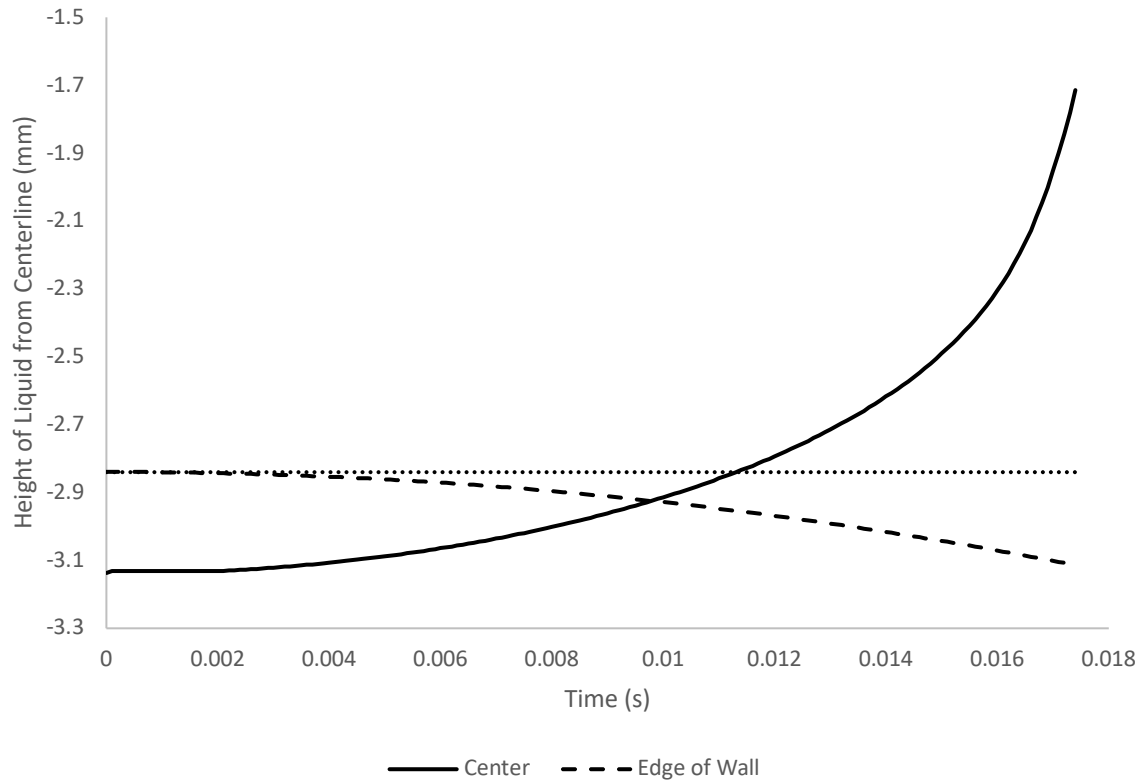
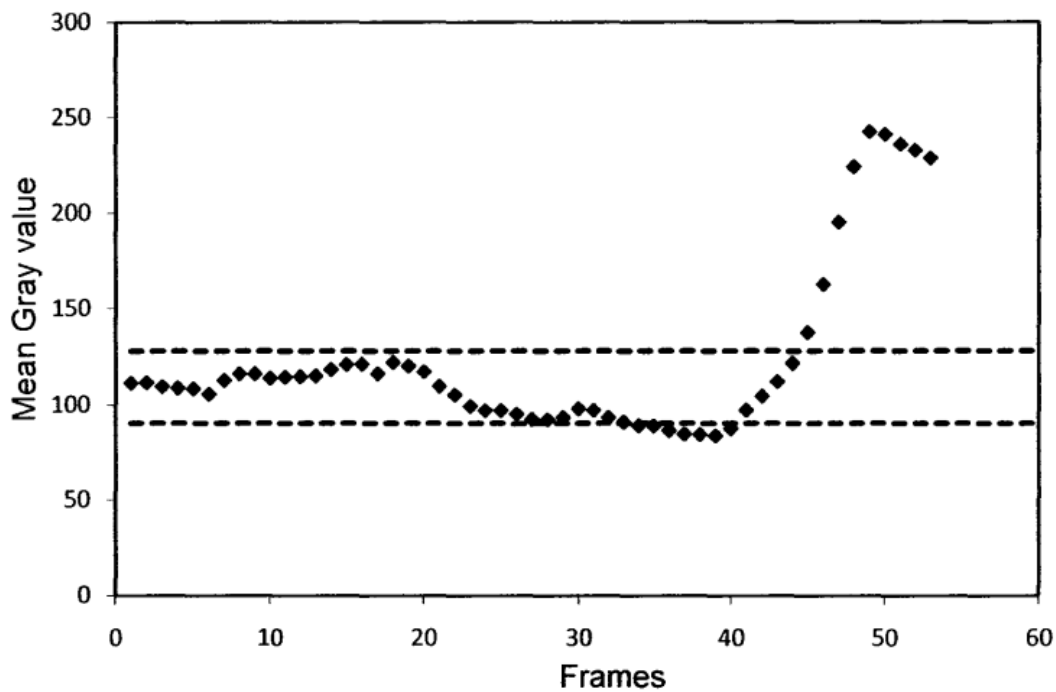
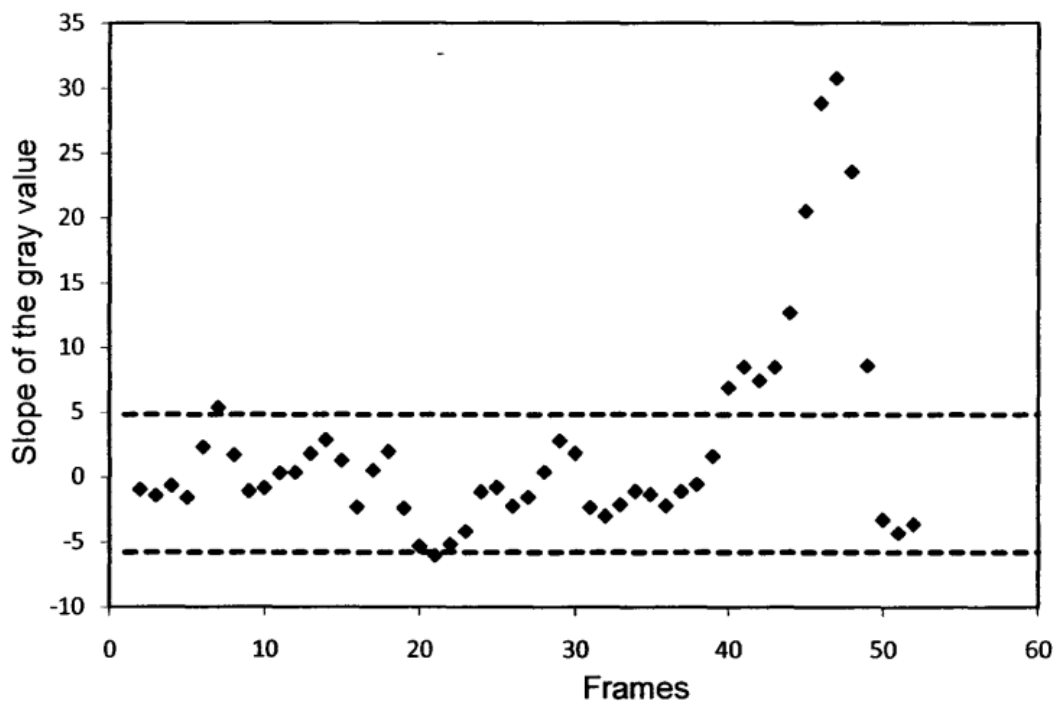


Figure 4.21: Fluid Levels at the center where liquid extraction occurs and at the edge of the domain where the contact angle rises the fluid. Dotted line represents the initial rise from surface tension.



(a)



(b)

Figure 4.22: Data collected by Sadek et al. 2012. (a) mean grey value (b) slope of mean grey value of the interface for different frames. Dotted lines show the ± 2 standard deviations.

A numerical method conducted by Nangle-Smith et al., 2012, used the same modelling software with the Moving Mesh and Level Set techniques. At the time of these models, the Moving Mesh numerics were unable to handle the circular geometry of the outer pipe so a square domain was instead used to estimate the extraction times. Figure 4.23 is the data from the numerical experiments conducted by Nangle-Smith et al.

It was found that the Level Set model showed a 25% reduction in extraction time unlike the decreased extraction time found in the model in this present work. A likely reasoning for this is that the reinitialization parameter in the model by Nangle-Smith et al. has a large value which suppresses phase advection. Increasing this value in the volume of fluids models makes the interface more stable but causes problems with time dependent studies. In the current investigation, the reinitialization and mobility numbers were tested and a value that had the best balance between advection and interface stability was chosen. As the column rose, the EHD force increases and there is more instability on the boundary. A variable weighting factor depending on EHD force might lead to a more stable interface without suppressing advection.

The rising time for the Moving Mesh models both have a comparable value. The value from Nangle-Smith et al.'s Moving Mesh model was 17.4ms which compared to the 17.5ms found in this present study has only a 0.6% error. They continued to estimate the liquid extraction time with a circular geometry using the Level Set model and a correction factor found from the comparison of the two models in the square domain. This value of liquid extraction on a circular domain with the Level Set model and corrected with the previous experiments was approximately 11ms. This may have been the wrong approach as the volume of fluid method rising time is so dependent on the mobility number that it could give different results with slightly different geometries.

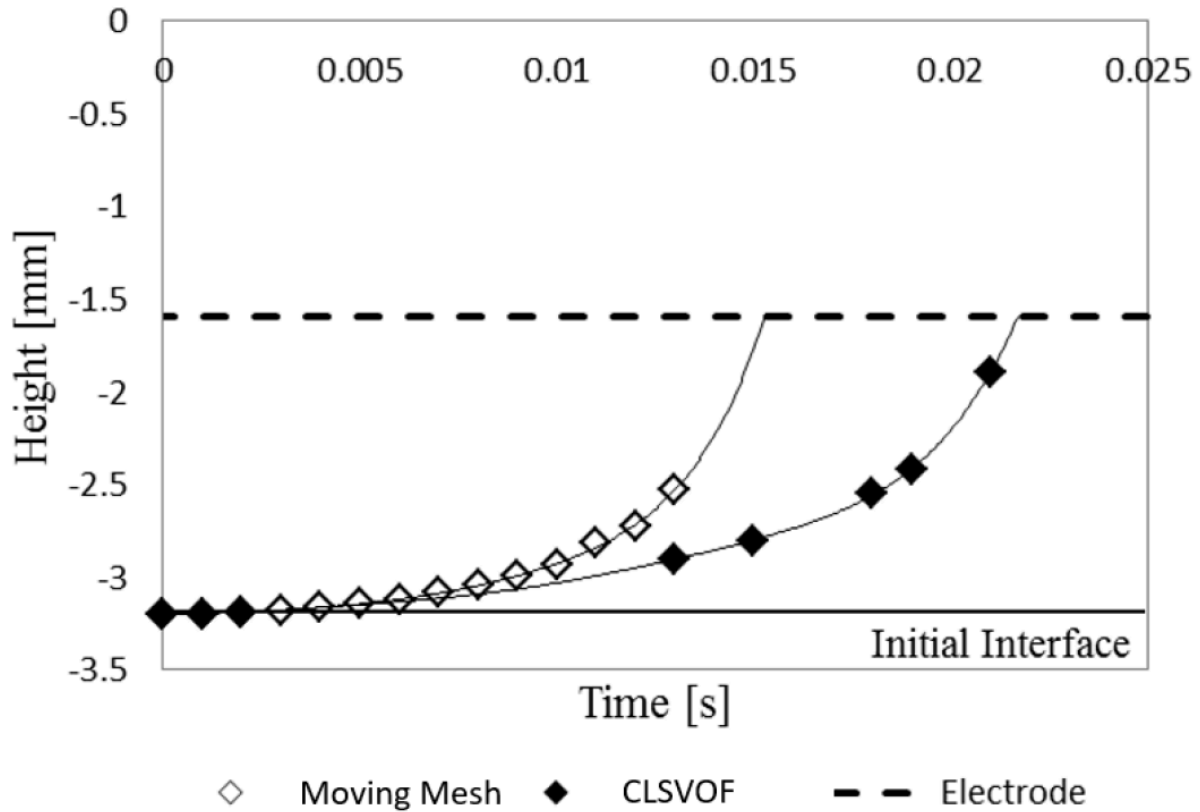


Figure 4.23: Height of the center of the fluid interface from numerical models performed by Nangle-Smith et al. 2012 [62].

Steady State Result

Although the column is thinner than the Moving Mesh model the shape of the column exhibits similar flow pattern characteristics. This means that after the attachment to the electrode the Phase Field model can be continued and if the interface recovers the final steady state shape of the fluid could be of interest. The Phase Field model was continued for 200ms until a steady state was reached. Simulating the topological change is only possible from the volume of fluid methods and shows why they should be improved further.

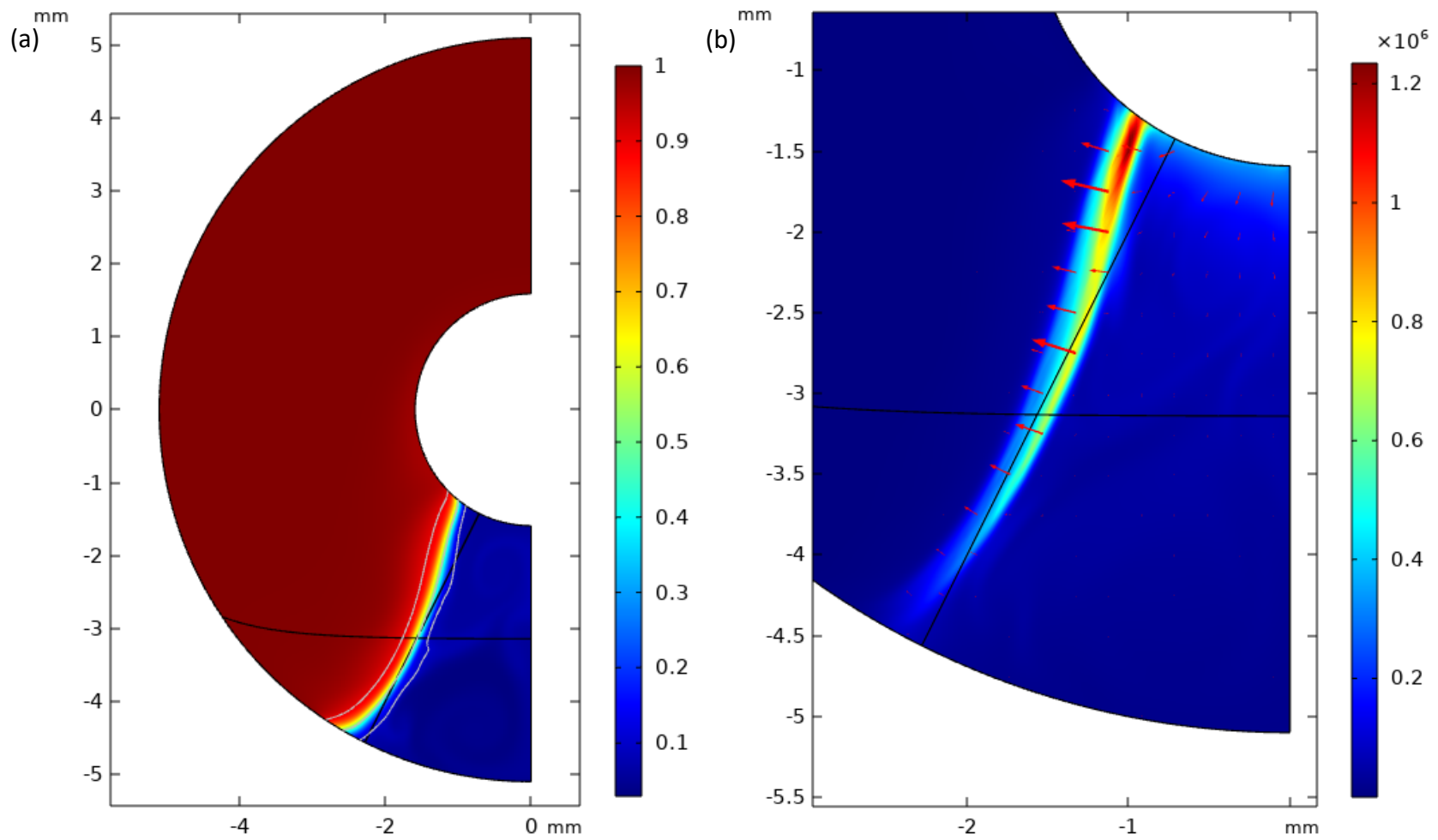


Figure 4.24: Results for the Phase Field model at steady state. (a) fluid fraction of vapour (b) body force magnitude in N/m^3 with proportional arrows.

Figure 4.24 shows the steady state fluid fraction and the forces on the boundary. After the liquid column contacted the electrode, it grew until it became this shape. Surface tension from the electrode helps to keep the fluid up and the body force pushes the boundary outwards to prevent necking. This structure is not seen in experiments due to three dimensional effects that would also occur.

Conclusions

A 2D adiabatic model was conducted to model liquid extraction in a circular pipe with a concentric electrode. Two segregated volume of fluids approaches, and one fully coupled interface tracking method were compared. Previous experimental and numerical work were also compared to the models performed in this study.

The previously validated Moving Mesh model had the slowest extraction time compared to the volume of fluid methods. The volume of fluids methods had interface expansion which degraded the surface tension force and lead to premature liquid extraction. It was found that the Moving Mesh model had the most trusted extraction as the infinitesimal interface was able to better estimate EHD and surface tension forces.

Comparing to the experiments conducted with liquid extraction, the Moving Mesh model had good agreement with the experiment as various significant points in the experimental data matched that estimated by the model. The volume of fluid models compared with previous work show that the advection to diffusion weighting parameter can change the results significantly and improvements should be made to make it less user dependent.

Chapter 5 - Summary and Conclusions

Two-phase EHD is a multi-physics problem which encompasses fluid dynamics, electrostatics, phase fields, and sometimes heat transfer. Modelling two-phase flows is difficult as it adds interactions between multiple fluids like surface tension, diffusion, and advection and when EHD forces are applied they can destabilize the current models used in two-phase cases. The EHD forces that are predominantly found in two-phase cases are the dielectrophoretic and electrostrictive components due to the large electrical permittivity change between the liquid and gas phases. As the permittivity change is located at the interface, which is infinitesimally small, certain modelling techniques have trouble maintaining a thin interface with the EHD force applied.

In this study, three two-phase flow modelling techniques were tested in the software package COMSOL. One of the methods was an interface tracking method that used mesh deformation to separate the two fluid domains, called the Moving Mesh model. The other two methods were volume of fluid methods that use a phase parameter that can experience advection and diffusion in the domain. The first model is the Phase Field model, which uses Hillard-Cahn diffusion to physically represent the diffusion term in the phase field. The other model is the Level Set model, which uses an artificial term that acts to decrease the thickness of the interface. These models were adapted to couple an electrostatics module by creating a surface pressure on the interface in the Moving Mesh model, and a body force in the Phase Field and Level Set models.

In Chapter 3, the three models were used to model a bubble undergoing a deformation due to EHD. The initial EHD force showed the volume of fluids methods had a reduction of EHD force compared to the Moving Mesh model. Breaking the EHD force into its components

showed that the dielectrophoretic and electrostrictive forces were equally important and of similar magnitude. Previous investigations suggested that the electrostriction forces were negligible. The Phase Field model had bubble detachment due to interface expansion degrading the surface tension force and the Level Set model experienced phase infiltration which caused the model not to converge. The Moving Mesh model was able to show the full bubble deformation at 20kV and when compared to the experiment there was good agreement with a maximum error of 0.007mm. The Moving Mesh model was found to have the best agreement with the experimental data between the models tested. It was shown that interface stability is crucial in volume of fluids methods as forces dependent on the gradient of the interface critically deteriorate when EHD forces destabilize the boundary.

In Chapter 4, the three models were used in an EHD liquid extraction case. Initial force comparison showed the volume of fluids model undercalculated the EHD force similar to the air bubble case presented in Chapter 3 and comparing the components of the EHD force showed that electrostriction was significant in this geometry as well. The volume of fluid models, Phase Field and Level Set models, extracted the fluid faster than the Moving Mesh model due to surface tension reduction from expanding interface thickness. In the Level Set case, the surface tension was completely deteriorated, and extraction was very fast after the interface expanded but the Phase Field maintained a relatively thin interface and, although it underpredicted the extraction time, the flow structure was similar to the Moving Mesh model. Previous experiments to find liquid extraction timing were investigated but with the new knowledge of how surface tension affects the fluid structure, the data was interpreted a different way that matched the results from the Moving Mesh model. The Phase Field model was continued until a steady state structure was found. This steady state structure is likely affected by 3D effects and is not what is seen in liquid

extraction experiments but shows the capability of the volume of fluids models to undergo topological changes and produce results that the Moving Mesh model is incapable of.

The Bubble Deformation and Liquid Extraction models show that the Moving Mesh model was the best of the three models tested. The Moving Mesh model accurately calculates the EHD force and maintains a stable fluid interface. It was the only model that was able to match both experimental results which shows its agreement in force balance with the steady state bubble and transient flows with a time-based liquid extraction model. The Moving Mesh model fails after the column reaches the electrode in the liquid extraction model which shows the importance of the other models in cases that require topological change throughout the model.

5.1 Recommendations for Future Work

This study showed that numerical modelling of cases with EHD forces have promising results when compared with experimental work. The modelling, as of now, is case specific and therefore there is room for improvement in implementation of EHD in the current models used and to develop better more robust two-phase models capable of EHD force.

This study showed that the Moving Mesh model was a very good approach in modelling 2D adiabatic cases involving EHD. Other interface tracking methods should be compared to it to find if there are cases that would benefit from a different interface tracking approach. Methods of reinitializing models after topological change that minimize error can be investigated or a method to allow for topological change.

Volume of fluids methods were found to be case dependent and unstable when it came to the EHD force on the boundary. The factor that weighs the phase advection to the diffusion of phase (mobility and reinitialization parameter) is user dependent which can lead to a large error

in time dependent cases like liquid extraction. Work to try and stabilize the boundary when more surface forces are applied should be investigated or a way to vary that parameter base on EHD force to ensure that advection is not suppressed when the EHD force is lower.

Diabatic and 3D systems are yet to be properly investigated due to their complexity and computational demand. In such two-phase systems, proper boiling and condensing models can be applied to show heat transfer enhancement of EHD. With three-dimensional modelling, there could be new flow structures that are made that are more consistent with the experiments that have been conducted. Also, the effect of EHD on two-phase flow can be studied with implementation of 3D heat transfer.

References

- [1] J. S. Cotton, “Numerical simulation of electric field distributions in electrohydrodynamic two-phase flow regimes,” *IEEE Trans. Dielectr. Electr. Insul.*, vol. 10, no. 1, pp. 37–51, 2003.
- [2] S. Nangle-Smith and J. S. Cotton, “A mechanistic approach to developing two phase flow pattern transition maps for two-phase dielectric fluids subject to high voltage polarization,” *Int. J. Heat Mass Transf.*, vol. 127, pp. 1233–1247, Dec. 2018, doi: 10.1016/j.ijheatmasstransfer.2018.06.076.
- [3] S. Siedel, S. Cioulachtjian, A. J. Robinson, and J. Bonjour, “Bubble Distortion due to EHD Stress,” p. 7, 2013.
- [4] J. Zhang, X. Luo, Z. Feng, and F. Guo, “Effects of pin and wire electrodes on flow boiling heat transfer enhancement in a vertical minichannel heat sink,” *Int. J. Heat Mass Transf.*, vol. 136, pp. 740–754, Jun. 2019, doi: 10.1016/j.ijheatmasstransfer.2019.03.043.
- [5] P. Di Marco, R. Kurimoto, G. Saccone, K. Hayashi, and A. Tomiyama, “Bubble shape under the action of electric forces,” *Exp. Therm. Fluid Sci.*, vol. 49, pp. 160–168, Sep. 2013, doi: 10.1016/j.expthermflusci.2013.04.015.
- [6] S. Nangle-Smith, H. Sadek, C. Y. Ching, and J. S. Cotton, “Numerical Modeling of EHD-Induced Liquid Extraction in a Cylindrical Electrode Configuration,” p. 7, 2016.
- [7] H. Sadek, “Electrohydrodynamic control of convective condensation heat transfer and pressure drop in a horizontal annular channel,” McMaster University, Hamilton ON, Canada, 2009.

- [8] M. R. Pearson and J. Seyed-Yagoobi, "Electrohydrodynamic Conduction Driven Single- and Two-Phase Flow in Microchannels With Heat Transfer," *J. Heat Transf.*, vol. 135, no. 10, p. 101701, Oct. 2013, doi: 10.1115/1.4007617.
- [9] K. Ng, "MECHANISMS OF ELECTROHYDRODYNAMIC TWO-PHASE FLOW STRUCTURES AND THE INFLUENCE ON HEAT TRANSFER AND PRESSURE DROP," p. 187.
- [10] J. S. Cotton, "Mechanics of Electrohydrodynamic (EHD) flow and heat transfer in horizontal convective boiling channels," McMaster University, Hamilton ON, Canada, 2000.
- [11] A. E. Bergles, "Recent developments in enhanced heat transfer," *Heat Mass Transf.*, vol. 47, no. 8, pp. 1001–1008, Aug. 2011, doi: 10.1007/s00231-011-0872-y.
- [12] S. Laohalertdecha, P. Naphon, and S. Wongwises, "A review of electrohydrodynamic enhancement of heat transfer," *Renew. Sustain. Energy Rev.*, vol. 11, no. 5, pp. 858–876, Jun. 2007, doi: 10.1016/j.rser.2005.07.002.
- [13] C. Qi, C. Min, S. Xie, and X. Kong, "Experimental Study of Fluid Flow and Heat Transfer in a Rectangular Channel with Novel Longitudinal Vortex Generators," *J. Enhanc. Heat Transf.*, vol. 17, no. 4, p. 11, 2010.
- [14] Z.-M. Xu and Z.-B. Zhang, "Experimental Investigation of the Applied Performance of Several Typical Enhanced Tubes," *J. Enhanc. Heat Transf.*, vol. 17, no. 4, p. 11, 2010.
- [15] N. Zuckerman and N. Lior, "Jet Impingement Heat Transfer: Physics, Correlations, and Numerical Modeling," in *Advances in Heat Transfer*, vol. 39, Elsevier, 2006, pp. 565–631. doi: 10.1016/S0065-2717(06)39006-5.

- [16] M. H. Mousa, N. Miljkovic, and K. Nawaz, "Review of heat transfer enhancement techniques for single phase flows," *Renew. Sustain. Energy Rev.*, vol. 137, p. 110566, Mar. 2021, doi: 10.1016/j.rser.2020.110566.
- [17] W. K. H. Panofsky and M. Phillips, *Classical Electricity and Magnetism*, Second Edition. Mineola, New York: Dover Publications, Inc., 1962.
- [18] J. S. Chang and A. Watson, "Electromagnetic Hydrodynamics," *IEEE Trans. Dielectr. Electr. Insul.*, vol. 1, no. 5, pp. 871–895, Oct. 1994.
- [19] P. Di Marco, "The Use of Electric Force as a Replacement of Buoyancy in Two-phase Flow," *Microgravity Sci. Technol.*, vol. 24, no. 3, pp. 215–228, Jun. 2012, doi: 10.1007/s12217-012-9312-y.
- [20] J. Cotton, A. J. Robinson, M. Shoukri, and J. S. Chang, "A two-phase flow pattern map for annular channels under a DC applied voltage and the application to electrohydrodynamic convective boiling analysis," *Int. J. Heat Mass Transf.*, vol. 48, no. 25–26, pp. 5563–5579, Dec. 2005, doi: 10.1016/j.ijheatmasstransfer.2005.05.032.
- [21] Y. Feng and J. Seyed-Yagoobi, "Control of adiabatic two-phase dielectric fluid flow distribution with EHD conduction pumping," *J. Electrostat.*, vol. 64, no. 7–9, pp. 621–627, Jul. 2006, doi: 10.1016/j.elstat.2005.10.034.
- [22] R. D. Selvakumar, D. Zhonglin, and J. Wu, "Heat transfer intensification by EHD conduction pumping for electronic cooling applications," *Int. J. Heat Fluid Flow*, vol. 95, p. 108972, Jun. 2022, doi: 10.1016/j.ijheatfluidflow.2022.108972.
- [23] Y. Liao, Z. Feng, and X. Zhou, "Predicting the pumping effects of electrohydrodynamic (EHD) gas pumps by numerical simulations and quantitative pressure drop vs. flow rate curves," *J. Electrostat.*, vol. 96, pp. 160–168, Dec. 2018, doi: 10.1016/j.elstat.2018.10.014.

- [24] J. Mizeraczyk and A. Berendt, "Introduction to investigations of the negative corona and EHD flow in gaseous two-phase fluids," *Plasma Sci. Technol.*, vol. 20, no. 5, p. 054020, May 2018, doi: 10.1088/2058-6272/aab602.
- [25] M. Huang and F. C. Lai, "Numerical study of EHD-enhanced water evaporation," *J. Electrostat.*, vol. 68, no. 4, pp. 364–370, Aug. 2010, doi: 10.1016/j.elstat.2010.05.003.
- [26] Sarah Nangle-Smith, "Performance of EHD assisted convective boiling heat exchangers utilizing dielectric fluids," McMaster University, Hamilton ON, Canada, 2018.
- [27] T. Fujino, Y. Yokoyama, and Y. H. Mori, "Augmentation of Laminar Forced Convective Heat Transfer by the Application of a Transverse Electric Field," *J. Heat Transf.*, vol. 111, pp. 345–351, May 1989.
- [28] G. McGranaghan and A. J. Robinson, "EHD Augmented Convective Boiling: Flow Regimes and Enhanced Heat Transfer," *Heat Transf. Eng.*, vol. 35, no. 5, pp. 517–527, Mar. 2014, doi: 10.1080/01457632.2013.833054.
- [29] S. Nangle-Smith and J. S. Cotton, "Phenomenological correlations for two phase heat transfer and pressure drop performance of electrohydrodynamic horizontal convective boiling of dielectric fluids," *Int. J. Heat Mass Transf.*, vol. 132, pp. 1018–1028, Apr. 2019, doi: 10.1016/j.ijheatmasstransfer.2018.12.019.
- [30] M. Sheikholeslami and M. M. Bhatti, "Active method for nanofluid heat transfer enhancement by means of EHD," *Int. J. Heat Mass Transf.*, vol. 109, pp. 115–122, Jun. 2017, doi: 10.1016/j.ijheatmasstransfer.2017.01.115.
- [31] M. Nahavandi and A. Mehrabani-Zeinabad, "Numerical simulation of electrohydrodynamic effect on natural convection through a vertical enclosure channel:

- ELECTROHYDRODYNAMIC EFFECT ON NATURAL CONVECTION,” *Asia-Pac. J. Chem. Eng.*, vol. 8, no. 5, pp. 756–766, Sep. 2013, doi: 10.1002/apj.1719.
- [32] J. Ogata and A. Yabe, “Basic study on the enhancement of nucleate boiling heat transfer by applying electric fields,” *Int. J. Heat Mass Transf.*, vol. 36, no. 3, pp. 775–782, Feb. 1993, doi: 10.1016/0017-9310(93)80053-W.
- [33] H. Sadek, J. S. Cotton, C. Y. Ching, and M. Shoukri, “Effect of frequency on two-phase flow regimes under high-voltage AC electric fields,” *J. Electrostat.*, vol. 66, no. 1–2, pp. 25–31, Jan. 2008, doi: 10.1016/j.elstat.2007.08.008.
- [34] P. Hanafizadeh, S. Ahmadi, S. Zeraati, M. Gharahasanlo, and M. A. Akhavan-Behabadi, “Effect of external electrode arrangements on R-134a two-phase flow regimes in the presence of AC electric fields,” *Appl. Therm. Eng.*, vol. 122, pp. 503–514, Jul. 2017, doi: 10.1016/j.applthermaleng.2017.05.030.
- [35] S. R. Mahmoudi, K. Adamiak, and G. S. P. Castle, “On the Thermodynamic Description of Electrohydrodynamic Flows,” p. 12, 2012.
- [36] G. L. Wedekind, B. L. Bhatt, and B. T. Beck, “A system mean void fraction model for predicting various transient phenomena associated with two-phase evaporating and condensing flows,” *Int. J. Multiph. Flow*, vol. 4, no. 1, pp. 97–114, Mar. 1978, doi: 10.1016/0301-9322(78)90029-0.
- [37] F. J. Lesage, S. Siedel, J. S. Cotton, and A. J. Robinson, “A mathematical model for predicting bubble growth for low Bond and Jakob number nucleate boiling,” *Chem. Eng. Sci.*, vol. 112, pp. 35–46, Jun. 2014, doi: 10.1016/j.ces.2014.03.011.

- [38] R. K. Verma and S. Ghosh, “Two-Phase Flow in Miniature Geometries: Comparison of Gas-Liquid and Liquid-Liquid Flows,” *ChemBioEng Rev.*, vol. 6, no. 1, pp. 5–16, Feb. 2019, doi: 10.1002/cben.201800016.
- [39] F. Almasi, M. Hopp-Hirschler, A. Hadjadj, U. Nieken, and M. Safdari Shadloo, “Coupled Electrohydrodynamic and Thermocapillary Instability of Multi-Phase Flows Using an Incompressible Smoothed Particle Hydrodynamics Method,” *Energies*, vol. 15, no. 7, p. 2576, Apr. 2022, doi: 10.3390/en15072576.
- [40] H. J. Cho, I. S. Kang, Y. C. Kweon, and M. H. Kim, “Study of the behavior of a bubble attached to a wall in a uniform electric field,” *Int. J. Multiph. Flow*, vol. 22, no. 5, pp. 909–922, Sep. 1996, doi: 10.1016/0301-9322(96)00024-9.
- [41] Y. C. Kweon, M. H. Kim, H. J. Cho, and I. S. Kang, “Study on the deformation and departure of a bubble attached to a wall in d.c./a.c. electric fields,” *Int. J. Multiph. Flow*, vol. 24, no. 1, pp. 145–162, Feb. 1998, doi: 10.1016/S0301-9322(97)00044-X.
- [42] M. Yang and J. Yagoobi, “A Numerical Study of Liquid-Vapor Interface in the Presence of Dielectrophoretic Force,” in *2019 IEEE Industry Applications Society Annual Meeting*, Baltimore, MD, USA, Sep. 2019, pp. 1–5. doi: 10.1109/IAS.2019.8912460.
- [43] K. Luo, J. Wu, H.-L. Yi, and H.-P. Tan, “Numerical analysis of two-phase electrohydrodynamic flows in the presence of surface charge convection,” *Phys. Fluids*, vol. 32, no. 12, p. 123606, Dec. 2020, doi: 10.1063/5.0028635.
- [44] H. B. Zhang, Y. Y. Yan, and Y. Q. Zu, “Numerical modelling of EHD effects on heat transfer and bubble shapes of nucleate boiling,” *Appl. Math. Model.*, vol. 34, no. 3, pp. 626–638, Mar. 2010, doi: 10.1016/j.apm.2009.06.012.

- [45] P. Hanafizadeh, M. Gharahasanlo, S. Ahmadi, S. Zeraati, and M. A. Akhavan-Behabadi, “Numerical investigation of EHD effects on heat transfer enhancement and flow pattern of R-134a two phase flow,” *J. Electrostat.*, vol. 82, pp. 63–71, Aug. 2016, doi: 10.1016/j.elstat.2016.05.007.
- [46] H. Sadek, J. S. Cotton, and C. Y. Ching, “Numerical simulation of the liquid extraction from a stratified liquid-vapor zone using electrohydrodynamic effects,” in *International Symposium on Advances in Computational Heat Transfer*, Marrakesh, Morocco, 2008, pp. 1–15. doi: 10.1615/ICHMT.2008.CHT.2290.
- [47] K. Ng, “Mechanisms of Electrohydrodynamic Two-Phase Flow Structures and the Influence on Heat Transfer and Pressure,” McMaster University, Hamilton ON, Canada, 2010.
- [48] J. Ogata and A. Yabe, “Augmentation of boiling heat transfer by utilizing the EHD effect—EHD behaviour of boiling bubbles and heat transfer characteristics,” *Int. J. Heat Mass Transf.*, vol. 36, no. 3, pp. 783–791, Feb. 1993, doi: 10.1016/0017-9310(93)80054-X.
- [49] E. Olsson and G. Kreiss, “A conservative level set method for two phase flow,” *J. Comput. Phys.*, vol. 210, no. 1, pp. 225–246, Nov. 2005, doi: 10.1016/j.jcp.2005.04.007.
- [50] Q. Liu, A. T. Pérez, R. D. Selvakumar, P. Yang, and J. Wu, “Numerical analysis of electrohydrodynamic (EHD) instability in dielectric liquid-gas flows subjected to unipolar injection,” *Phys. Rev. E*, vol. 104, no. 6, p. 065109, Dec. 2021, doi: 10.1103/PhysRevE.104.065109.
- [51] COMSOL, “Microfluidics Module - User Guide.” COMSOL, 2018.
- [52] M. A. Mianmahale, A. Mehrabani-Zeinabad, M. H. Zare, and M. Ghadiri, “Single-bubble EHD behavior into water two-phase flow under electric-field stress and gravitational

- acceleration using PFM,” *Npj Microgravity*, vol. 7, no. 1, p. 6, Dec. 2021, doi: 10.1038/s41526-021-00134-y.
- [53] F. Chen, Y. Peng, Y. Z. Song, and M. Chen, “EHD behavior of nitrogen bubbles in DC electric fields,” *Exp. Therm. Fluid Sci.*, vol. 32, no. 1, pp. 174–181, Oct. 2007, doi: 10.1016/j.expthermflusci.2007.03.006.
- [54] Y. Q. Zu and Y. Y. Yan, “A numerical investigation of electrohydrodynamic (EHD) effects on bubble deformation under pseudo-nucleate boiling conditions,” *Int. J. Heat Fluid Flow*, vol. 30, no. 4, pp. 761–767, Aug. 2009, doi: 10.1016/j.ijheatfluidflow.2009.03.008.
- [55] A. Bateni, S. Laughton, H. Tavana, S. S. Susnar, A. Amirfazli, and A. W. Neumann, “Effect of electric fields on contact angle and surface tension of drops,” *J. Colloid Interface Sci.*, vol. 283, no. 1, pp. 215–222, Mar. 2005, doi: 10.1016/j.jcis.2004.08.134.
- [56] S. Siedel, S. Cioulachtjian, and J. Bonjour, “Experimental analysis of bubble growth, departure and interactions during pool boiling on artificial nucleation sites,” *Exp. Therm. Fluid Sci.*, vol. 32, no. 8, pp. 1504–1511, Sep. 2008, doi: 10.1016/j.expthermflusci.2008.04.004.
- [57] Z. Yan, C. Louste, J. Wu, and J. Fang, “Coupling characteristics of fluid and charge behaviors in an EHD wall jet produced by a surface dielectric barrier injection actuator,” *J. Electrostat.*, vol. 119, p. 103737, Sep. 2022, doi: 10.1016/j.elstat.2022.103737.
- [58] H. B. Chae, J. W. Schmidt, and M. R. Moldover, “Surface tension of refrigerants R123 and R134a,” *J. Chem. Eng. Data*, vol. 35, no. 1, pp. 6–8, Jan. 1990, doi: 10.1021/jc00059a002.
- [59] K. Stephan and M. Abdelsalam, “Heat-transfer correlations for natural convection boiling,” *Int. J. Heat Mass Transf.*, vol. 23, no. 1, pp. 73–87, Jan. 1980, doi: 10.1016/0017-9310(80)90140-4.

- [60] R. Thirumalaisamy, G. Natarajan, and A. Dalal, “Towards an improved conservative approach for simulating electrohydrodynamic two-phase flows using volume-of-fluid,” *J. Comput. Phys.*, vol. 367, pp. 391–398, Aug. 2018, doi: 10.1016/j.jcp.2018.04.024.
- [61] J. M. López-Herrera, S. Popinet, and M. A. Herrada, “A charge-conservative approach for simulating electrohydrodynamic two-phase flows using volume-of-fluid,” *J. Comput. Phys.*, vol. 230, no. 5, pp. 1939–1955, Mar. 2011, doi: 10.1016/j.jcp.2010.11.042.
- [62] S. Nangle-Smith, “The Effect of High Voltage Electric Fields on Two Phase Flow Pattern Redistribution & Heat Exchanger Performance,” M.A.Sc., McMaster University, Hamilton ON, Canada, 2012.

Appendix A - Independence Test for Bubble Deformation

Introduction

This appendix shows the mesh independence studies for the bubble deformation model seen in Chapter 3. The models consist of coupled fluid flow, electrostatic, and two-phase modules in COMSOL. Three different models are used including the Moving Mesh, Phase Field, and Level Set models. A ramp voltage was used to reduce momentum and made the models approach steady state so time dependent tests were all similar and will not be discussed.

Mesh Independence Study

As this model acts like it is in steady state at every timestep, the calculation of forces like surface tension, EHD, and buoyancy is important to predict the shape of the bubble. Mesh spacing is important in these models as the interface between the fluids has a gradient of electrical permittivity and density that creates the EHD and surface tension forces. This interface is often resolved over several nodes so reducing the mesh spacing acts to reduce the interface thickness.

Three maximum mesh spacings around the bubble were chosen to do an independence test on which include 0.008mm, 0.004mm, and 0.002mm. The models included larger mesh spacing farther from the bubble as there was only single-phase liquid under a small electric field. An example of the mesh is shown in Figure A.1. The volume of fluid models are run with an interface thickness of 50% of the maximum grid spacing as recommended by the COMSOL user guide to ensure convergence.

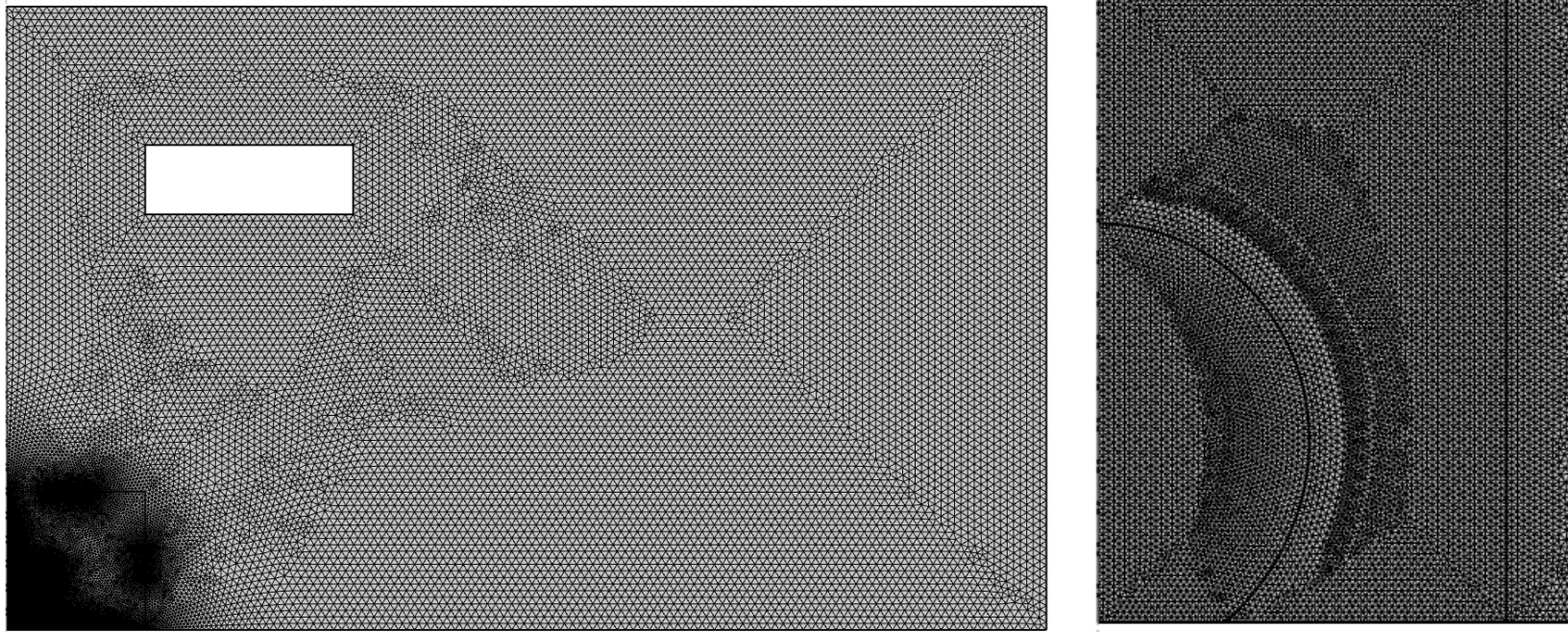


Figure A.1: Mesh used for bubble deformation. Example is from maximum grid spacing of 0.008mm. Left is full domain with a close up on the bubble on the right.

To evaluate the meshes the initial EHD forces on the boundary was compared. The values in the radial and axial direction were calculated in each of the two-phase flow models with each mesh. Figure A.2 to A.4 show the EHD force with different size meshes.

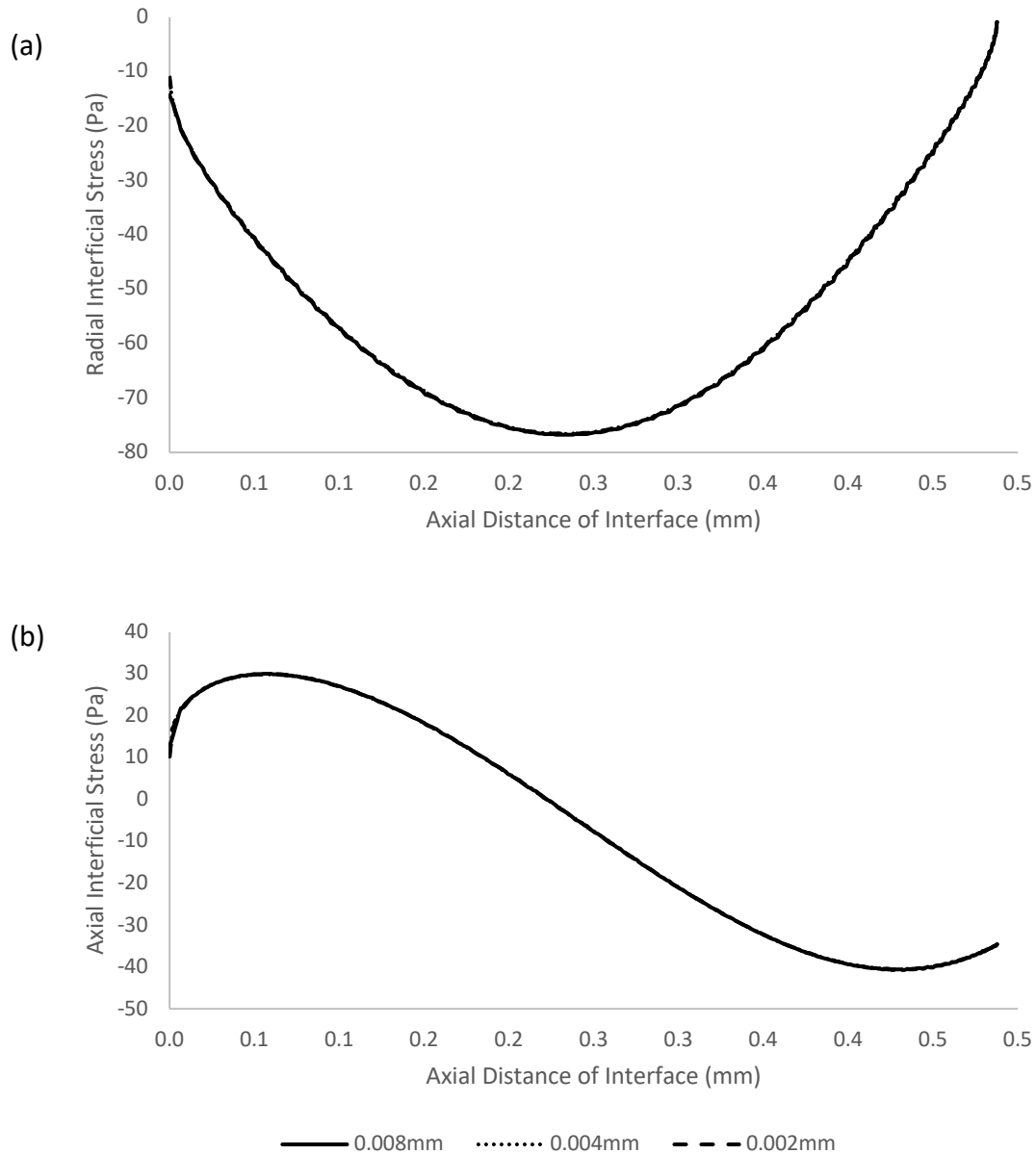


Figure A.2: Radial and axial interfacial stress of the bubble with various maximum mesh spacings for the Moving Mesh model. (a) Radial Stress Component (b) Axial Stress Component

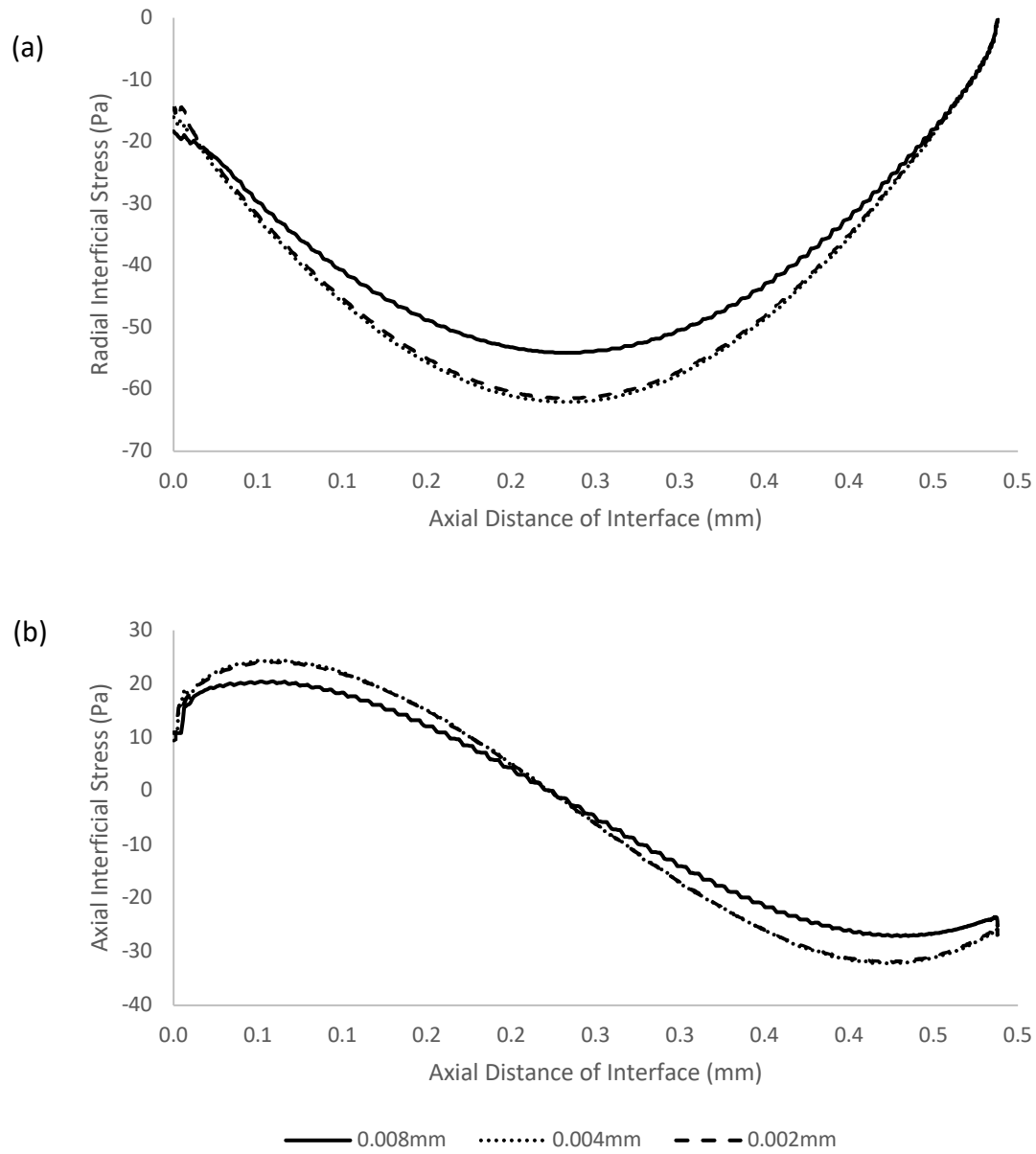


Figure A.3: Radial and axial interfacial stress of the bubble with various maximum mesh spacings for the Phase Field model. (a) Radial Stress Component (b) Axial Stress Component

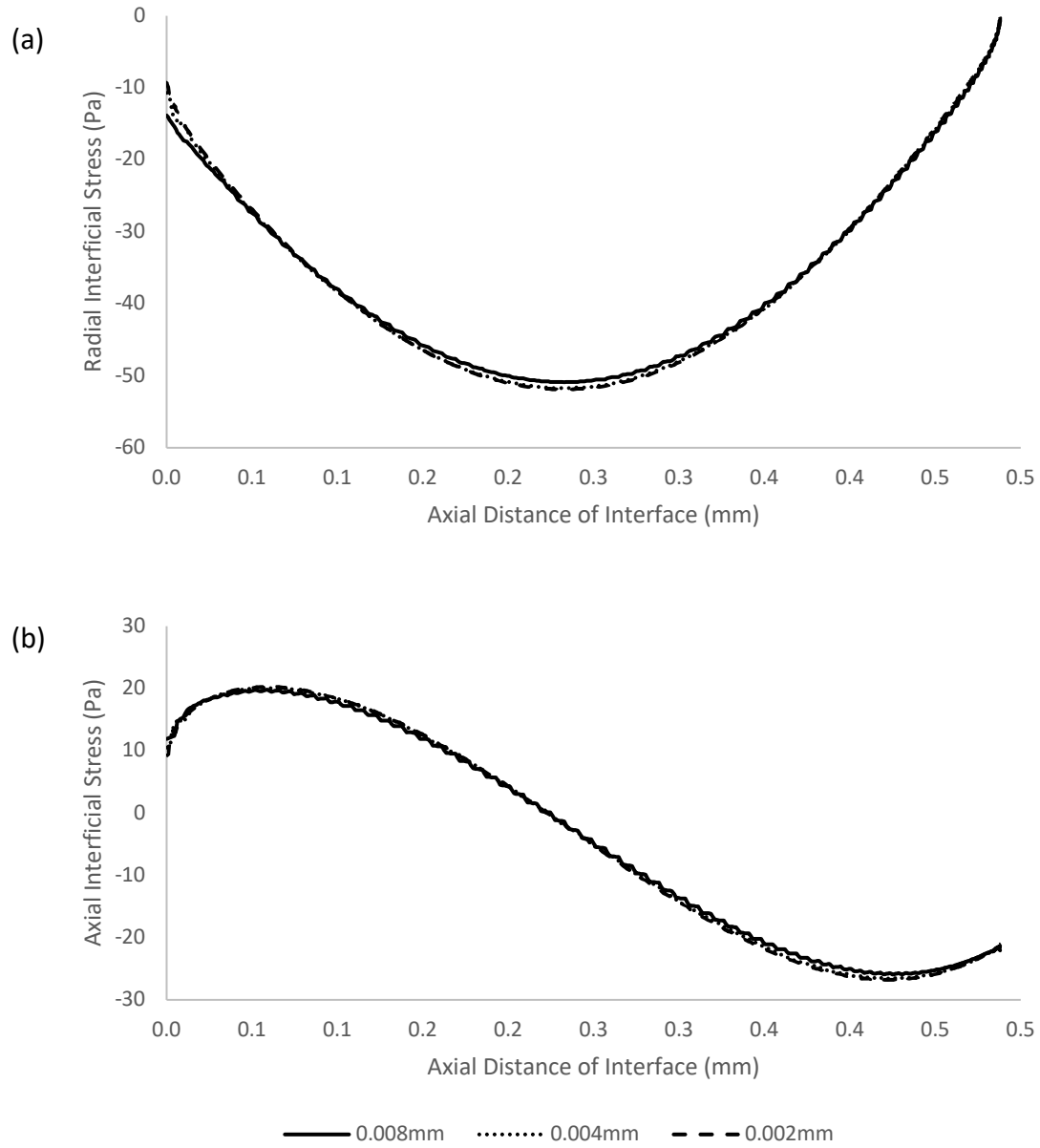


Figure A.4: Radial and axial interfacial stress of the bubble with various maximum mesh spacings for the Level Set model. (a) Radial Stress Component (b) Axial Stress Component

Table A.1: Maximum radial interfacial pressure differences with mesh spacing between the fine mesh, 0.002mm, and the other densities.

Model	% Difference Fine to Coarse	% Difference Fine to Medium
Moving Mesh	-0.2%	-0.005%
Phase Field	12%	-0.9%
Level Set	1.9%	0.3%

Table A.2: Maximum axial interfacial pressure differences with mesh spacing between the fine mesh, 0.002mm, and the other densities.

Model	% Difference Fine to Coarse	% Difference Fine to Medium
Moving Mesh	-0.3%	-0.07%
Phase Field	15%	-0.9%
Level Set	3.1%	0.7%

Table A.1 and A.2 show the deviation of the maximum interfacial stress in each direction compared to the model with the finest mesh. The Moving Mesh model has very close results regardless of the mesh size due to the infinitesimally small interface, but some deviation can be seen in the volume of fluid methods. The deviation is below 1% when the mesh is reduced from the medium to the fine mesh so it is unlikely there will be any significant change with a further mesh reduction. Therefore, a mesh size of 0.002mm is sufficient to estimate the forces correctly in this case.

Appendix B - Independence Tests for Liquid Extraction Model

Introduction

This appendix shows the mesh independence and time dependent tolerance studies for the liquid extraction model seen in Chapter 4. The models consist of coupled fluid flow, electrostatic, and two-phase modules in COMSOL. Three different models are used including the Moving Mesh, Phase Field, and Level Set models.

Mesh Independence Study

Mesh spacing have an important role in the estimation of the EHD force on the interface. EHD force is created from the phase gradient between the liquid and vapour phase which differs in size depending on the nodes a volume of fluid method takes to resolve the boundary and the spacing of those nodes. Three maximum mesh spacings were chosen to do an independence test on which include 0.1mm, 0.05mm, and 0.02mm. The meshes are shown in Figure A2.1. The volume of fluid models are run with an interface thickness of 50% of the maximum grid spacing as recommended by the COMSOL user guide and allows the models to converge. The relative tolerance is set to 0.005 as the default in the program.

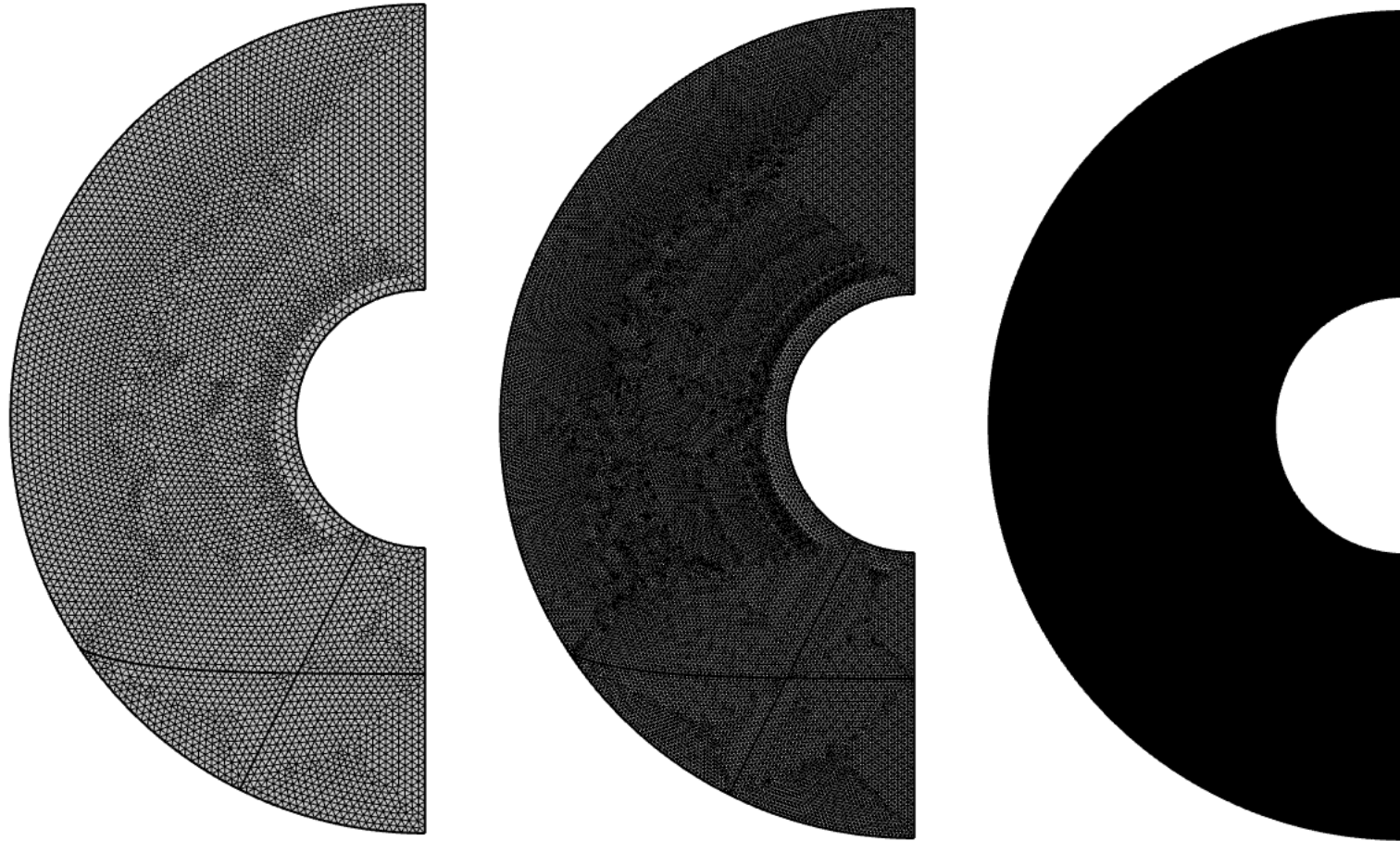


Figure B.1: Three meshes that were used to show mesh independence. The maximum node spacing from left to right is 0.1mm, 0.05mm, and 0.02mm.

The effect on EHD force is focused on to compare the different mesh densities as it is the key factor that will change with a smaller interface resolution. The initial force on the interface is compared for the mesh independence test.

The volume of fluid methods have a variable body force due to a smaller interface causes a large force to compensate. For simplicity, the normal stress component in the y-direction, T22, is used to compare these models. This component causes the interfacial stress and therefore will converge with the interfacial force.

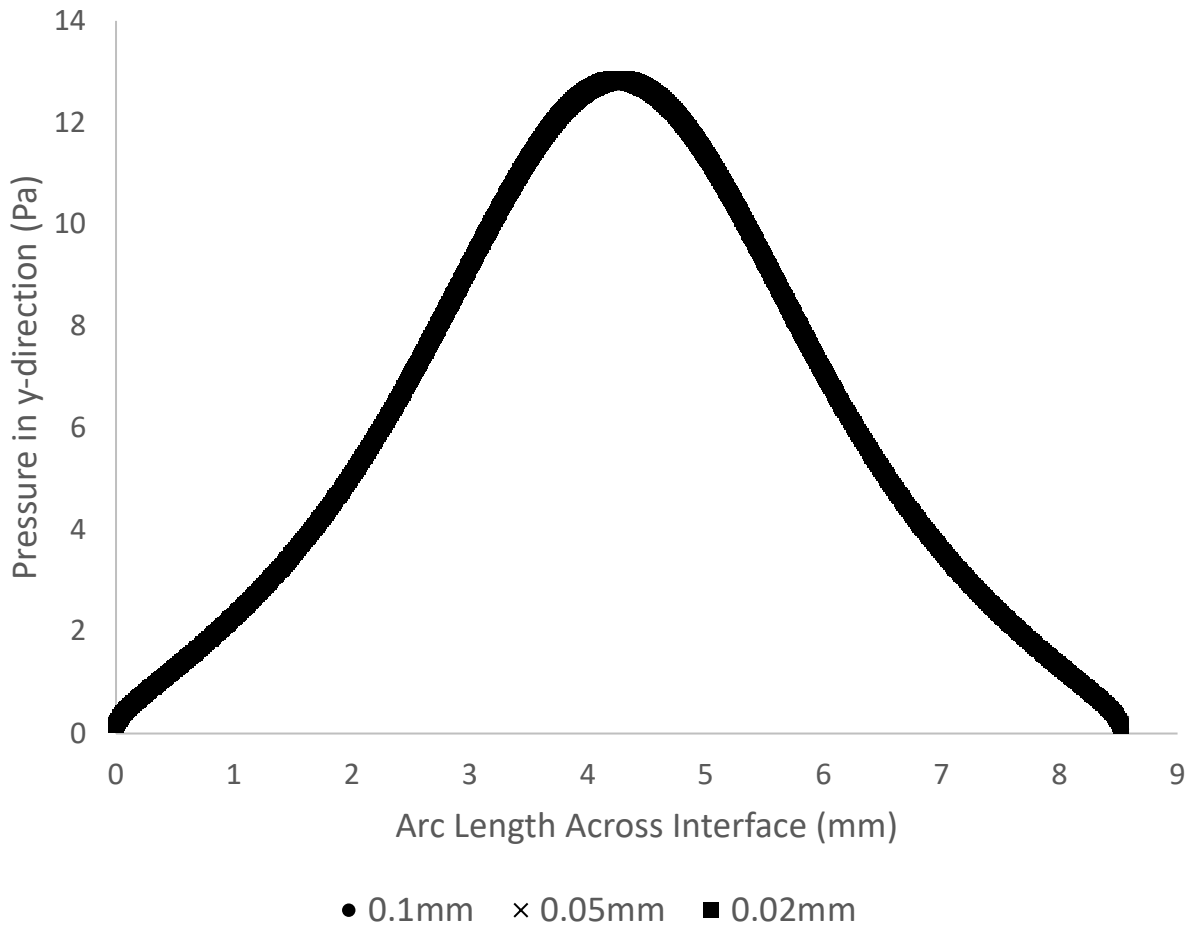


Figure B.2: Comparison of principle stress component with different mesh spacing with the Moving Mesh model

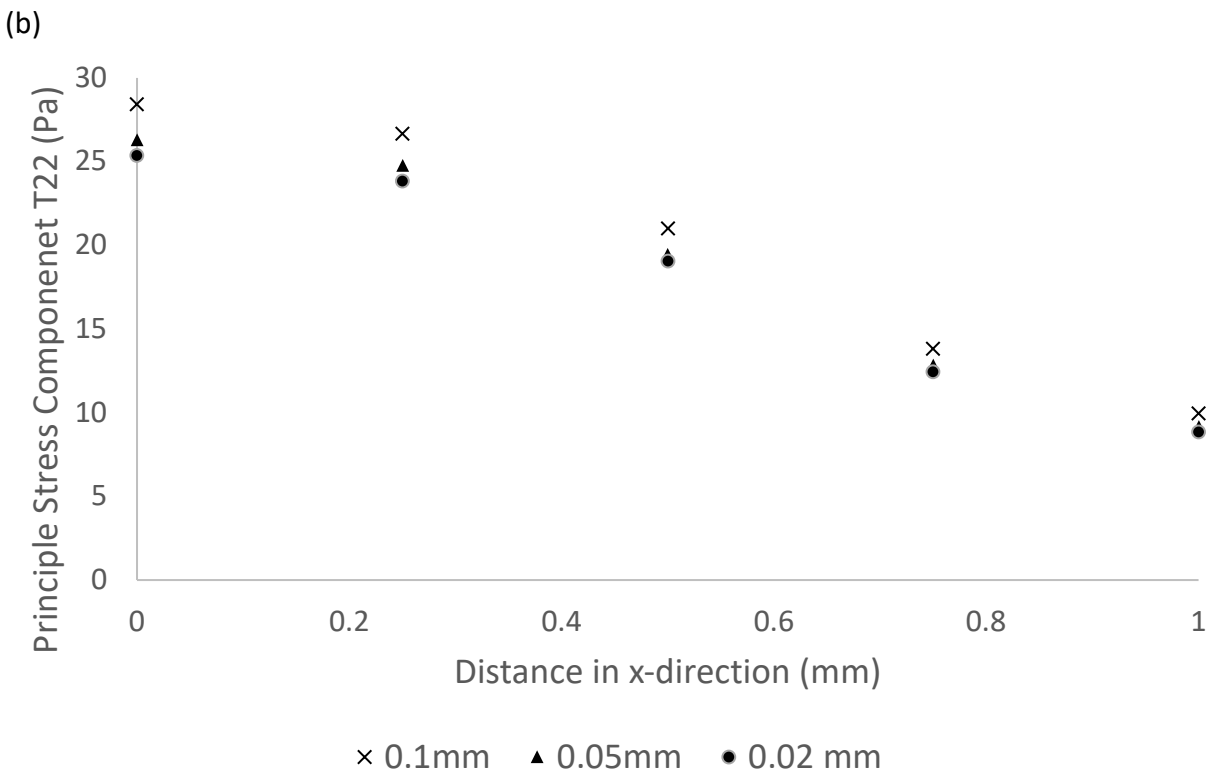
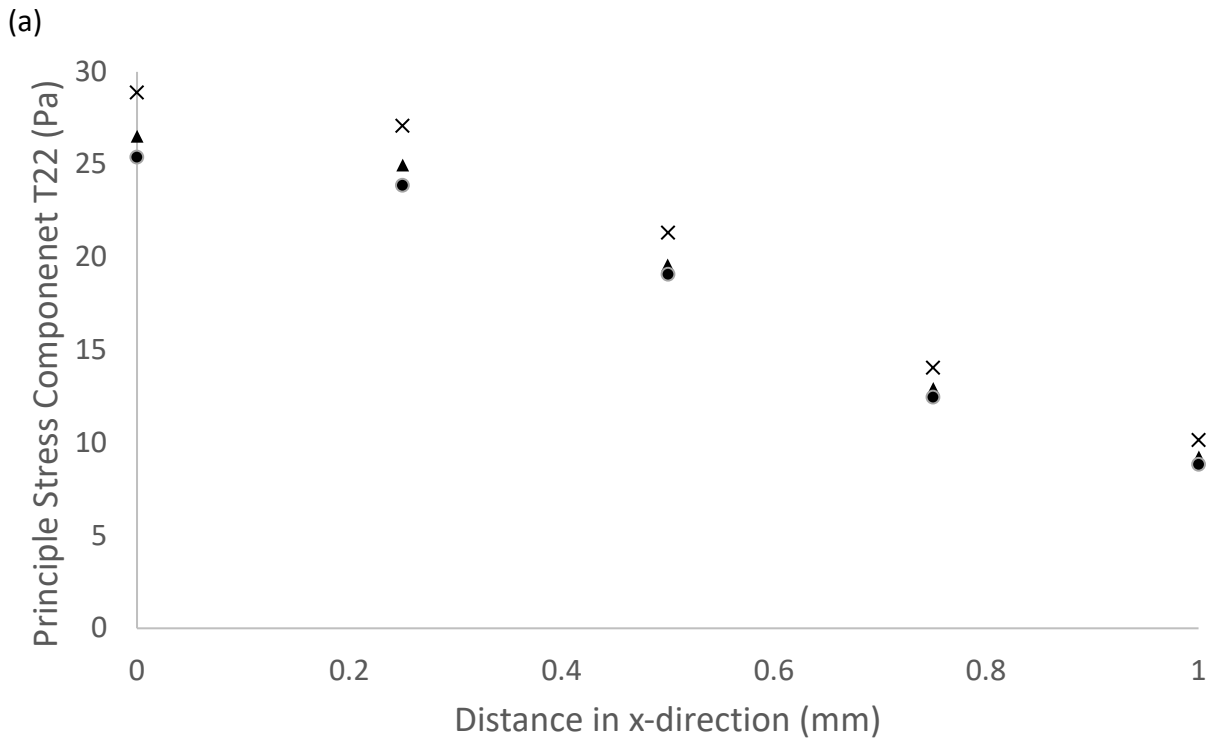


Figure B.3: Comparison of principle stress component with different mesh spacing (a) Phase Field Model (b) Level Set Model

Table B.1: Force differences with mesh spacing between the fine mesh, 0.02mm, and the other densities.

Model	% Difference Fine to Coarse	% Difference Fine to Medium
Moving Mesh	0.2%	0.02%
Phase Field	-14%	-4%
Level Set	-12%	-4%

The Moving Mesh model was shown to approximate the force with any grid spacing chosen. This is due to its step change interface which is less affected by the mesh spacing. The fine mesh, 0.02mm, will be used for the actual models as it has the most information and is shown to be stable.

The volume of fluid methods showed a difference depending on the mesh size. Table A2-1 shows the percent difference comparing the medium mesh, 0.05mm, and the coarse mesh, 0.1mm, to the fine mesh, 0.02mm. There is a 14% difference between the coarse and the fine mesh but only 4% difference between fine and medium meshes. This shows that the fine mesh has the best resolution of the EHD force and should be used with all the models moving forward. Reduction of the mesh beyond 0.02mm causes a significant increase in computational time for minimal force difference so the models were all continued with 0.02mm maximal grid spacing.

Time Independence Tests

In COMSOL Multiphysics, the timesteps are adaptive meaning they vary depending on parameters the gradients of phases, flow velocities, and magnitude of forces. When a model is undergoing large advection, the timesteps become smaller to better resolve the flow pattern. The software uses an implicit solver with timesteps that correspond to a given relative error. The step size is varied to keep the relative error below a specified number. When the error exceeds the tolerance, the step size is reduced or if the timestep converges in few iterations then the step size is doubled for the next timestep. There is also an input for time steps, but this is only for data retrieval and does not affect how the model is run. Therefore, in order to ensure there is time independence, the relative error must be reduced and compared.

To compare the relative error, three relative errors were chosen and tested. In the Moving Mesh model, relative errors of 0.02, 0.01, and 0.005 were chosen. The volume of fluid methods were not able to converge to a physical solution with a relative error of 0.02, so another relative error model was made which is 0.0025. The mesh used was 0.1mm maximum grid spacing to reduce the computational time and it was within 5% of the fine mesh solution.

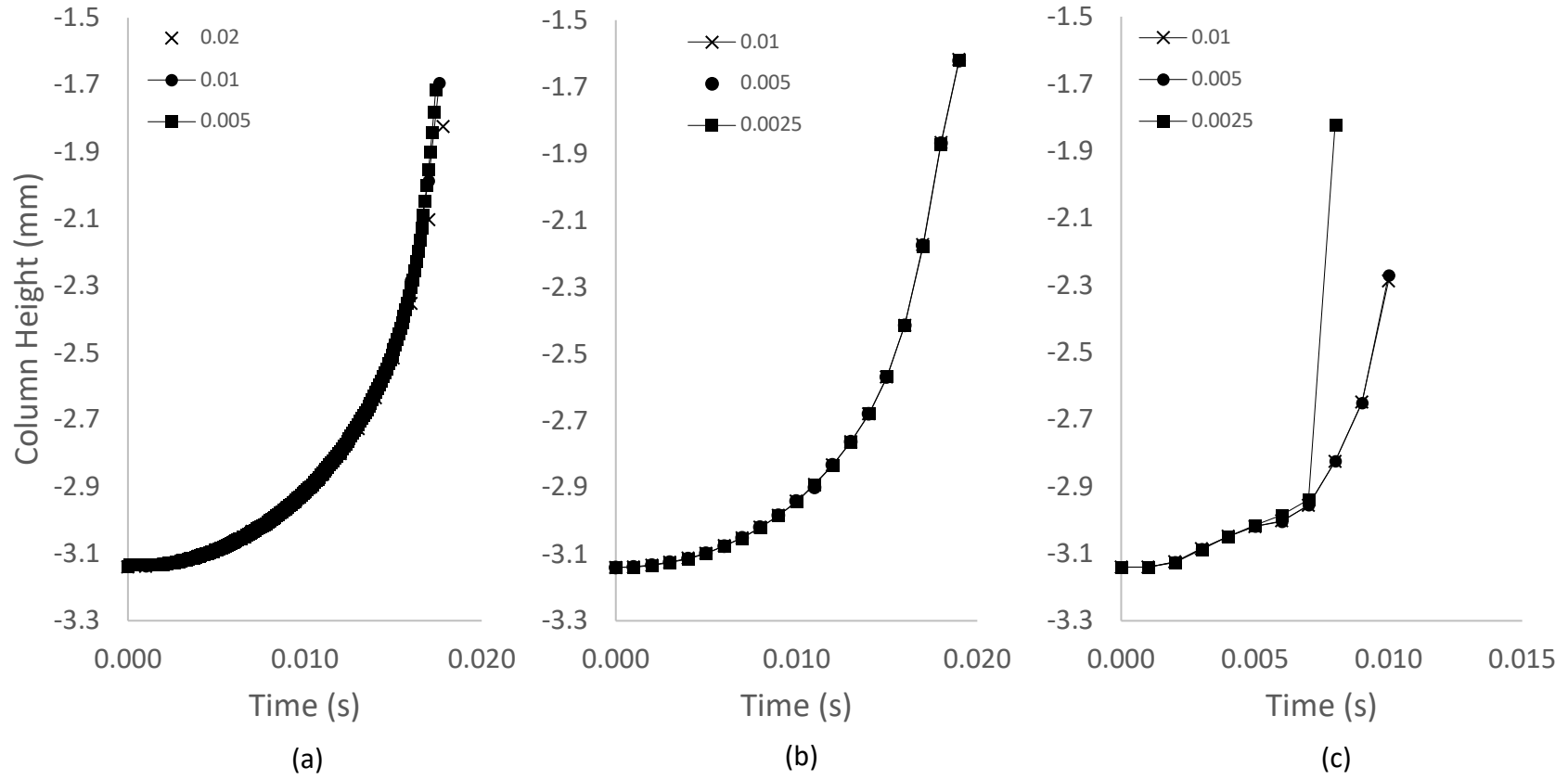


Figure B.4: Comparison of liquid extraction height with different relative tolerances (a) Moving Mesh Model (b) Phase Field Model (c) Level Set Model

Table B.2: Liquid extraction timing differences between the low relative error, 0.005 & 0.0025 for Moving Mesh and volume of fluid methods respectively, and the other relative errors.

Model	% Difference with High	% Difference with Middle
Moving Mesh	5%	1%
Phase Field	0.06%	0.03%
Level Set	1%	-

A linear extrapolation was used on the last two timesteps in each model to approximate the time for the liquid height to reach the bottom of the electrode at -1.59mm. Comparing the lowest relative error used with the other two relative errors, Table A2.2 shows all the different liquid extraction times are within 5% of each other.

The Level Set model was compared between the high and middle relative tolerances of 0.01 and 0.005. This is due to the divergence that happened at 0.0025 relative error. The model made a very sharp edge that had a high EHD force and caused the interface to rise very quickly. The column went away from the centerline and entrapped a bubble on the electrode. All the results from this test were non-physical and is likely due to very small timesteps causing large numerical errors in the system. The Level Set model is the only model to show extraction times and column height profiles that are different from the other models, and this again shows that it is not ideal for high force cases.

For all three cases a relative error of 0.005 was chosen for the rest of the experiments as it performed well in all the scenarios. The concern of choosing a relative error that is too low for the volume of fluids methods also made it the best choice for the Phase Field model so that the model does not diverge like the Level Set model did.